# Circulating Neutrophil Extracellular Traps Promote Gasdermin-D Dependent Lung Injury in Sickle Cell Disease

by

**Ravi Vats**

B.Tech in Biotechnology, Maharshi Dayanand University, India

M.Sc in Imaging and Microscopy, University College Dublin, Ireland

Submitted to the Graduate Faculty of the

Swanson School of Engineering in partial fulfillment

of the requirements for the degree of

Doctor of Philosophy

University of Pittsburgh

2021

UNIVERSITY OF PITTSBURGH

SWANSON SCHOOL OF ENGINEERING

This dissertation was presented

by

**Ravi Vats**

It was defended on

July 7, 2021

and approved by

**Sanjeev Shroff**, PhD, Distinguished Professor, Gerald E. McGinnis Chair of the Bioengineering Department, and Department of Medicine

**Gregory J. Kato**, MD, Senior Director, Global Clinical Programs, Hematology Clinical Research and Development of CSL Behring

**Kang Kim**, PhD, Associate Professor of Department of Biomedical Engineering and Department of Medicine

**Jesus Tejero**, PhD, Assistant Professor of Medicine, Division of Pulmonary, Allergy and Critical Care Medicine, Vascular Medicine Institute

Dissertation Director: **Prithu Sundd**, PhD, Associate Professor of Medicine and Bioengineering

**Circulating Neutrophil Extracellular Traps Promote Gasdermin-D Dependent Lung Injury in Sickle Cell Disease**

Ravi Vats, PhD

University of Pittsburgh, 2021

Sickle Cell Disease (SCD) is a monogenic disorder caused by the homozygosity of the beta-S (βs) allele of the β-globin gene, which results in generation of mutant hemoglobin (HbS). Intra-erythrocytic polymerization of mutant hemoglobin promotes hemolysis, which leads to the development of sterile inflammation and acute systemic painful vaso-occlusive episodes (VOE). VOE is the predominant pathophysiology responsible for emergency hospitalization of SCD patients and often serves as an antecedent to development of Acute Chest Syndrome (ACS), which is a type of acute lung injury (ALI) and one of primary cause of mortality among SCD patients. Although epidemiological findings in humans and *in-vivo* imaging in transgenic-humanized SCD mice suggest a potential role for lung vaso-occlusion in development of ACS, the cellular, molecular, and biophysical mechanisms that promote lung vaso-occlusion and injury in SCD remain incompletely understood.

Using quantitative fluorescence intravital microscopy of the intact lung, liver, and kidney in live SCD mice, confocal microscopy of freshly isolated organs, and Imaging Flow Cytometry of SCD mice or patient plasma, I show that intravenous (IV) administration of oxy-Hb or hemin promotes neutrophil-platelet aggregates-dependent lung vaso-occlusion in SCD mice. Importantly, IV administration of recombinant tandem-P-selectin−glycoprotein ligand−immunoglobulin (TSGL-Ig) significantly attenuated IV oxy-Hb induced lung vaso-occlusion in SCD mice. These findings highlighted the therapeutic potential of TSGL-Ig in preventing VOE and ACS in SCD.

Remarkably, I also discovered a previously unknown phenomenon of the shedding of neutrophil extracellular traps (NETs) from parent neutrophils in the liver and how it contributes to development of lung vaso-occlusion in SCD mice. NETs were shed primarily in the liver of SCD mice administered IV oxy-Hb, and then traveled to the lung as circulating NETs (cNETs) to promote P-selectin independent pulmonary vaso-occlusion. I found that inhibiting caspase-4 (humans)/caspase-11 (mouse)-dependent activation of pore forming protein gasdermin-D (GSDMD), prevented shedding of cNETs in the liver, their translocation to the lung and the development of lung vaso-occlusion in SCD mice. Taken together, these studies introduce a novel paradigm that translocation of DAMPs from liver to lung promotes lung injury in SCD, and identify a new GSDMD-mediated, P-selectin-independent mechanism of lung injury in SCD.

## Table of Contents

## List of Figures

## Preface

Throughout my doctoral work in the Sundd lab there were many people both in and outside of the lab who have helped me reach this day and aided in my development as a researcher.

Dr. Prithu Sundd has been an amazing advisor throughout the five years I have been at Pitt. His mentorship has helped me become an independent researcher and has aided in my development. The knowledge and skills I have gained in his lab have been invaluable and will help me in the next stages of my career. As he began his lab, he took a chance and chose me as his first international graduate student and for that I am forever grateful.

My committee members, Dr. Sanjeev Shroff, Dr. Gregory Kato, Dr. Jesus Tejero, and Dr. Kang Kim have each played an essential role throughout my dissertation and development. With their help and guidance, I have not only become a more well-rounded researcher but a better person.

The friendships that I have developed with my fellow Sundd lab members have been great and have helped those crazy research days become more bearable. Maggie, Maritza, Tomasz Brzoska, Tomasz Kaminski and Egemen, our group has been small throughout the way, and I could not have asked for a better lab group. Maggie and Tomasz B, you both have been my inspiration. You have been there since the very first day and have blazed a path on your way to becoming a professor while showing me what I could become as I move forward with my career as a postdoctoral scholar and beyond.

I would also like to mention my cricket family and friends in Pittsburgh. They have been an outstanding support, not only on the cricket field but outside as well and considering me as one of their closest friends.

Finally, my family who I dedicate this dissertation to. Without each one of you I probably wouldn't be here right now. My parents, Laxman and Sushila, have made me into the person I am today and have taught me that I can achieve anything I put my mind to, no matter how difficult it may seem in the beginning. You have been the steady hand as I've gone through this journey and taught me the value of perseverance even in the face of insurmountable odds. My sister Rachna, you have provided me with the support and relief from the daily grind. I would like to especially thank you for taking care of our parents in my absence when I am thousands of miles away spending time in dark room of microscope looking for something new (and yes, I did), and you were close to them in every up and down taking care of them. Without you this PhD wouldn't have been completed.

## Abbreviations

| | |
|---|---|
| ACS | Acute Chest Syndrome |
| ADP | Adenosine di-phosphate |
| AF | Alexa Fluor |
| APO | Apochromatic |
| BBIB | Blood Bile Barrier |
| CBI | Center for Biologic Imaging |
| CDE | Choline deficient, Ethionine-supplement |
| CF | Carboxyfluorescein |
| CM-DiI | Chloromethyl-Dialkylcarbocyanine |
| cNETs | circulating Neutrophil Extracellular Traps |
| DDC | 3,5-diethoxycarbonyl 1,4-dihydrocollidine |
| DNA | Deoxyribonucleic acid |
| DNase-1 | Deoxyribonuclease I |
| DRP | Drag-reducing polymer |
| eDAMP | erythrocyte Damage-Associated Molecular Pattern |
| EV | Extracellular Vesicles |
| FDA | Food and Drug Administration |
| FITC | Fluorescein Isothiocyanate |
| FOV | Field of view |
| GSDMD | Gasdermin-D |
| GSK484 | PAD-4 inhibitor |

| | |
|---|---|
| H3-CitH3 | Citrullinated Histones |
| HbF | Fetal hemoglobin |
| HbS | Sickle Hemoglobin |
| HU | Hydroxyurea |
| ICAM-1 | Intercellular Adhesion Molecule 1 |
| ICAM-4 | Intercellular Adhesion Molecule-4 (ICAM-4) |
| IgG | Immunoglobulin G |
| IL-1RA | Interleukin-1 Receptor Antagonist |
| IL1β | Interleukin-1β |
| IL-8 | Interleukin – 8 (CXCL8) |
| IV | Intravenous |
| IVC | Inferior-Vena-Cava |
| LDC7559 | GSDMD inhibitor |
| LEVD-CHO | Caspase-4 inhibitor |
| LPS | Lipopolysaccharide, gram negative bacteria |
| LWD | Large Working Distance |
| MPO | Myeloperoxidase |
| NA | Numeric Aperture |
| NAC | N-Acetyl-L-cysteine |
| NADPH | Nicotinamide Adenine Dinucleotide Phosphate |
| NE | Neutrophil Elastase |
| NEi | Neutrophil Elastase inhibitor; BAY-85-8501 |
| NETs | Neutrophil Extracellular Traps |

| | |
|---|---|
| NK-T | Natural Killer T |
| NO | Nitric Oxide |
| NSA | Necrosulfonamide; GSDMD inhibitor |
| Oxy-Hb | Oxy-hemoglobin |
| PAD-4 | Protein Arginine deiminase-4 |
| PBS | Phosphate Buffer Saline |
| PMA | Phorbol-2-Myristate-13-Acetate |
| PPP | Platelet Poor Plasma |
| PS | Phosphatidyl Serine |
| PSGL-1 | P-selectin glycoprotein ligand-1. |
| PVO | Pulmonary Vaso-occlsuion |
| qFILM | quantitative Fluorescence Intravital Lung Microscopy |
| qKIM | quantitative Kidney Intravital Microscopy |
| qLIM | quantitative Liver Intravital Microscopy |
| qMFM | quantitative Microfluidic Fluorescence Microscopy |
| RBC | Red Blood cell (Erythrocyte) |
| rh | recombinant human |
| ROS | Reactive Oxygen Species |
| SCA | Sickle Cell Anemia. Most common form of SCD. |
| SCD | Sickle Cell Disease |
| SNP | Single Nucleotide Polymorphism |
| sRBC | sickle Red Blood Cells |
| TJ | Tight Junction |

| | |
|---|---|
| TLR4 | Toll Like Receptor-4 |
| TNF | Tumor Necrosis Factor |
| TSGL-Ig | Tandem P-selectin Glycoprotein Ligand Immunoglobulin |
| TXR-dextran | Texas Red-dextran |
| UN | United Nations |
| UNESCO | United Nations Educational, Scientific, Cultural Organization |
| VOC | Vaso-occlusive Crisis |
| VOE | Vaso-occlusive Episodes |
| WHO | World Health Organization |
| WT | Wild-Type |
| YVAD-CHO | Caspase-1 inhibitor |
| Z-VAD-FMK | Pan-caspase inhibitor |

# 1.0 Introduction

## 1.1 Sickle Cell Disease

### 1.1.1 Background

Sickle Cell Disease (SCD) is one of the most common monogenetic disorders in the world[1]. Sickle Cell Anemia (SCA), the most common form of SCD is caused by the homozygosity of the beta-S (βs) allele of the β-globin gene, which is located in the short arm of chromosome 11 (11p15.5)[1]. The βs allele differs from wild type β allele by a single nucleotide polymorphism (SNP) dbSNP Rs334(T;T), which involves replacement of GAG by GTG as the 6th triplet-codon, leading to substitution of valine (hydrophobic amino acid) for glutamic acid (hydrophilic amino acid) at the 6th position in the β-globin chain of hemoglobin[2, 3]. Figure 1 shows the global distribution of βs-allele, and it is particularly common in humans with ancestry of sub-Saharan Africa, Saudi Arabia, and India[4]. In United States, there are 50-100 births with SCA per 100,000 births[4]. According to the data available in 2013, globally 3.2 million people

had SCD, 43 million people had sickle cell trait (carriers), and more than 150,000 people died of SCD (115,000 deaths in 2015)[5].

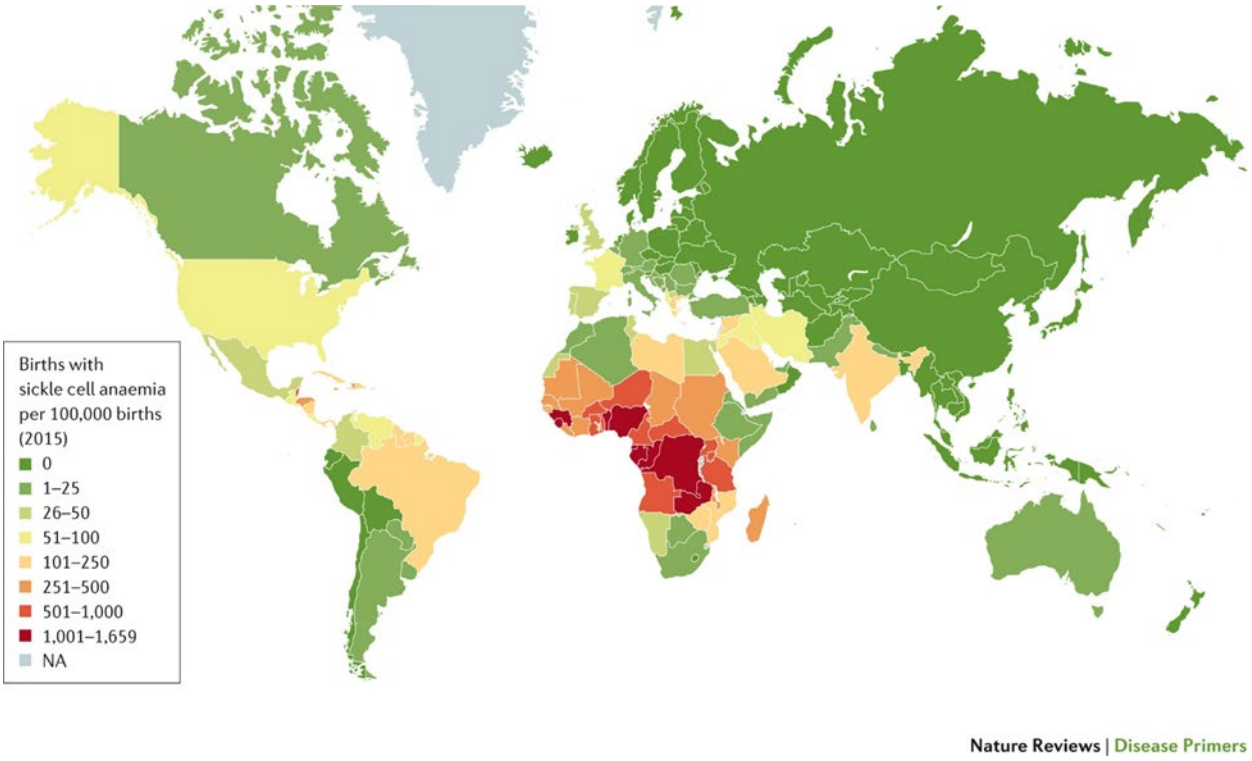


**Areas in red shows the highest prevalence of SCA whereas in green shows the lowest prevalence of SCA.**

**Figure is used with permission from reference [4].**

In 1910, sickled erythrocytes were first described by James B. Herrick as "peculiar elongated and sickle-shaped red blood corpuscles in a case of severe anemia"[6]. Fourteen years later in 1924, V.P. Sydenstricker identified hemolysis as a pathophysiology in Sickle Cell Disease[7]. In 1949, Linus Pauling described SCD as a defect in hemoglobin and described it as a molecular disease[8]. The abnormal form of hemoglobin resulting from the homozygosity of βs allele in SCA patients is referred to as HbSS[1]. Although SCA is the most common form of SCD responsible for severe disease among majority of SCD patients, there are other less common

variants of SCD caused by the compound inheritance of one βs allele with an another β allele carrying mutations such as βC (HbSC), βD (HbSD), βO (HbSO/Arab), βE (HbSE), or a β-thalassemia allele (HbS/β-thal0 or HbS/β-thal+), resulting in varying levels of disease severity[1, 2, 4, 9]. Sickle Cell Trait (HbAS) is caused by the compound heterozygosity of βs and wild type β alleles, and it is believed to be asymptomatic [1, 2, 4]. Although SCD was discovered over a century ago, a cure for this disease still not exist. In the last three decade, four drugs were FDA approved for the treatment of SCD (Hydroxyurea (1995), Adakveo (2019) and L-glutamine (2018), and Oxbryta (2020) that only partially attenuate disease morbidity, thus warranting the need to identify the mechanism responsible for the remaining morbidity in SCD.

### 1.1.2 Pathophysiology of SCD

SCD is an inherited and autosomal recessive molecular disease caused by mutation in β-globin gene, this mutation resulted in change of amino acid from glutamic acid to valine, and hence the resultant hemoglobin (HbS) has abnormal physiochemical properties [1, 2, 4]. Following deoxygenation, HbS forms polymer bundles and hence results in sickling of Red Blood Corpuscles (RBCs) and hemolysis. Sickled RBCs causes impaired rheology and adhesion between leukocytes and platelets[2, 4]. Hemolysis release free heme in the blood circulation which causes activation of platelets, endothelium, and leukocytes[10]. Release of heme in the blood circulation causes sterile inflammation which further activates Toll Like Receptors 4 (TLR4), Neutrophil Extracellular Traps (NETs), and Reactive Oxygen Species (ROS) generation[10]. These combined events lead to vaso-occlusion and multi-organ failure[2]. Pathophysiology of SCD can be divided into four parts viz; HbS polymerization, Vaso-occlusion, Endothelial dysfunction, and Sterile inflammation described in Figure 2[2]. Detailed explanation of each part is discussed below:

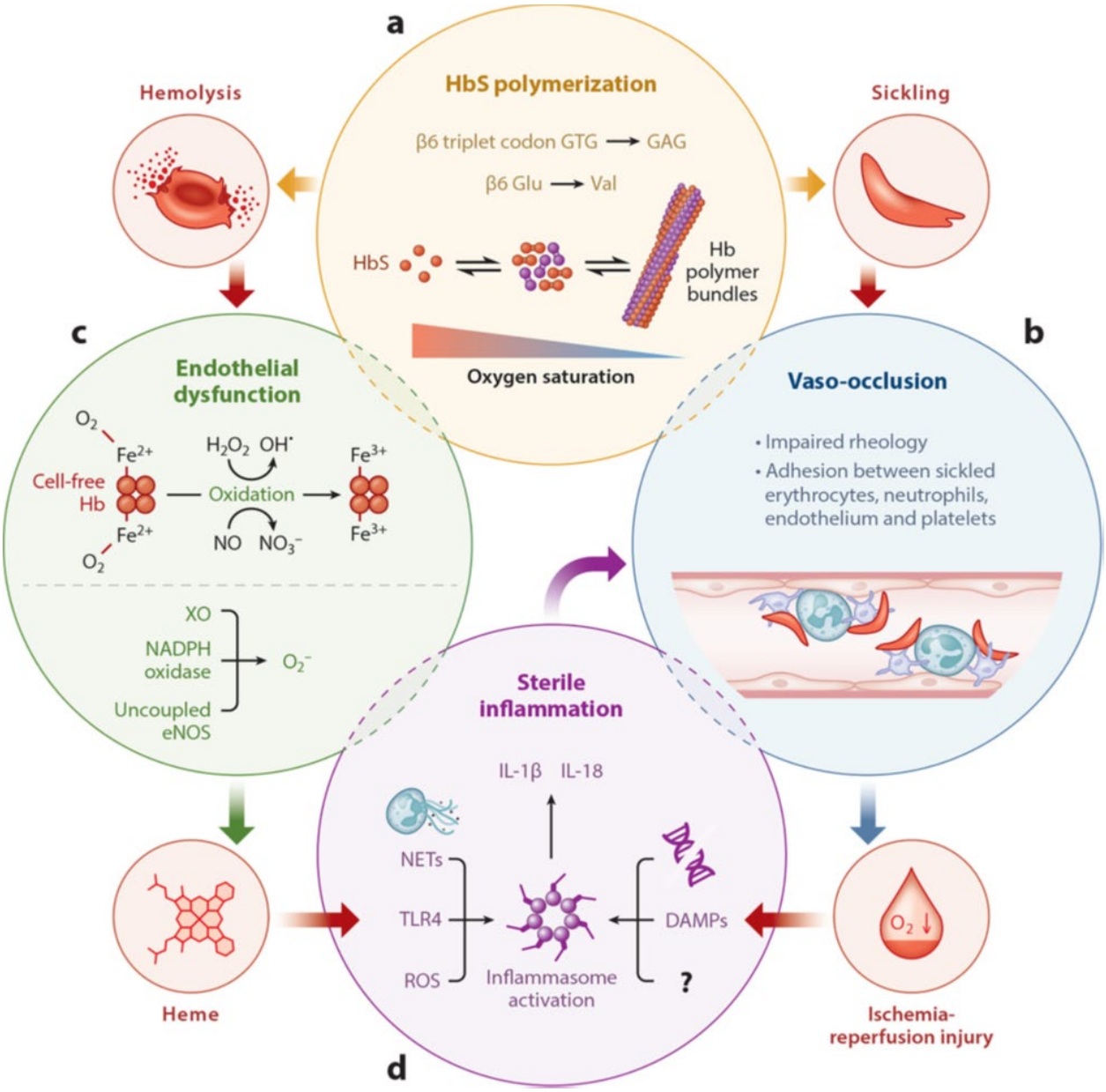


**Figure 2: Pathophysiology of Sickle Cell Disease.**

**A. HbS polymerization B. Vaso-occlusion C. Endothelial dysfunction D. Sterile Inflammation. This figure is used with permission from reference[2].**

#### 1.1.2.1 HbS Polymerization

Intraerythrocytic HbS in deoxygenated conditions forms HbS tetramers, further these tetramers bind to each other thus initiating the nucleation of a HbS polymer[2, 11]. These HbS polymers grows rapidly in deoxygenation condition resulting in HbS polymerization. Due to HbS polymerization and long bundle formation, erythrocyte cellular rigidity increases, and erythrocyte membrane gets deformed, thus causing the erythrocytes to take a sickle shape. Initially the process of sickling is reversible but due to change in membrane numerous times, it becomes irreversible[11]. These subsequent changes in RBCs shape made changes in its rheological properties, and RBCs plasma viscosity changes, membrane flexibility decreases, and cellular dehydration increases[11]. It has been stated that the rate of polymerization is inversely proportional to the concentration of fetal Hb (HbF), and directly proportional to the concentration of HbS[2, 11].

#### 1.1.2.2 Vaso-occlusion

As a result of HbS polymerization and sickling of RBCs, there is an impaired rheology which result in an adhesion between sickled erythrocytes, neutrophils, endothelium, and platelets[11]. These adhesions between different cell types form large aggregates which blocks the blood flow in capillaries, post-capillaries, and arterioles, leading to ischemia and organ failure[1, 4]. Hence, it is responsible for acute systemic painful vaso-occlusive episode (VOE) in SCD patients. Importantly, sickle RBCs membrane exposure of adhesion molecules such as phosphatidyl serine (PS), integrin-associated protein, and intercellular adhesion molecule-4 (ICAM-4) make RBCs adhere to the endothelium, leukocytes and platelets[2]. Also, bone marrow in chronic anemia undergoes stress and produces immature erythrocytes decorated with adhesion molecules such as integrin and CD36[2]. Recently, it has been shown that external stimulus like

lipopolysaccharide (LPS) [3] and oxy-Hemoglobin (oxy-Hb) [12] causes neutrophil-platelets aggregates in the bottlenecks of a SCD mouse lung, which leads to stoppage of blood flow to promote lung vaso-occlusion. Lung vaso-occlusion may lead to ACS, and accounts for most of morbidity and mortality in SCD patients [13].

#### 1.1.2.3 Endothelial Dysfunction

Under normal conditions, cell free hemoglobin released after intravascular hemolysis binds to haptoglobin forming a hemoglobin-haptoglobin complex, which then binds to CD163 receptors on reticuloendothelial macrophages in the spleen, liver and bone marrow leading to endocytosis of hemoglobin for recycling of iron for erythropoiesis [9, 14, 15]. However, the haptoglobin reserve is depleted in SCD because of chronic intravascular hemolysis, leading to impairment of CD163-dependent pathway of cell-free Hb scavenging [9, 15]. The unscavenged heme ($Fe^{2+}$) reacts with hydrogen peroxide ($H_2O_2$) via Fenton reaction to generate highly reactive hydroxyl radical, hydroxyl ion, and hemin ($Fe^{3+}$). On the other side, oxy-Hb ($HbFe^{2+}$) is also released post hemolysis which reacts with nitric oxide (NO) via dioxygenation reaction to form inert nitrate ($NO^{3-}$), and highly unstable methemoglobin ($HbFe^{3+}$), which degrades to release a potent pro-oxidant and pro-inflammatory cell, oxidized form of heme (ferric protoporphyrin IX)[15]. NO scavenging by oxy-Hb further promotes endothelial dysfunction by impairing NO-dependent basal vasodilation, promoting activation of platelets, endothelial cells and leukocytes, and uncoupling endothelial nitric-oxide-synthase (eNOS) leading to generation of endothelial reactive oxygen species (ROS)[2, 15]. These pathophysiological events triggered by the impaired scavenging of cell free heme, and hemin synergistically result in endothelial dysfunction, which promotes proliferative vasculopathy of the pulmonary and systemic vasculature and the vaso-occlusive pathophysiology (discussed earlier)[2, 13, 15].

#### 1.1.2.4 Sterile Inflammation

Heme and its oxidized form, hemin serve as a potent erythroid-derived DAMPs (eDAMPs) to activate TLR4 pathway, generation of NETs, and ROS[2]. Ischemia-reperfusion injury secondary to vaso-occlusion leads to generation of diverse cell and tissue-derived DAMPs such as oxidized DNA and plasma membrane fragments, chromatin-binding protein such as HMGB1, adenosine triphosphate, mitochondrial proteins such as cardiolipin, loss of mitochondrial membrane potential, cytoplasmic proteins, proteases, lysosomal products, histones, and nucleosomes[2, 9]. These combined events lead to activation of inflammasome pathways in leukocytes, platelets and endothelial cells, leading to extracellular release of interleukin-1β (IL-1β) and interleukin-18 (IL-18)[2]. TLR4 (Toll Like Receptors 4) is a transmembrane protein which acts as a specific pattern recognition receptor. TLR4 activation leads to further activation of NF-κB pathway and innate immune system[10]. NETs (Neutrophil Extracellular Traps) are web-like structures which are produced from neutrophils under inflammatory or thrombotic conditions[10]. NETs are composed of decondensed chromatin decorated with citrullinated histones and neutrophil proteases[16]. NETs and their role in inflammation and SCD will be discussed in later section 1.1.4.

### 1.1.3 Vaso-occlusive Episodes and Acute Chest Syndrome in SCD

Acute systemic painful vaso-occlusive episode (VOE) is the major cause of hospitalization among SCD patients, and often leads to development of Acute Chest Syndrome (ACS)[2, 17]. ACS is a type of acute lung injury (ALI) in patients with SCD defined as a condition with new pulmonary infiltrates, fever, labored breathing and chest pain[17]. ACS is one of the leading causes of death and hospitalization in SCD[13, 17, 18], and develops within 2.5 days of patient's

hospitalization with VOE[17]. It has been reported that the episodes of ACS are more common in SCD children but has a mild clinical course, whereas adults typically have a more severe clinical course that develops into substantial morbidity and mortality[13, 17]. Severe hemolysis, low hemoglobin levels, fat embolism, high neutrophil-platelet aggregates (NPAs) and neutrophil counts, hypoventilation and atelectasis, and pulmonary thrombosis has been described as the potential cause of ACS[13, 17]. The current treatments for ACS are typically exchange transfusion and antibiotics, which are primarily supportive, but the mechanism of action of these treatments remains largely unknown[13, 17].

### 1.1.4 Neutrophil Extracellular Traps in SCD

Neutrophil extracellular traps (NETs) are the web-like structures of chromatin filaments which contain histones, proteases, granular and cytosolic proteins that are assembled on a scaffold of decondensed chromatin[19, 20]. NETs are released from neutrophils under proinflammatory and prothrombotic conditions, and they help to catch and kill pathogens under normal conditions[19]. The process of releasing of NETs from neutrophils is called NETosis, which helps in elimination of bacteria, viruses, and other pathogens[19-21]. However, recently it is known that NETs play a vital role in non-infectious disease, sterile inflammation, and auto-immune diseases as well[19]. The main protein content of NETs are histones, serine proteases such as neutrophil elastase, myeloperoxidase (MPO), calprotectin, cathelicidins, defensins and actin[20]. As shown in Figure 3, NETosis can be divided into two pathways based on activation and release of NETs viz. late suicidal NETosis or early vital NETosis[19]. In late suicidal NETosis, stimulation of neutrophils with phorbol-2-myristate-13-acetate (PMA) activates NADPH (nicotinamide adenine dinucleotide phosphate)-oxidase production leading to ROS generation. ROS results in activation

of protein arginine deiminase 4 (PAD4), an enzyme responsible for conversion of arginine to citrulline on histones and chromatin de-condensation in the neutrophil nucleus[19]. This results in chromatin de-condensation and release of neutrophil elastase (NE) and myeloperoxidase (MPO) from the neutrophil azurophilic granules and translocated into the nucleus, which further promotes de-condensation of chromatin[21, 22]. As a repercussion of these events, the nuclear membrane breaks, and chromatin is released into the cytosol which is decorated with cytosolic proteins. Finally, NETosis occurs through disruption of plasma membrane, and the neutrophil dies [19]. The induction of late suicidal NETosis depends mostly on the type of stimulus (PMA, foreign antibodies or cholesterol crystals) used to activate neutrophils and has been reported to occur primarily in in-vitro studies with isolated neutrophils following 12- 24 hour incubation with the stimuli[19].

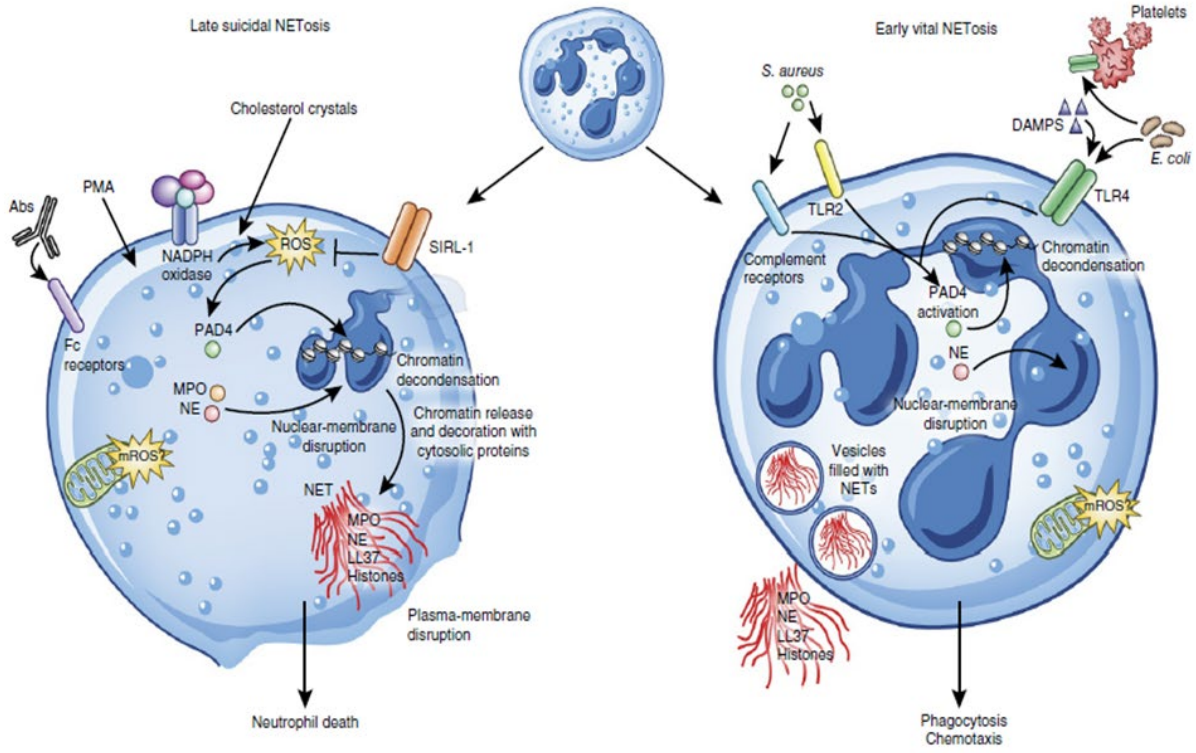


**Figure 3: Overview of NETosis.**

**Late suicidal NETosis, and Early vital NETosis10. Figure taken with permission from reference[19].**

In contrast, the early vital NETosis occurs within minutes of stimulation of neutrophils (both in-vivo and in-vitro) following exposure to bacteria, complement component 5a, TLR2 ligands, activated platelets, and eDAMPs[19, 22]. PAD4 is activated which results in chromatin de-condensation, further NE and MPO are translocated to the nucleus, and disruption of nuclear membrane occurs. Here, NETs are released via nuclear-envelope blebbing without disruption of plasma membrane and hence neutrophils are still able to stay alive and carry out their phagocytosis, chemotaxis, and killing of bacteria function[19]. Recently, NETs were shown to be present in the lung of SCD mice administered TNFα, however, the molecular mechanism promoting NETs generation in SCD remains unknown[10] and their role in promoting lung vaso-occlusion remains also unknown. Furthermore, recent clinical findings suggest that circulating NETs are present in the blood of SCD patients, which suggest that NETs contribute to the pathobiology of SCD but

the molecular mechanism remains to be determined[23]. This gap of knowledge formed the basis of my doctoral thesis looking at molecular pathway that can be inhibited to prevent NETs-dependent lung vaso-occlusion and the development of lung injury in SCD.

### 1.1.5 Emerging role of Gasdermin-D in NETs generation

Gasdermins has been shown to play an important role in inflammation and inflammatory signaling[24-26]. Gasdermins are a pore-forming effector proteins which causes membrane permeabilization and then pyroptosis of a cell[24-26]. So far, six gasdermins have been known and our interest is mostly on GSDMD (Gasdermin D) effector protein because of it influential affect in inflammation[26-28]. GSDMD is composed of a cytotoxic N-terminal, flexible linker, and a C-terminal repressor domain. Cleavage of GSDMD leads to Pyroptosis[24-26], and is defined as a highly specific programmed inflammatory cell death initiated by inflammasome. An inflammatory cascade of inflammasomes is activated in response to microbial infection and foreign danger signals. Inflammasomes are set a complex protein which form inflammatory cascade in response to microbes, and they activate inflammatory caspases to produce cytokines and to induce pyroptotic cell death[29]. Furthermore, in response to microbial infection and foreign danger signals, pro-caspase-4/5/11 are activated to from mature caspase-4/5/11. This leads to cleavage of Gasdermin D (GSDMD) from a cytotoxic N-terminal, resulting in large oligomerization of N-GSDMD which forms pores into the cell membranes and disrupts ion homeostasis, and induces cell death[26]. Recently, a new mechanism has been identified in infectious models where intracellular translocation of LPS or cytosolic release of neutrophil elastase results in GSDMD-dependent generation of NETs[24]. A new study also shows that caspase-4/5 in humans and caspase-11 in mouse cleave GSDMD to promote NETs generation

triggered by cytosolic LPS and cytosolic gram-negative bacteria (Figure 4)[30]. These new pathways of GSDMD dependent NETosis may play an important role in SCD. I propose that caspase-4 in human and caspase-11 in mouse activation leads to GSDMD-dependent NETs generation in SCD via hemolytic-milieu induced oxidative stress, and this is the focus of my PhD research.

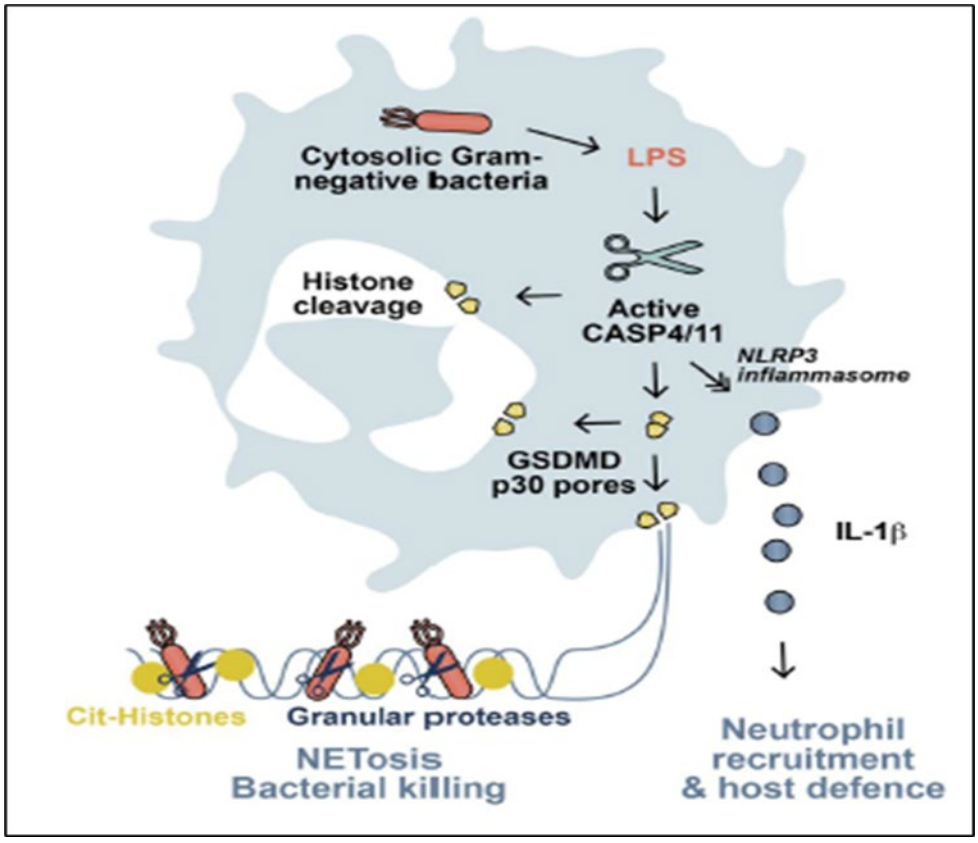


**Figure 4: LPS driver activation of caspase-4/11 induces GSDMD cleavage, pore formation and NETosis.**

**Figure taken with permission from reference[30]**

### 1.1.6 Current treatment and ongoing clinical trials

UNESCO (in 2005), WHO (2006), and the UN (2008) recognized sickle cell disease as a public health priority and declared 19th June of each year to be celebrated as the World Sickle Cell Day to raise awareness of the disease in the world[31]. Hydroxyurea (HU) was the 1st FDA approved drug in 1998 for the prevention of VOE in SCD patients[32]. HU, a myelosuppressive agent, works by raising the level of fetal hemoglobin (HbF), thereby interfering with HbS polymerization[32]. However, not all patients are adherent to HU because of adverse side effects (headache, mild gastrointestinal symptoms, nausea etc), and the disease morbidity is only reduced by half in those taking HU[32]. L-glutamine was the 2nd FDA approved drug in 2017 for the prevention of VOE in sickle cell anemia and sickle β-thalassemia. L-glutamine also known as Endari® increases the amount of free glutamine in the blood circulation and hence generate antioxidant molecules, such as reduced glutathione and the cofactors NAD(H) and NADP(H), and nitric oxide[33, 34]. The main side effects of L-glutamine in SCD clinical trials were abdominal pain, cough, constipation, nausea, and chest pain. L-glutamine is not recommended for patients with renal and hepatic impairment and therefore there is a requirement for additional treatment options for SCD patients with renal and hepatic impairment until these population are studied further[34]. Crizanlizumab was the 3rd FDA approved drug in 2019 for the prevention of VOE in sickle cell disease. Also known as Adakveo®, it is a humanized anti-P-selectin antibody which prevents vaso-occlusion by blocking adhesion of leukocyte and sickle erythrocytes to endothelial and platelet P-selectin[35], P-selectin is an adhesion binding protein which is present on the surface of endothelial cells and activated platelets. Adakveo was effective in reducing the frequency of hospitalizations by 45.3% compared to placebo[35], suggesting the presence of a P-selectin independent mechanism contributing to remaining ~50% morbidity. Additionally, there have been

reports of adverse effect of Adakveo among few SCD patients which include joint pain, diarrhea, itching, vomiting and chest pain[35]. Oxbryta was the 4th FDA approved drug in 2019 for the treatment of sickle cell disease. Also known as voxelotor (GBT-440), it is an oral therapy drug, which binds to hemoglobin and increases its affinity for oxygen[36]. This helps prevents Hb polymerization by maintaining hemoglobin in the oxygenated R-state conformation and subsequently reduces sickling of RBC[36]. Voxelotor was found to reduce hemolysis and improve erythrocyte function in SCD patients without having any beneficial effects on frequency of VOE. The most common side effects of Voxelotor were headaches, diarrhea, fatigue, and nausea[36].

There are several clinical trials going on for the treatment of VOE in sickle cell disease. One of them is rivipansel (GMI-1070), a pan-selectin inhibitor, which blocks adhesion molecules called selectins in the blood vessels. Selectins family contains E-, P-, and L-selectin which regulate interactions between red blood cells, endothelial cells, and platelets. However, rivipansel failed to the meet the primary outcome criteria in its Phase 3 clinical trial (NCT02187003)[37]. Intravenous immunoglobulin (IVIG) is another agent in clinical trials for the treatment of VOE in SCD. IVIG has been shown to inhibit leukocyte activation and adhesion to endothelium as well as circulating RBC by inhibiting Mac-1 dependent interactions[38]. IVIG is now in a Phase 2 trial to test its effectiveness at reversing acute VOE (NCT01757418)[38]. Prasugrel or ticagrelor, is a P2Y12 ADP receptor antagonist, inhibits ADP mediated platelet activation and aggregation. The drug showed promising results during Phase 1 and Phase 2 clinical trials with decreased platelet activation in SCD patients[39]. Unfortunately phase 3 clinical trials (NCT01794000) were terminated due to a lack in efficacy in reducing acute vaso-occlusive complications but have opened the door to new drugs targeting platelet activation[40]. Canakinumab also known as ACZ885 is an interventional study type for the prevention of inflammation in sickle cell

disease[41]. ACZ885 acts as an anti-inflammatory protein which prevents or inhibits the action of interleukin-1 beta (IL-1β). ACZ885 just completed the phase 2 trial (NCT02961218)[41].

Several gene therapies such as LentiGlobin, are currently being investigated in clinical trial as a curative therapy for SCD. These therapies involve replacement of βs-allele with the βA-allele in autologous stem cells or induction of constitutively activated γ-globin gene in SCD patients. Although early findings from these gene therapy trials seem promising, however, all the gene-therapy clinical trials have been temporarily paused due to development of acute myeloid leukemia in patients[42].

## 1.2 Summary

Sickle Cell Disease is a genetic disease which affects millions of people all over the world, and so far, only four drugs have been approved by FDA but the disease morbidity remains high[2, 4, 13]. Therefore, there is a critical need to study previously unknown pathways contributing to VOE/ACS morbidity in SCD, and how these new pathways can be therapeutically targeted to provide further protection beyond the benefits of currently approved therapies. In severe condition SCD patients develop vaso-occlusive episodes and ACS within couple of days and this accounts for high mortality of SCD patients[13]. As per literature the pathophysiology of SCD includes: HbS polymerization, vaso-occlusion, endothelial dysfunction, and sterile inflammation[2]. Recently, my mentor's (Dr. Sundd) lab has shown that nanogram dose of intravenous LPS administered to SCD but not control mice triggered micro-embolism of pulmonary arteriole bottle-necks (junction of pulmonary arterioles with pulmonary capillaries) by large neutrophil-platelet aggregates[3], which was attenuated by ~50% following inhibition or genetic deletion of P-selectin

from endothelium and platelets[3]. These results supported the phase-2 study of crizanlizumab, which reported ~45.3% reduction in VOE-related hospitalization among SCD patients prophylactically treated P-selectin blocking Ab crizanlizumab (now known as Adakveo®)[35]. However, the remaining adverse events are still a matter of concern for SCD patients and a focus of research for many researchers. This emphasizes the importance to determine alternative approaches to decrease these adverse events. Recently, it has been shown that NETs and circulating NETs contribute to the pathogenesis of SCD[23], but whether they are involved downstream of vaso-occlusion or upstream is still debatable. NETs are released from neutrophils under pro-inflammatory and pro-thrombotic conditions. However, NETs are formed before neutrophil-platelet aggregation or after is still unknown, or NETs primarily contribute to these aggregates is also unknown. I propose that the remaining 50% P-selectin-independent pathophysiology of VOE/ACS involves GSDMD-dependent mechanism leading to generation of intravascular NETs in SCD. My current findings support that these NETs are primarily shed in the liver, which serves as the natural sink for Hb and heme in SCD, then these NETs are carried by the blood to the lung where they promote lung injury.

### 1.3 Hypothesis and Aims of Study

Sickle Cell Disease is a debilitating disease without any cure. VOC remains as the major cause of morbidity face by SCD patients, yet the mechanisms remain unknown. The purpose of this study is to determine the role of cNETs and GSDMD in Sickle Cell Disease. This study is driven by primary hypothesis and three aims mentioned below:

### 1.3.1 Primary Hypothesis

*Liver-derived cNETs arrive in the lung to promote neutrophil-platelet aggregate-enabled pulmonary arteriole micro-embolism in SCD and inhibiting GSDMD activation in neutrophils prevents cNETs generation and development of ACS.*

This hypothesis was tested using the following aims:

**1.3.2 Aim 1: To determine whether erythrocyte-derived damage associated molecular patterns promote neutrophil-platelet aggregates dependent lung vaso-occlusion in SCD mice.**

**1.3.3 Aim 2: To determine whether circulating NETs (cNETs) shed in the liver, travel to the lung to promote P-selectin independent pulmonary vaso-occlusion in SCD mice.**

**1.3.4 Aim 3: To determine whether caspase-4/11-dependent activation of neutrophil GSDMD promotes shedding of cNETs and development of ACS in SCD.**

# 2.0 Materials and Methods

## 2.1.1 Reagents

Alexa Fluor 546 (AF546) rat anti-mouse Ly6G mAb (clone 1A8) and Pacific Blue (PB) anti-mouse Ly6G mAb (clone 1A8) were purchased from BioLegend (San Diego, CA). Fluorescein Isothiocyanate (FITC) dextran (MW 70,000) was purchased from Molecular Probes Inc. (Eugene, OR). Violet 450 (V450) rat-anti mouse CD49b mAb (clone DX5) was purchased from BD Biosciences (San Jose, CA). LDC7559 and BAY-85-8501 were purchased from MedChemExpress (Monmouth Junction, NJ). Pan-caspase inhibitor (Z-VAD-FMK) and Necrosulfonamide (NSA) were purchased from Millipore Sigma (St. Louis, MO). GSK484 was purchased from Cayman Chemical (Ann Arbor, MI). DNase-1 was purchased from Roche (Basel, Switzerland). Oxy-Hemoglobin was prepared from lysed human erythrocytes as described elsewhere49. Hemin was purchased from Frontier Scientific (Logan, UT). VetStarch was purchased from Henry Schein Animal Health (Dublin, OH). Recombinant human lgG1 Fc (rh IgG1 Fc) was purchased from BioCell (West Lebanon, NH, USA). Recombinant tandem P-selectin−glycoprotein ligand−immunoglobulin (TSGL-Ig)1 fusion molecule was provided by Quell Pharma Inc. (Plymouth, MA). N-Acetyl-L-cysteine (NAC) was purchased from Millipore Sigma. Anti-Neutrophil Elastase Ab (ab21595), Rabbit anti-Histone H2A.X mAb (ab124781), and Rabbit anti-citrullinated-Histone H3 Ab (ab5103) were purchased from Abcam (Cambridge, MA). Rabbit anti-neutrophil elastase polyclonal antibody, sytox orange, and sytox green were purchased from Thermo Fisher Scientific (Waltham, MA). Ketamine HCl (100 mg/ml) was purchased from Henry Schein Animal Health (Dublin, OH) and xylazine (20 mg/ml) was purchased from LLOYD

Laboratories (Shenandoah, IA). BD Vacutainer 3.2% sodium citrate blood collection 4.5 ml tubes (cat# 369714), 5 ml polystyrene round-bottom tubes (cat# 352058) and BD PrecisionGlide® needles (cat# 305159) were purchased from BD (Franklin Lakes, NJ).

### 2.1.2 Mice

Male and female (age ~12-16 weeks) Townes SCD mice (SS, homozygous for $Hba^{tm1(HBA)Tow}$, homozygous for $Hbb^{tm2(HBG1,HBB*)Tow}$) and non-sickle control mice (AS, homozygous for $Hba^{tm1(HBA)Tow}$, compound heterozygous for $Hbb^{tm2(HBG1,HBB*)Tow}$/$Hbb^{tm3(HBG1,HBB)Tow}$) were used in this study[43]. Townes sickle SS mice have human α and β-sickle (βS) genes knocked into the locus where mouse α and β genes were knocked out. Townes AS mice are sickle trait mice and thus do not develop SCD. Townes SS and AS mice have been used previously as SCD and control non-sickle mice, respectively [3, 10, 12, 44-47]. Townes SS and AS mice were bred and genotyped in-house. P-selectin-deficient SCD mice (SCD-*Selp-/-*) were generated as described elsewhere[48]. Breeding pairs of Gasdermin-D (GSDMD) knock-out (*Gsdmd-/-*) mice (Stock# 032410) homozygous for Gsdmdem4Fcw allele and the corresponding wild-type (WT) control C57BL/6NJ mice (Stock# 005304) were purchased from Jackson Laboratories (Bar Harbor, ME)[49]. Townes SCD and control mice, SCD-*Selp-/-*, and *Gsdmd-/-* mice were bred and genotyped in-house at the University of Pittsburgh, Division of Laboratory Animal Resources (DLAR) facility. All animal experiments were approved by the Institutional Animal Care and Use Committee at the University of Pittsburgh.

### 2.1.3 Blood collection and Handling

Healthy race matched control human subjects (control) and steady state (not in crisis) SCD (SS or S/$\beta^o$) patient blood was collected via venipuncture in a blue-cap glass BD Vacutainer tube containing sodium citrate (BD Biosciences, Franklin Lakes, NJ) in accordance with the guidelines set by the Institutional Review Board at the University of Pittsburgh. The procedure for blood draw has been described elsewhere in detail[3, 45]. Only non-smokers who were not on chronic transfusion therapy (no transfusion within the last 1 month) were included in the study. Informed written consent was obtained from all the participants in accordance with the Declaration of Helsinki. All blood samples were used within 2 hours of blood draw.

### 2.1.4 Multiphoton Microscopy

Multiphoton microscopy also referred as two-photon laser scanning microscopy or non-linear microscopy enables to visualize sample in three-dimensional imaging with deep penetration, and less photobleaching and phototoxicity of the live specimens in comparison to conventional confocal microscope[50, 51]. Multiphoton microscope uses longer wavelength laser, which allows to penetrate more deeply into live specimens without tissue damage[50, 51]. Principle of multiphoton microscope is based on a non-linear principle where two or more photons are simultaneously excited, this excitation results in emission of a fluorescence photon[50, 51].

We have used AAA Nikon Multiphoton microscope located in Center for Biologic Imaging (CBI) at University of Pittsburgh. This upright microscope comes with a femtosecond infrared pulse laser with a wide range from 700 nm to 1100 nm, equipped with an apochromatic (APO) large working distance (LWD) 25x water immersion objective with 1.1 Numeric Aperture (NA).

This microscope holds the capacity to provide high resolution images (512 X 512 pixels) with up to 0.5 µm lateral resolution, with 8 times zoom capability, and 30 fps image acquisition speed.

Figure 5


**Figure 5: Nikon AAA Multiphoton Excitation microscope located in Center for Biologic Imaging at University of Pittsburgh.**

### 2.1.5 Experimental Design of qFILM studies

Quantitative fluorescence intravital lung microscopy (qFILM) has been used widely for in-vivo assessment of pulmonary vaso-occlusion in SCD mice[3, 12, 45, 48, 52]. In the current study,

qFILM was used to assess pulmonary vaso-occlusion and detect neutrophil extracellular traps (NETs) in the intact lung microcirculation of live SCD, Control, SCD-*Selp-/-*, *Gsdmd-/-* and WT mice following intravenous (IV) challenge with saline, oxy-hemoglobin (oxy-Hb) or hemin with or without pretreatment with GSDMD inhibitors LDC7559[25] or NSA[53] or the pan-caspase inhibitor Z-VAD-FMK[25, 54]. The qFILM experimental setup and approach has been described elsewhere in detail[3, 52] and is also mentioned in Sundd lab protocols Appendix section A1.1. Briefly, mice were IV administered via tail vein with 80 µl of either: 1) saline or vehicle, 2) 10 µmole/kg oxy-Hb, 3) 20 µmole/kg hemin, 4) 0.004 µmol/kg Z-VAD-FMK or 10 mg/kg LDC7559 or 20 mg/kg NSA, 30 min prior to 10 µmole/kg oxy-Hb. Approximately 2-2.5 hours following IV administration, qFILM was conducted with a Nikon multi-photon-excitation fluorescence microscope using an excitation wavelength of 850 nm and an APO LWD 25x water immersion objective with 1.1 NA. Time-series of 2D qFILM images were collected at ~15 frames per second (fps) using a resonant scanner. Each field of view (FOV) was 256 µm x 256 µm (~65,536 µm2) with a resolution of ~0.5 µm per pixel in the x-y plane.

### 2.1.6 Experimental Design of qLIM studies

Recently, we developed quantitative liver intravital microscopy (qLIM) to study liver pathophysiology in SCD mice[44, 55, 56]. In the current study, qLIM was used to assess vaso-occlusion and detect NETs generation in the intact liver microcirculation of live mice. qLIM was conducted on same strains of mice as described under qFILM studies. The qLIM experimental setup has been described previously in detail[44, 55, 56]. Briefly, mice were IV administered via tail vein with 80 µl of either: 1) saline, 2) 10 µmole/kg oxy-Hb, 3) 0.004 µmol/kg Z-VAD-FMK or 10 mg/kg LDC7559 or 20 mg/kg NSA, 30 min prior to 10 µmole/kg oxy-Hb. Approximately 2-

2.5 hours following IV administration, qLIM was conducted with a Nikon multi-photon-excitation fluorescence microscope using an excitation wavelength of 850 nm and an APO LWD 25x water immersion objective with 1.1 NA. Time-series of 2D qFILM images were collected at ~15 frames per second (fps) using a resonant scanner. Each field of view (FOV) was 256 μm x 256 μm (~65,536 $\mu m^2$) with a resolution of ~0.5 μm per pixel in the x-y plane. Detail explanation of qLIM imaging strategy and set up in mentioned in Appendix section A1.2.

### 2.1.7 Experimental Design of qKIM studies

We have also developed quantitative Kidney Intravital Microscopy (qKIM) approach, which enables in-vivo visualization of blood flow, blood cell trafficking and detection of NETs in the intact kidney of a SCD mice. qKIM uses an experimental set-up and approach identical to the one used for qLIM imaging with few modifications. Briefly, control and SCD mice were intravenously (IV) injected via tail vein with 10 μmole/kg oxy-Hb, anesthetized, and prepared for intravital imaging as described under qLIM experimental approach. Detail explanation of qKIM imaging strategy and set up in mentioned in Appendix section A1.3.

### 2.1.8 Strategy to halt blood flow from liver to lung in mice

As shown in Figure 6, blood enters the liver through the hepatic artery and portal vein, travels through the liver sinusoids, and then exits through the multiple short branches of hepatic vein that drain into the Inferior-Vena-Cava (IVC). IVC carries blood to the right-heart and lung. In mice, the hepatic vein branches are short in length, primarily embedded inside the liver tissue and drain individually into IVC, thus making it hard to clamp all of them simultaneously without

causing trauma. Therefore, the blood flow through the liver to lung was stopped by simultaneously clamping the hepatic artery and portal vein (Figure 6) using a silk suture ligature. For qFILM studies, the arrival of cNETs in the lung was confirmed using qFILM, then the hepatic artery and portal vein were simultaneously clamped to stop the blood outflow from the liver into the IVC, and the effect on cNETs arrival into the lung was again assessed using qFILM in the same mouse.

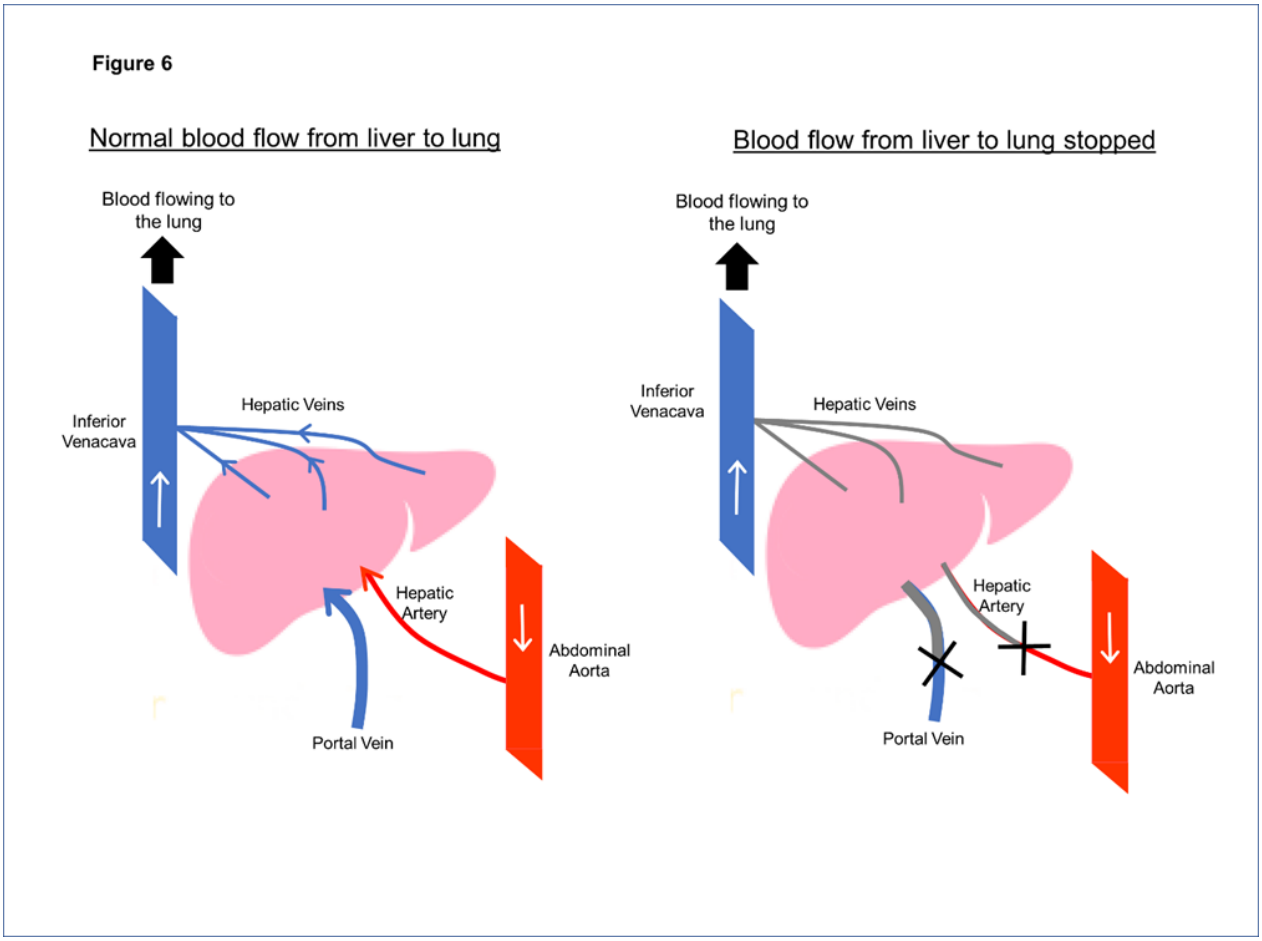


**Figure 6: Strategy to halt blood flow from liver to lung.**

**Shows the schematic to understand the normal blood from liver to lung (left), blood from liver travels from inferior vena cava to right side of heart and then to lung. Right side image shows that after blocking hepatic artery and portal vein, blood flow from liver to lung is stopped.**

### 2.1.9 Image processing and analysis

Time series of qFILM 2D-images were processed and analyzed using Nikon's NIS-Elements software (Nikon Instruments; Tokyo, Japan) as described elsewhere[3, 45]. First, image subtraction was performed to remove autofluorescence between channels. Second, signal to noise ratio was improved by using median filter, smoothing and denoising functions. Third, each channel was pseudo-colored as following: microcirculation as purple, neutrophils primarily as red or blue in some instances, platelets as green, extracellular DNA as green, NE as red and histones as red. Pulmonary vaso-occlusions were defined using the following criteria described previously[3, 12, 45]. Briefly, a pulmonary vaso-occlusion was defined as a neutrophil-platelet aggregate (> 500 $\mu m^2$ in size) occluding a pulmonary arteriole (> 20 μm ID) or the arteriolar bottleneck (junction between a pulmonary arteriole and the downstream pulmonary capillaries), leading to impairment of arteriolar blood flow. Pulmonary vaso-occlusions were quantified and compared between treatment groups using the following four parameters as described previously[3, 12, 45]: 1) Average number of pulmonary vaso-occlusions per FOV, 2) Percent FOVs with at least one pulmonary vaso-occlusion, 3) Average number of large pulmonary vaso-occlusions (size > 1000 $\mu m^2$) per FOV, and 4) Neutrophil rich or platelet rich PVOs. Based on previous studies [10, 57, 58], a NET in the qFILM image was identified using one of the following criteria: 1) a strand of extracellular DNA colocalizing with NE or citrullinated-histones (H3-cit); 2) a strand of extracellular DNA either colocalizing or within ~ 5 μm proximity of one or more neutrophil (Ly6G-staining). Number of NETs were counted in each FOV, and average number of NETs per FOV compared between treatment groups. Circulating NETs (cNETs) were identified as micro-fragments of extracellular DNA flowing into the lung through the pulmonary arteriole. NIS-Elements software was used to quantify the number of cNETs entering each FOV over a 30 second

duration, to estimate average number of cNETs entering per FOV per minute (#cNETs/FOV/min), which was compared between treatment groups.

Time series of qLIM 2D-images were processed and analyzed using Nikon's NIS-Elements software, each channel was pseudo-colored (microcirculation as violet, neutrophils as red, and extracellular DNA as green) and NETs in the liver were quantified using the same strategy as the one used for qFILM image processing. Average number of NETs per FOV was quantified and compared between treatment groups. Vaso-occlusion in the liver was quantified as percent occluded area in each FOV (~65,536 $\mu m^2$) using the threshold binary function in NIS-Elements as described recently[59] ,and the mean percent occluded area per FOV was compared between treatment groups.

Time series of qKIM 2D-images were processed and analyzed using a strategy similar to the one used for qLIM.

### 2.1.10 Imaging flow cytometry of SCD mice plasma

SCD or SCD-*Selp-/-* mice were intravenously administered with 10 µmole/kg Oxy-Hb ± 10 mg/kg LDC7559. After 3 hours, mice were sacrificed, blood was drawn via inferior vena cava into tubes containing 3.2% sodium citrate (0.105M) in a ratio of 1:10 (sodium citrate: blood) and processed to generate platelet-poor-plasma (PPP) as described elsewhere[45]. For each treatment group, 30 µl of PPP was mixed with 70 µl of physiological saline, and incubated with sytox green, AF546-conjugated anti-NE Ab, and AF647-conjugated-anti-H3cit or H2A.X Ab for in situ staining of extracellular DNA, NE, and histones, respectively. Image Flow Cytometry was conducted using Image Stream equipment Amnis Imagestream and data was analyzed using

IDEAS application software version 6.2.187.0. Detail explanation of Imaging flow cytometry imaging strategy and set up in mentioned in Appendix section A1.4.

### 2.1.11 Imaging flow cytometry of SCD patient plasma

SCD patient blood was split into following treatment groups: 1) untreated or incubated for 15 min with 2) 20 μM hemin, 3) 20 μM hemin + 10 μM LDC7559, 4) 20 μM hemin + 20 μM caspase-4 inhibitor LEVD-CHO, and 5) 20 μM hemin + 20 μM NAC. Following incubation, blood samples were processed to generate platelet-poor-plasma (PPP) as described elsewhere[45]. For each treatment group, 30 μl of PPP was mixed with 70 μl of physiological saline, and incubated with sytox green, AF546-conjugated anti-NE Ab, and AF647-conjugated-anti-H3cit or H2A.X Ab for in situ staining of extracellular DNA, NE, and histones, respectively. Image Flow Cytometry was conducted using Image Stream equipment Amnis Imagestream and data was analyzed using IDEAS application software version 6.2.187.0. Detail explanation of Imaging flow cytometry imaging strategy and set up in mentioned in Appendix section A1.4.

### 2.1.12 Immunofluorescence microscopy of mouse liver sections

The method of liver confocal imaging is described elsewhere[56]. Briefly, SS and control mouse were intravenously injected with 10 μmole/kg oxy-Hb and after 3 hours of waiting liver was isolated from them. Freshly obtained unfixed liver tissue was sectioned and picked up on a glass slide. Antibody staining was performed on unfixed tissue as described here6. Coverslips were stained with Pacific Blue Ly6G for neutrophils staining, sytox green for extracellular DNA staining, and AF546-conjugated anti-NE antibody present in neutrophil. Images were captured

using a Nikon spectral confocal microscope. NETs were identified as triple-positive for NETs markers (neutrophil elastase), extracellular DNA, and neutrophil. Confocal images were processed and analyzed using Nikon's NIS-Elements software, neutrophil channel was pseudo-colored in white for better visualization, and extracellular DNA is in green and neutrophil elastase is in red.

Figure 7

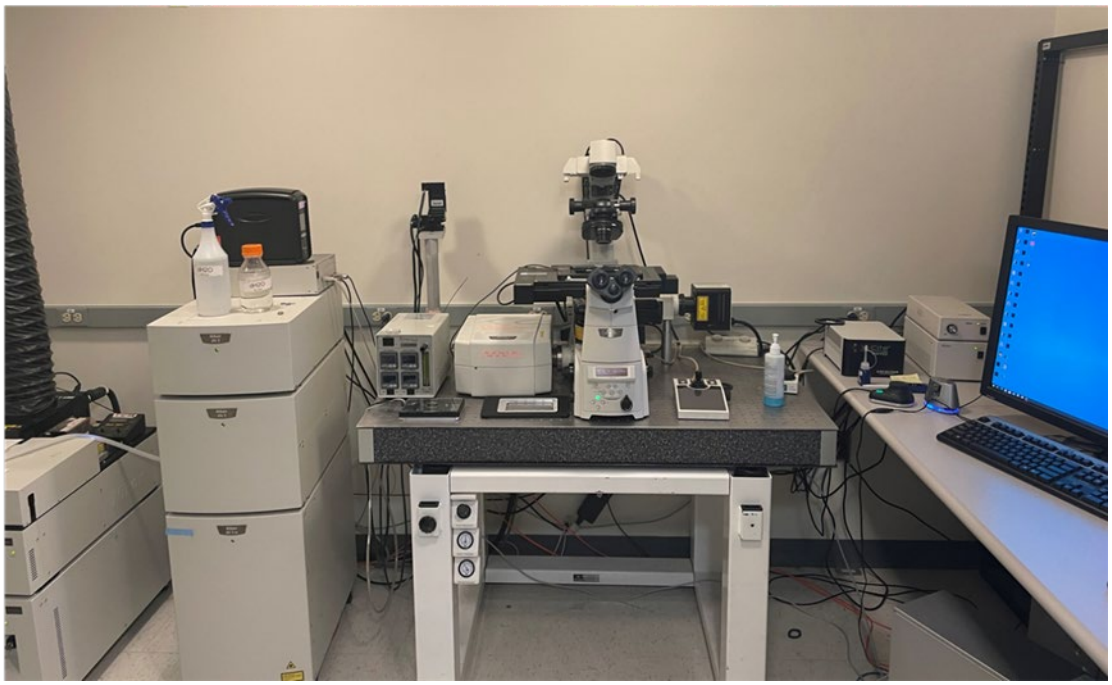

**Figure 7: Nikon A1 Confocal microsocpe located at the Center for Biologic Imaging at the University of Pittsburgh.**

### 2.1.13 Oxy-hemoglobin and hemin treatment

Oxy-hemoglobin (oxy-Hb) preparation is described in detail somewhere else[12, 60]. In brief, oxy-hemoglobin was prepared from expired, leukocyte-reduced red blood cell units from healthy human donors. These red blood cell units were provided by the Institute for Transfusion Medicine (ITxM, Pittsburgh, PA). Red blood cells were centrifuge with phosphate-buffered saline

(PBS) at 5000g for 10 min to obtain a packed cell pellet[12]. Further, cells were lysed hypotonically by resuspension in distilled water (3:1, v/v) and mixing for 30 min at room temperature1. Cell debris was removed by centrifugation at 25,000g for 30 min. The supernatant was dialyzed against PBS, and the final product stored at −80°C[12]. After multiple titrations, a non-lethal dose of intravenous Oxy-Hb i.e., 10 µmole/kg was established for intravital microscopy studies. Vet-starch or saline is used as a control for oxy-Hb studies. Hemin was purchased from Frontier Scientific (Logan, UT). After multiple titrations, a non-lethal dose of intravenous hemin i.e., 20 µmole/kg was established for intravital microscopy studies. Saline is used as a control for hemin studies.

### 2.1.14 TSGL-Ig treatment

Recombinant tandem P-selectin−glycoprotein ligand−immunoglobulin (TSGL-Ig) fusion molecule was provided by Quell Pharma Inc. (Plymouth, MA)[12]. TSGL-Ig was produced in HEK293 cells after transfection with plasmids encoding human FucT-VII cDNA and TSGL-Ig, essentially as described elsewhere[61]. Secreted TSGL-Ig was purified from conditioned medium using protein A−Sepharose, and P-selectin binding kinetics were subsequently confirmed via multiple Octet binding assays[12]. Townes-SS (SCD) mice or control mice were administered intravenous (IV) with 10 µmol/kg oxy-Hb or 80 µL VetStarch or 10µmol/kg oxy-Hb with 100 µg/mouse of TSGL-Ig or 10 µmol/kg oxy-Hb with 100 µg/mouse of recombinant human IgG1-Fc (rh IgG1-Fc)1. Two hours later, mice were IV administered fluorescein isothiocyanate (FITC) −dextran, AlexaFluor546 (AF546)-conjugated anti-mouse Ly6G mAb and Violet450 (V450)-conjugated anti-mouse CD49b mAb for visualization of blood vessels and in vivo staining of neutrophils and platelets, respectively[12]. Lung microcirculation in live mice was assessed using

the qFILM imaging approach described previously in detail[3, 12, 45, 59]. Recombinant human lgG1 Fc (rh IgG1 Fc) was purchased from BioCell (West Lebanon, NH, USA). IgG1-Fc is used as a negative control in these experiments[12].

### 2.1.15 DNase-1 treatment

DNase-1 was purchased from Roche (Basel, Switzerland). SCD mice were administrated IV with 10mg/kg of DNase-1[10] just 30 min prior to IV 10μmol/kg oxy-Hb. As discussed above in section 2.0.5 in detail, qFILM was performed on SCD mice administrated with DNase-1 and oxy-Hb. Mice were IV administered fluorescein isothiocyanate (FITC) −dextran, AlexaFluor546 (AF546)-conjugated anti-mouse Ly6G mAb and Violet450 (V450)-conjugated anti-mouse CD49b mAb for visualization of blood vessels and in vivo staining of neutrophils and platelets, respectively. Lung microcirculation was accessed using the qFILM imaging approach. For visualization, and analysis of NETs and circulating NETs; Pacific Blue Ly6G Ab, sytox orange, and FITC dextran was IV administrated for in-vivo staining of neutrophils, extracellular DNA, and blood vessels, respectively.

### 2.1.16 NETs inhibition by PAD-4 inhibitor

Protein arginine deiminase- 4 (PAD-4) is an enzyme present in neutrophils which is responsible for the conversion of arginine to citrulline[62]. Activation of PAD-4 in presence of calcium leads to histone citrullination, and NETs generation[62]. GSK484 act as a reversible PAD-4 inhibitor in a dose dependent manner[62]. GSK484 was purchased from Cayman Chemical (Ann Arbor, MI). 10mg/kg dose of GSK484 has been shown to effective in inhibiting PAD-4 activity,

and there by inhibiting NETs generation[62]. SCD mice were administrated IV with 10mg/kg GSK484 just 30 min prior to IV 10µmol/kg oxy-Hb. As discussed above in section 2.0.5 in detail, qFILM was performed on SCD mice administrated with GSK484 and Oxy-Hb. Mice were IV administered fluorescein isothiocyanate (FITC)−dextran, AlexaFluor546 (AF546)-conjugated anti-mouse Ly6G mAb and Violet450 (V450)-conjugated anti-mouse CD49b mAb for visualization of blood vessels and in vivo staining of neutrophils and platelets, respectively. Lung microcirculation was accessed using the qFILM imaging approach. For visualization, and analysis of NETs and circulating NETs; Pacific Blue Ly6G Ab, sytox orange, and FITC dextran was IV administrated for in-vivo staining of neutrophils, extracellular DNA, and blood vessels, respectively.

### 2.1.17 Treatment of SCD mice with Gasdermin-D inhibitors

As discussed in section 1.1.5, Gasdermin D (GSDMD) has been shown to play an important role in NETs generation. Therefore, specific GSDMD inhibitors viz. LDC7559[25] and NSA[53] (necrosulfonamide) are used for this study. LDC7559 at 10 mg/kg is effective in inhibiting GSDMD and therefore, this dose is used for this study[25]. NSA 20 mg/kg is effective in inhibiting GSDMD and therefore, this dose is used for this study[53]. LDC7559 was purchased from MedChemExpress (Monmouth Junction, NJ), and Necrosulfonamide (NSA) was purchased from Millipore Sigma (St. Louis, MO). SCD mice were administrated IV with 10 mg/kg LDC7559 or 20 mg/kg NSA just 30 min prior to IV 10µmol/kg oxy-Hb. As discussed above in section 2.0.5 in detail, qFILM was performed on SCD mice administrated with LDC7559 and oxy-Hb or NSA and oxy-Hb. Mice were IV administered fluorescein isothiocyanate (FITC) −dextran, AlexaFluor546 (AF546)-conjugated anti-mouse Ly6G mAb and Violet450 (V450)-conjugated anti-mouse CD49b

mAb for visualization of blood vessels and in vivo staining of neutrophils and platelets, respectively. Lung microcirculation was accessed using the qFILM imaging approach. For visualization, and analysis of NETs and circulating NETs; Pacific Blue Ly6G Ab, sytox orange, and FITC dextran was IV administrated for in-vivo staining of neutrophils, extracellular DNA, and blood vessels, respectively.

### 2.1.18 Treatment of SCD mice with Neutrophil Elastase inhibitor

It has been shown that cytosolic release of neutrophil elastase enables GSDMD dependent generation of NETs[24]. Hence, specific neutrophil elastase inhibitor (NEi) i.e., BAY-85-8501[25] is used for this study. NEi at 10 mg/kg is effective in inhibiting NETs generation and therefore, this dose has been used for this study[25]. BAY-85-8501 was purchased from MedChemExpress (Monmouth Junction, NJ). SCD mice were administrated IV with 10 mg/kg NEi just 30 min prior to IV 10µmol/kg oxy-Hb. As discussed above in section 2.0.5 in detail, qFILM was performed on SCD mice administrated with NEi and Oxy-Hb. Mice were IV administered fluorescein isothiocyanate (FITC) −dextran, AlexaFluor546 (AF546)-conjugated anti-mouse Ly6G mAb and Violet450 (V450)-conjugated anti-mouse CD49b mAb for visualization of blood vessels and in vivo staining of neutrophils and platelets, respectively. Lung microcirculation was accessed using the qFILM imaging approach. For visualization, and analysis of NETs and circulating NETs; Pacific Blue Ly6G Ab, sytox orange, and FITC dextran was IV administrated for in-vivo staining of neutrophils, extracellular DNA, and blood vessels, respectively.

### 2.1.19 Treatment of SCD mice with Pan-caspase inhibitor

Pan-caspase inhibitor (Z-VAD-FMK)[25] was purchased from Millipore Sigma (St. Louis, MO). Pan-caspase inhibitor at 0.004 μmol/kg has been shown to be effective in reducing neutrophil-platelet aggregation and pulmonary vaso-occlusion, hence this dose is used for this study[45]. SCD mice were administrated IV with 0.004 μmol/kg Z-VAD-FMK just 30 min prior to IV 10μmol/kg oxy-Hb. As discussed above in section 2.0.5 in detail, qFILM was performed on SCD mice administrated with Z-VAD-FMK and Oxy-Hb. Mice were IV administered fluorescein isothiocyanate (FITC) −dextran, AlexaFluor546 (AF546)-conjugated anti-mouse Ly6G mAb and Violet450 (V450)-conjugated anti-mouse CD49b mAb for visualization of blood vessels and in vivo staining of neutrophils and platelets, respectively. Lung microcirculation was accessed using the qFILM imaging approach. For visualization, and analysis of NETs and circulating NETs; Pacific Blue Ly6G Ab, sytox orange, and FITC dextran was IV administrated for in-vivo staining of neutrophils, extracellular DNA, and blood vessels, respectively.

### 2.1.20 Statistical Analysis

The average number of pulmonary vaso-occlusions per FOV, the average number of pulmonary vaso-occlusions (per FOV) with area > 1000 $\mu m^2$, average number of NETs per FOV, average number of cNETS per FOV per minute, average number of cNETs per μL of plasma, and mean percent occluded area per FOV were compared between groups using the unpaired Student's t test with Bonferroni correction when comparing more than two groups. The percent FOVs with pulmonary vaso-occlusions were compared between groups using four-fold table analysis with $\chi 2$

statistics as described elsewhere[3, 12, 45]. Error bars shown represent mean ± standard error (SE). A p value less than 0.05 was considered as significant.

## 3.0 AIM-1: To determine whether erythrocyte-derived damage associated molecular patterns promote neutrophil-platelet aggregates dependent lung vaso-occlusion in SCD mice.

*Rationale:* Intravascular hemolysis promotes the release of erythrocyte-derived damage associated molecular patterns (eDAMPs) such as oxy-hemoglobin and hemin. Therefore, IV oxy-Hb and hemin was used to determine whether eDAMPs promotes neutrophil-platelets aggregates dependent lung vaso-occlusion in SCD mice. qFILM imaging technique was used to visualize the blood circulation and PVOs in the lung micro-circulation of live control or SCD mice.

*Hypothesis:* Oxy-Hb and hemin promotes neutrophil-platelet aggregates dependent lung vaso-occlusion in SCD mice.

## 3.1 Results

### 3.1.1 eDAMPs trigger statistically higher neutrophil-platelet aggregates and pulmonary vaso-occlusion in SCD mice than control mice.

Quantitative fluorescence intravital lung microscopy (qFILM) has been used extensively for in-vivo assessment of pulmonary vaso-occlusion in control or SCD mice[3, 12, 45]. In the current study, qFILM was used to assess the presence or absence of neutrophil-platelets aggregates and pulmonary vaso-occlusion in the intact lung microcirculation of live control and SCD mice following intravenous (IV) challenge with saline or oxy-Hb. The qFILM experimental setup and approach has been described elsewhere in detail[3, 12, 45], and is also mentioned in section 2.1.5. Briefly as shown in Figure 8 A, mice were IV administered via tail vein with 10 μmole/kg oxy-Hb. Approximately 2-2.5 hours following IV challenge, qFILM was conducted with a Nikon multi-photon-excitation fluorescence microscope using an excitation wavelength of 850 nm and an APO LWD 25x water immersion objective with 1.1 NA. Time-series of 2D qFILM images were collected at ~15 frames per second (fps) using a resonant scanner. Each field of view (FOV) was 256 μm x 256 μm (~65,536 $\mu m^2$) with a resolution of ~0.5 μm per pixel in the x-y plane. A snapshot of control and SCD mice administered IV oxy-Hb is shown in Figure 8 B and C, and it reveals that more neutrophil-platelet aggregates were present in the pulmonary arteriole-bottleneck of a SCD mouse given oxy-Hb in the lung micro-circulation. However, there is absence of neutrophil-platelet aggregates in the lung micro-circulation of a control mouse given oxy-Hb. The aggregates composed of platelets (green) and neutrophils (red) can be seen sequestered in the arteriole of SCD mice leading to the onset of pulmonary vaso-occlusion (PVO). Quantitative analysis of several time-series of qFILM images reveled that the total average number of PVOs

per FOV present in SCD mice given IV oxy-Hb is almost twice than control mice given oxy-Hb (Figure 8 D). Percent field of views (FOVs) with PVOs shows that about 70% of the total FOVs contain PVOs in SCD mice given Oxy-Hb, which is statistically significant and higher than control mice given Oxy-Hb (Figure 8 E). To quantify how many of these PVOs are bigger in size, we quantified total of number of FOVs having PVOs greater than 1000 $\mu m^2$. This estimation shows that PVOs greater than 1000 $\mu m^2$ were two-times more numerous in SCD than control mice given IV oxy-Hb (Figure 8 F). Finally, we distributed the PVOs as per most prominent cells present in them i.e., either neutrophil-rich or platelet-rich (Figure 8 G). These in-vivo qFILM studies suggest that neutrophil-platelet aggregates were significantly more frequent and higher in the lung of SCD mice than control mice given IV oxy-Hb.

## Figure 8

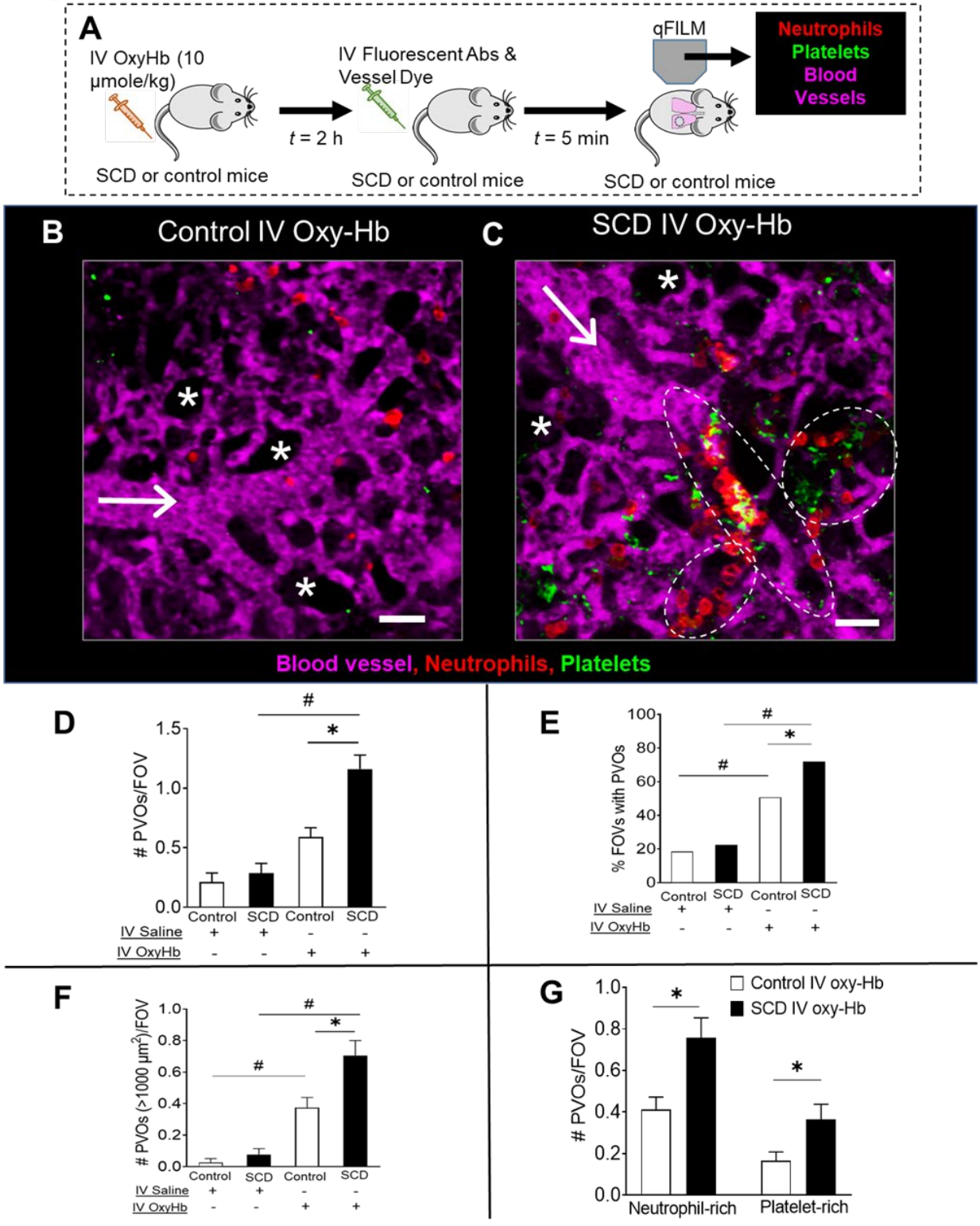


**Figure 8: IV oxy-Hb induces neutrophil-platelet aggregates formation in the lung of SCD mice.**

**(A) shows the schematic of qFILM imaging approach. (B) & (C) are the representative images obtained from qFILM after administered of 10 µmole/kg oxy-Hb to control and SCD mice, respectively. * Shows the air alveoli and arrow shows the direction of blood flow. Dotted eclipses are drawn around neutrophil-platelet aggregates and scale bar 20 µm. (D) Average number of pulmonary vaso-occlusion per field of view; SCD IV oxy-Hb mice had significantly higher PVOs/FOV in comparison to control mice IV oxy-Hb, also SCD IV oxy-Hb had significantly higher PVOs/FOV in comparison to SCD saline. Control mice IV saline (n = 3 mice; FOVs 38), SCD IV saline (n = 4 mice; FOVs 49), Control IV oxy-Hb (n = 5 mice; FOVs 71), SCD IV oxy-Hb (n = 5 mice; FOVs 75). Control IV saline comparison to SCD IV saline, and Control IV oxy-Hb comparison to SS oxy-Hb is denoted by * whereas Control IV saline comparison to Control IV oxy-Hb, and SCD IV saline comparison to SCD IV oxy-Hb is denoted as #. Comparisons were done using t-test with Bonferroni correction between control mice vs. SCD mice (significance indicated as *), saline vs. IV oxy-Hb (significance indicated as #), p-value < 0.05 considered as significant and data represent mean ± SE. (E) Shows percent FOVs with PVOs in SCD and control mice administrated with IV saline or IV 10 µmole/kg oxy-Hb. Compared using 4-fold table analyses with Bonferroni $\chi 2$ statistics, $p < 0.05$ significance level. (F) Average number of PVOs per FOV with area greater than 1000 $\mu m^2$. Compared using t-test with Bonferroni correction, $p < 0.05$ significance level and data represent mean ± SE. (G) Average number of PVOs per FOV, in which PVOs are characterized as per more neutrophils or more platelets. Statistically higher neutrophils PVOs/FOV were present in SCD IV oxy-Hb than Control IV oxy-Hb, similarly higher platelets PVOs/FOV were present in SCD IV oxy-Hb than Control IV oxy-Hb.**

Like results shown for IV oxy-Hb, we have also used a hemin-infusion model to perform the same set of experiments and analysis. In the current study, qFILM was used to assess the presence or absence of neutrophil-platelets aggregates and pulmonary vaso-occlusion in the intact lung microcirculation of live control and SCD mice following intravenous (IV) challenge with saline or hemin. The qFILM experimental setup and approach has been described elsewhere in detail[3, 12, 45] and is also presented in section 2.1.5. Briefly as shown in Figure 9 A, mice were IV administered via tail vein with 20 μmole/kg hemin. Approximately 2-2.5 hours following IV challenge, qFILM was conducted with a Nikon multi-photon-excitation fluorescence microscope. A snapshot of control and SCD mice administrated with IV hemin is shown in Figure 9 B and C, and it reveals that more neutrophil-platelet aggregates were present in the pulmonary arteriole bottleneck of a SCD mouse given hemin in the lung micro-circulation. However, there was absence of neutrophil-platelet aggregates in the lung micro-circulation of a control mouse given hemin. The aggregates were composed of platelets (green) and neutrophils (red), sequestered in the arteriole of a SCD mice leading to the onset of pulmonary vaso-occlusion (PVO) in SCD mice. Quantitative analysis of several time-series of qFILM images reveled that the total average number of PVOs present in SCD mice given hemin is almost twice than control mice given hemin (Figure 9 D). Percent field of views (FOVs) with PVOs showed about 80% of the total FOVs contain PVOs in SCD mice given hemin, which was statistically significant and higher than control mice given hemin (Figure 9 E). To quantify how many of these PVOs are bigger in size, we quantified total of number of FOVs having PVOs greater than 1000 $\mu m^2$. This estimation showed that PVOs greater than 1000 μm2 were two-times more numerous in SCD mice than control mice given IV hemin (Figure 9 F). Finally, we distinguished the PVOs as per most prominent cells present in them i.e., either neutrophil-rich or platelet-rich (Figure 9 G). These in-vivo qFILM studies suggest

that neutrophil-platelet aggregate-dependent PVOs were significantly more in SCD mice than control mice given IV hemin.

## Figure 9

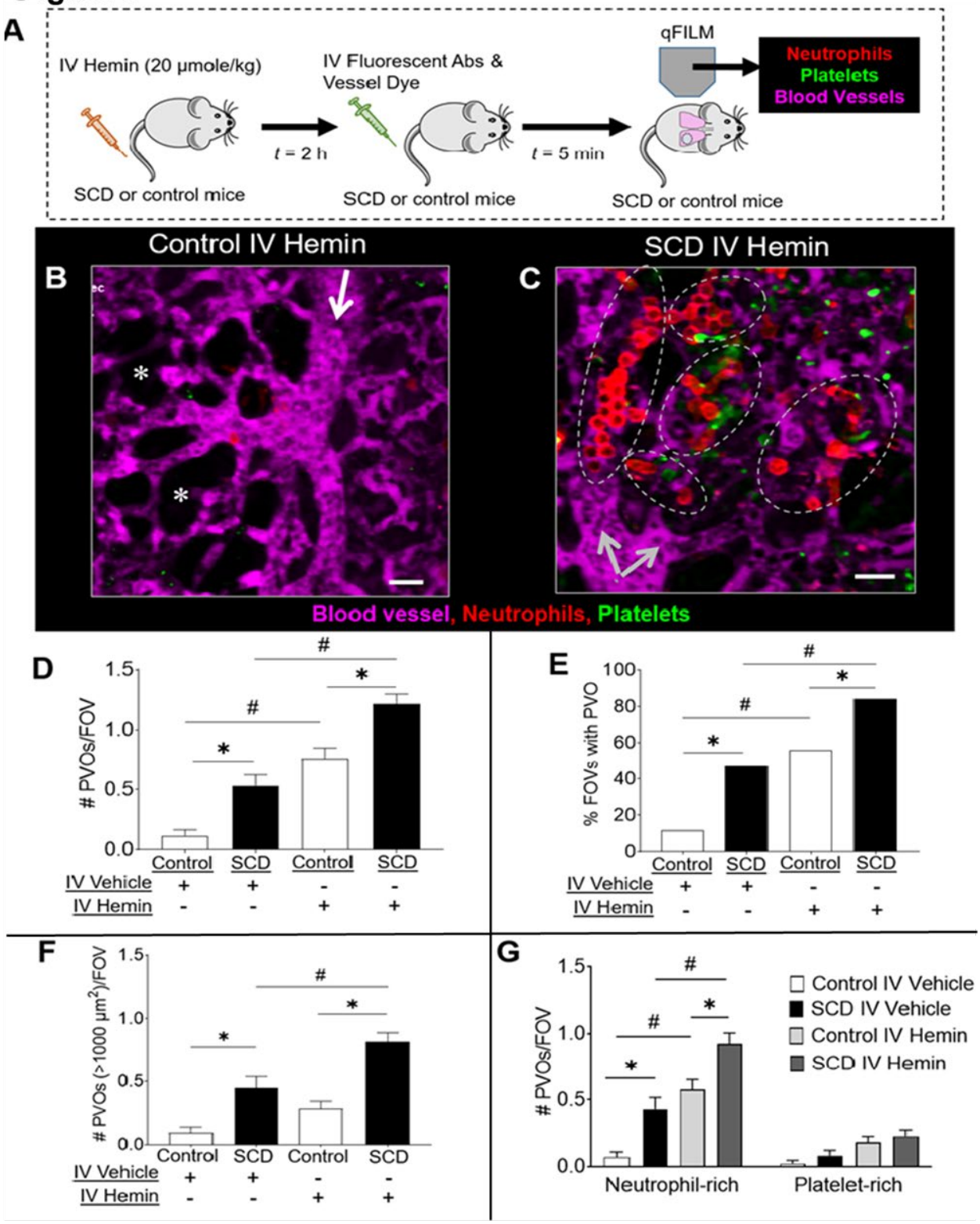


**Figure 9: IV hemin induces neutrophil-platelet aggregate formation in the lung of a SCD mice.**

**(A) Shows the schematic of qFILM imaging approach. (B) & (C) are the representative images obtained from qFILM after IV challenge of 20 μmole/kg hemin to control and SCD mice, respectively. * Shows the air alveoli and arrow shows the direction of blood flow. Dotted eclipses are drawn around neutrophil-platelet aggregates and scale bar 20 μm. (D) Average number of pulmonary vaso-occlusion per field of view; SCD IV hemin mice had significantly higher PVOs/FOV in comparison to Control IV hemin, also SCD IV hemin had significantly higher PVOs/FOV in comparison to SCD IV vehicle. Control IV vehicle (n = 3 mice; FOVs 43), SCD IV vehicle (n = 3 mice; FOVs 44), Control IV hemin (n = 5 mice; FOVs 77), SCD IV hemin (n = 5 mice; FOVs 88). Control IV vehicle comparison to SCD IV vehicle, and Control IV hemin comparison to SCD IV hemin is denoted by * whereas Control IV vehicle comparison to Control IV hemin, and SCD IV vehicle comparison to SCD IV hemin is denoted as #. Comparisons were done using t-test with Bonferroni correction between control mice vs. SCD mice (significance indicated as *), saline vs. IV oxy-Hb (significance indicated as #), p-value < 0.05 considered as significant and data represent mean ± SE. (E) Percent FOVs with PVOs in SCD and control mice administrated with IV saline or IV 20 μmole/kg hemin. Compared using 4-fold table analyses with Bonferroni $\chi 2$ statistics, $p < 0.05$ significance level. (F) Average number of PVOs per FOV with area greater than 1000 $\mu m^2$. Compared using t-test with Bonferroni correction, $p < 0.05$ significance level and data represent mean ± SE. (G) Average number of PVOs per FOV, in which PVOs were characterized as per more neutrophils or more platelets. Control IV vehicle comparison to SCD IV vehicle, and Control IV hemin comparison to SCD IV hemin is denoted by * whereas Control IV vehicle comparison to Control IV hemin, and SCD IV vehicle comparison to SCD IV hemin is denoted as #. Comparisons are done using t-test with Bonferroni correction between control mice vs. SCD mice (significance indicated as *), saline vs. IV oxy-Hb (significance indicated as #), p-value < 0.05 considered as significant and data represent mean ± SE.**

### 3.1.2 TSGL-Ig prevents lung vaso-occlusion in SCD mice.

*Note:* Result of this section was previously published as: Vats R, Tutuncuoglu E, Pradhan-Sundd T, Tejero J, Shaw GD, and Sundd P. Tandem P-selectin glycoprotein ligand immunoglobulin prevents lung vaso-occlusion in sickle cell disease mice. Exp Hematol. 2020; 84:1-6 e[12].

Here we have used quantitative fluorescence intravital lung microscopy (qFILM) to illustrate that tandem P-selectin−glycoprotein ligand−immunoglobulin (TSGL-Ig) fusion molecule containing four P-selectin binding sites, significantly attenuated intravenous (IV) oxy-hemoglobin triggered lung vaso-occlusion in SCD mice[12]. These findings highlight the therapeutic potential of TSGL-Ig in preventing VOE and ACS in SCD[12]. TSGL-Ig is a recombinant fusion protein that carries two P-selectin sulfated glycopeptide-binding domains in a tandem configuration on a single polypeptide chain[12]. Two such polypeptide chains are fused to an inactivated Fc domain of human IgG1, resulting in a dimer with four P-selectin binding sites per molecule of TSGL-Ig[12]. A nonlethal dose of intravenous oxy-Hb (10 μmole/kg) was established after multiple titrations and administered IV to SCD mice to trigger VOE. Based on previous studies[63], intravenous VetStarch was used as a control (vehicle) to account for the changes in volume and viscosity caused by intravenous oxy-Hb administration. As illustrated in the experimental scheme (Figure 10 A) and described in section 2.1.14, SCD mice were administered IV with 10 μmole/kg oxy-Hb or 80 μl VetStarch or 10 μmole/kg oxy-Hb with 100 μg/mouse of TSGL-Ig or 10 μmole/kg oxy-Hb with 100 μg/mouse of recombinant human IgG1-Fc (rh IgG1-Fc). Two hours later, mice were IV administered fluorescein isothiocyanate (FITC)−dextran, AlexaFluor546 (AF546)-conjugated anti-mouse Ly6G mAb and Violet450 (V450)-conjugated anti-mouse CD49b mAb for visualization of blood vessels and in vivo staining

of neutrophils and platelets, respectively. Lung microcirculation in live mice was assessed using the qFILM imaging approach described previously in detail[3, 12, 45]. A snapshot of SCD mice challenged with IV oxy-Hb as shown in Figure 10 B revealed occlusion of arteriolar bottleneck by neutrophil-platelet aggregates in the lung micro-circulation. However, there was absence of neutrophil-platelet aggregates in the lung micro-circulation of a SCD mouse given Vet-starch (control), Figure 10 C[12]. Not only that, when SCD mice was challenged with IV oxy-Hb and TSGL-Ig, there was absence of neutrophil-platelet aggregates in the lung micro-circulation, figure 10 D. Figure 10 E, showed aggregates of neutrophil-platelet in lung micro-circulation of a SCD mouse challenged with IV oxy-Hb and IgG1-Fc, which depicts no effect of IgG1-Fc on lung vaso-occlusion in SCD mice[12]. After challenge with IV oxy-Hb, SCD mice manifested an average of at least one PVO per FOV (black bar in Figure 10 F), at least one PVO in 80% of all the FOVs examined (black bar in Figure 10 G), and an average of 0.4 large PVO per FOV (black bar in Figure 10 H)[12]. Although TSGL-Ig treatment led to significant reduction in all three parameters (Figure 10 F-H), the largest reduction was observed in the number of large vaso-occlusions (Figure 10 H)[12]. The average number of PVO per FOV was reduced by 40% (gray bar in Figure 10 F), percentage of FOVs with PVO was reduced by 33% (gray bar in Figure 10 G), and average number of large PVO per FOV was reduced by 50% (gray bar in Figure 10 H) in SCD mice administered IV oxy-Hb + TSGL-Ig compared with SCD mice administered only IV oxy-Hb[12]1. In contrast, the average number of PVO per FOV was unchanged in SCD mice administered IV oxy-Hb + rh IgG1-Fc compared with SCD mice administered IV oxy-Hb only (Figure 10 I)[12].

# Figure 10

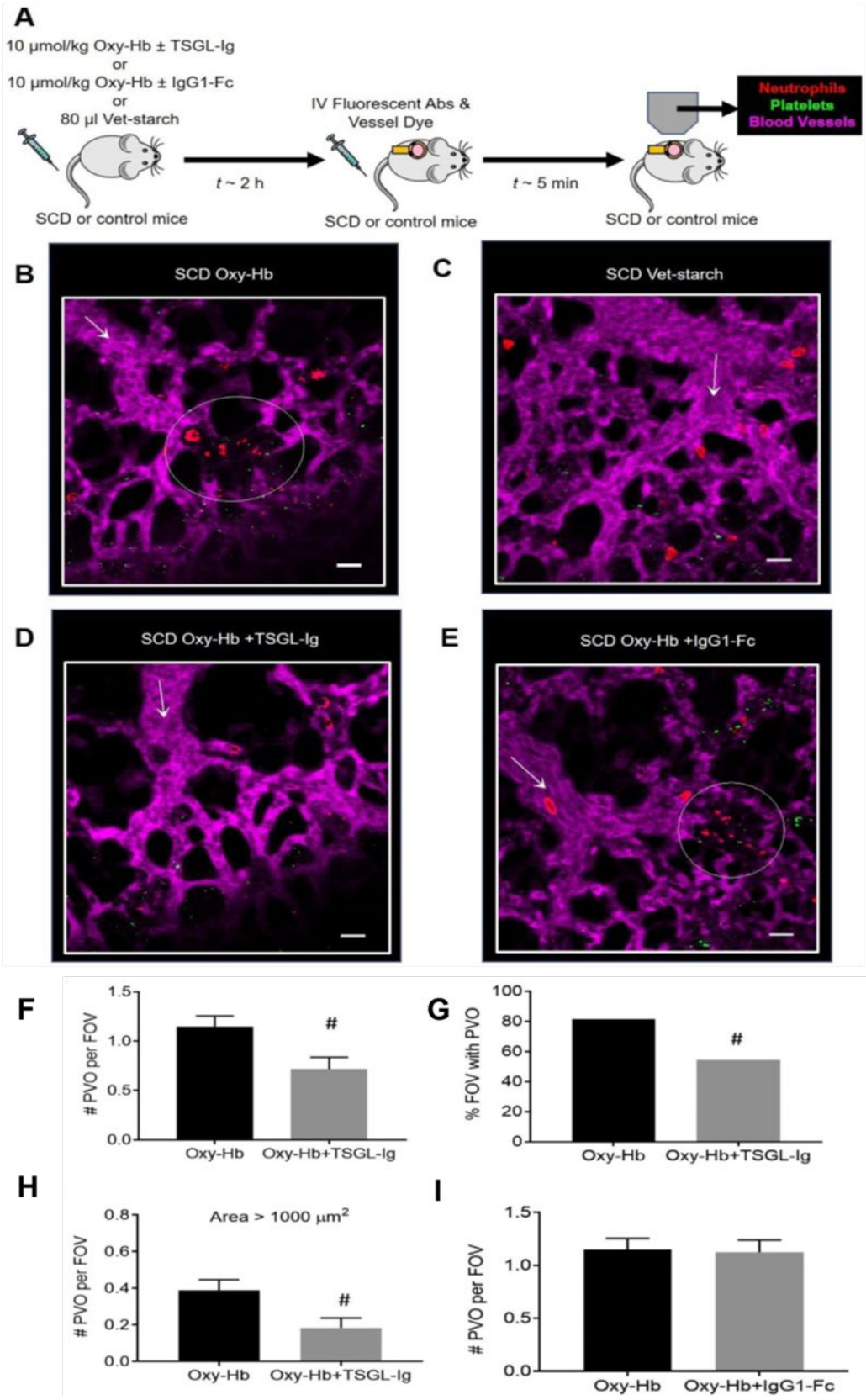
A
10 µmol/kg Oxy-Hb ± TSGL-Ig
or
10 µmol/kg Oxy-Hb ± IgG1-Fc
or
80 µl Vet-starch
IV Fluorescent Abs &
Vessel Dye
Neutrophils
Platelets
Blood Vessels
t ~ 2 h
t ~ 5 min
SCD or control mice
SCD or control mice
SCD or control mice
B
SCD Oxy-Hb
C
SCD Vet-starch
D
SCD Oxy-Hb +TSGL-Ig
E
SCD Oxy-Hb +IgG1-Fc
F
# PVO per FOV
1.5
1.0
0.5
0.0
#
Oxy-Hb
Oxy-Hb+TSGL-Ig
G
% FOV with PVO
100
80
60
40
20
0
#
Oxy-Hb
Oxy-Hb+TSGL-Ig
H
Area > 1000 µm²
# PVO per FOV
0.8
0.6
0.4
0.2
0.0
#
Oxy-Hb
Oxy-Hb+TSGL-Ig
I
# PVO per FOV
1.5
1.0
0.5
0.0
Oxy-Hb
Oxy-Hb+IgG1-Fc

**Figure 10: TSGL-Ig prevents lung vaso-occlsuion in SCD mice in-vivo.**

**(A) shows the schematic used for qFILM imaging approach. Control or SCD mice were IV challenged with 10 µmole/kg oxy-Hb ±100 µg/mouse TSGL-Ig or 10 µmol/kg oxy-Hb ± 100 µg/mouse rh IgG1-Fc or 80 µl vet-starch. qFILM was used to access pulmonary vaso-occlusion in the lung micro-circulation. Representative images obtained from qFILM shows that oxy-Hb promotes neutrophil-platelet aggregates and pulmonary vaso-occlusion in the bottleneck of arteriole (highlighted in eclipse) in SCD mice (B), whereas no aggregates were noticed in SCD mice given IV vet-starch (C) and SCD mice given IV oxy-Hb with TSGL-Ig (D). However, challenge of SCD mice with IV oxy-Hb and IgG1-Fc promotes pulmonary vaso-occlusion as shown in (E). Pulmonary microcirculation (pseudo-colored purple), neutrophils (red) and platelets (pseudo-colored green) were labeled in-vivo by IV administration of FITC dextran, AF546-anti-Ly6G Ab and V450-anti-CD49b Ab, respectively. White arrows denote the direction of blood flow within the arterioles. FOV~65,536 $\mu m^2$. Quantitative analysis of 2D image data sets obtained from qFILM revealed that average number of PVO per FOV in SCD mice given IV oxy-Hb and TSGL-Ig attenuated PVOs by almost half in comparison to SCD mice given IV oxy-Hb (F). Percent FOV with PVO shows that SCD mice given IV oxy-Hb had 80% of FOV with PVOs, however SCD mice given IV oxy-Hb with TSGL-Ig bring it down to 50% (G). PVOs greater than 1000 µm2 were also reduced in SCD mice given IV oxy-Hb with TSGL-Ig (H), however no change was noticed in SCD mice given IV oxy-Hb and SCD mice given IV oxy-Hb with IgG1-Fc (used as a negative control) as shown in (I). Means were compared using unpaired student's t test and percent analysis was compared using four-fold table analysis with $\chi 2$ statistics to assess the effect of TSGL-Ig or rh IgG1-Fc on IV oxy-Hb triggered lung vaso-occlusion in SCD mice. # $p < 0.05$, data represent mean ± SE. IV oxy-Hb SCD (n = 4 mice; 54 FOVs); IV oxy-Hb + TSGL-Ig SCD (n = 3 mice; 46 FOVs); IV oxy-Hb + rh IgG1-Fc SCD (n = 2 mice; 28 FOVs). Scale bar is 20 µm[12].**

## 3.2 Discussion

Epidemiological evidence shows that vaso-occlusive episodes and chest pain in SCD patients are often precursors to acute chest syndrome (ACS), a type of acute lung injury which has the highest mortality rates among SCD patients[17, 18]. The current treatment for ACS is primarily supportive, but the molecular mechanism remains largely unknown[17, 18]. In a recent autopsy study[64], ACS patient's pulmonary histopathology showed presence of platelets, neutrophils and erythrocytes aggregates suggesting the role of molecular events responsible for pulmonary vaso-occlusion in ACS patients leading to lung injury.

Recent intravital studies from my mentor's lab have revealed a potential role for neutrophil-platelet aggregates, which are present in the bottle-necks (the junction of pulmonary arteriole with pulmonary capillaries) of arteriole lung micro-circulation in SCD mice administered with IV LPS[3] or IV oxy-Hb[12]. Using a qFILM in-vivo approach, we have modeled vaso-occlusive crisis in SCD mice by administering a non-lethal dose of oxy-Hb[12] or hemin, to determine whether neutrophil-platelet aggregates promote in the lung micro-circulation of a SCD mice. The 2D time frame snapshots obtained from qFILM enable us to quantify average number of PVOs, size of PVOs, and frequency of neutrophil-rich or platelet-rich PVOs.

qFILM is a useful technique, but there are few limitations associated with this approach. qFILM is an operator method which requires years of practice, handling of mice, and surgical skills[52]. Due to heartbeat and lung movement of a mouse, the qFILM 2D time frame contains drift, that can be avoided only if a mechanical clamp is placed in a correct position on the lung, mostly lower part of the right lung has less drift and movement. This lower half of the lung has more clinical relevance because lung injury in ACS patients is often localized to the lower region of the lung[52].

## 3.3 Conclusion

This study uses previously introduced qFILM approach to visualize the cellular interaction in live lung micro-circulation of control or SCD mice administered with IV oxy-Hb or hemin. qFILM reveals that average number of PVOs present in SCD mice administered with IV oxy-Hb or hemin is significantly higher than control mice. Our data published in 2017[3], showed that administration of P-selectin blocking antibody to SCD mice given nano-gram dose of IV LPS decreased neutrophil-platelet aggregates and PVOs by 50% in comparison to SCD mice given only IV LPS. Based on these findings, TSGL-Ig was used to quantify the effect of blocking P-selectin-PSGL-1 interaction on neutrophil-platelet aggregates and PVOs in SCD mice given IV oxy-Hb[12]. TSGL-Ig has four p-selectin binding sites per TSGL-Ig molecule, which binds to P-selectin on endothelium and platelets, there by interfering with platelet-neutrophil and neutrophil-endothelium interactions. TSGL-Ig decreased neutrophil-platelet aggregates and PVOs in SCD mic, thus highlighting its potential as a future therapy to prevent VOEs and development of ACS among SCD patients. Taken together, this study concludes that eDAMPs (oxy-Hb and hemin) promotes neutrophil-platelet aggregation-dependent lung vaso-occlusion in SCD mice, and TSGL-Ig prevents lung vaso-occlusion in SCD mice by attenuating P-selectin-dependent neutrophil-platelet aggregation in lung arterioles.

## 4.0 Aim-2: To determine whether circulating NETs (cNETs) shed in the liver, travel to the lung to promote P-selectin independent pulmonary vaso-occlusion in SCD mice.

*Rationale:* Cell-free DNA levels in SCD patient blood correlates with onset of ACS30, but their origin and role in promulgating ACS remains unknown. Our findings suggest that these cell-free DNA fragments are cNETs shed by neutrophils in the liver, and then carried in blood to the lung to promote P-selectin-independent occlusion of pre-capillary pulmonary arterioles by neutrophil-platelet aggregates.

*Hypothesis:* cNETs are shed in the liver and then travel to the lung to promote P-selectin-independent pulmonary vaso-occlusion and ACS in SCD mice.

## 4.1 Results

### 4.1.1 Circulating NETs arrive in the lung micro-circulation from other organs in SCD mice.

In the current study, qFILM was used to assess presence or absence of neutrophil extracellular traps (NETs) in the intact lung microcirculation of live control or SCD mice after intravenous (IV) challenge with oxy-hemoglobin (oxy-Hb). The qFILM experimental setup and approach has been described elsewhere in detail[3, 12, 45], and is also mentioned in section 2.1.5. Briefly as shown in figure 11 A, SCD or control mice were IV administered via tail vein with 10 µmole/kg oxy-Hb. Approximately 2-2.5 hours following IV administration, qFILM was conducted with a Nikon multi-photon-excitation fluorescence microscope using an excitation wavelength of 850 nm and an APO LWD 25x water immersion objective with 1.1 NA. Time-series of 2D qFILM images were collected at ~15 frames per second (fps) using a resonant scanner. Each field of view (FOV) was 256 µm x 256 µm (~65,536 $\mu m^2$) with a resolution of ~0.5 µm per pixel in the x-y plane. A snapshot of SCD mice administered with IV oxy-Hb is shown in Figure 11 B and C, and it reveals that NETs are present in the lung micro-circulation of a SCD mouse given IV oxy-Hb. NETs are identified based on colocalization of NETs marker i.e., citrullinates histones (H3-Cit) or neutrophil elastase (NE) with extracellular DNA described somewhere else[16, 19-21]. Quantitative analysis of several time-series of qFILM images revealed that the average number of NETs per FOV present in SCD mice given IV oxy-Hb is significantly more than SCD mice given IV saline (Figure 11 D). The average number of NETs per FOV were also significantly more in SCD mice than control mice IV administered oxy-Hb (Figure 11 E). Schematic diagram of Figure 11 F shows SCD, or control mice were IV administered via tail vein with 10 µmole/kg oxy-Hb.

Approximately 2-2.5 hours following IV administration, qFILM was conducted with a Nikon multi-photon-excitation fluorescence microscope. Here, qFILM imaging approach was used to detect and quantify the presence or absence of circulating NETs in the lung micro-circulation of a SCD or control mice after IV oxy-Hb challenged. As shown in Figure 11 G, IV oxy-Hb led to arrival of cNETs in the lung micro-circulation a SCD mice. cNETs were found to flow into the lung via the pulmonary arteriole suggesting that they are arriving from non-pulmonary vascular beds. However, no cNETs were reported in the lung micro-circulation of a control mice given IV oxy-Hb (Figure 11 H). Quantification of 2D qFILM time frames revealed that average number of cNETs flowing into the lung per FOV per min was significantly higher in SCD mice given IV saline than control mice given IV saline (Figure 11 I). The average number of cNETs flowing into the lung per FOV per min was also higher in SCD mice given IV oxy-Hb than SCD mice given IV saline (Figure 11 J). After challenge of IV oxy-Hb to both control and SCD mice, average number of cNETs flowing per FOV per min were significantly higher in SCD mice than control mice (Figure 11 K). Finally, we also quantified the average number of cNETs flowing per FOV per min into the lung of SCD-*Selp-/-* mice, which was not significantly different from SCD mice administered IV oxy-Hb (Figure 11 L).

These in-vivo qFILM data suggest that IV oxy-Hb results in statistically higher number of NETs in the lung of SCD mice than control mice, and these NETs primarily arrive as cNETs from other organs.

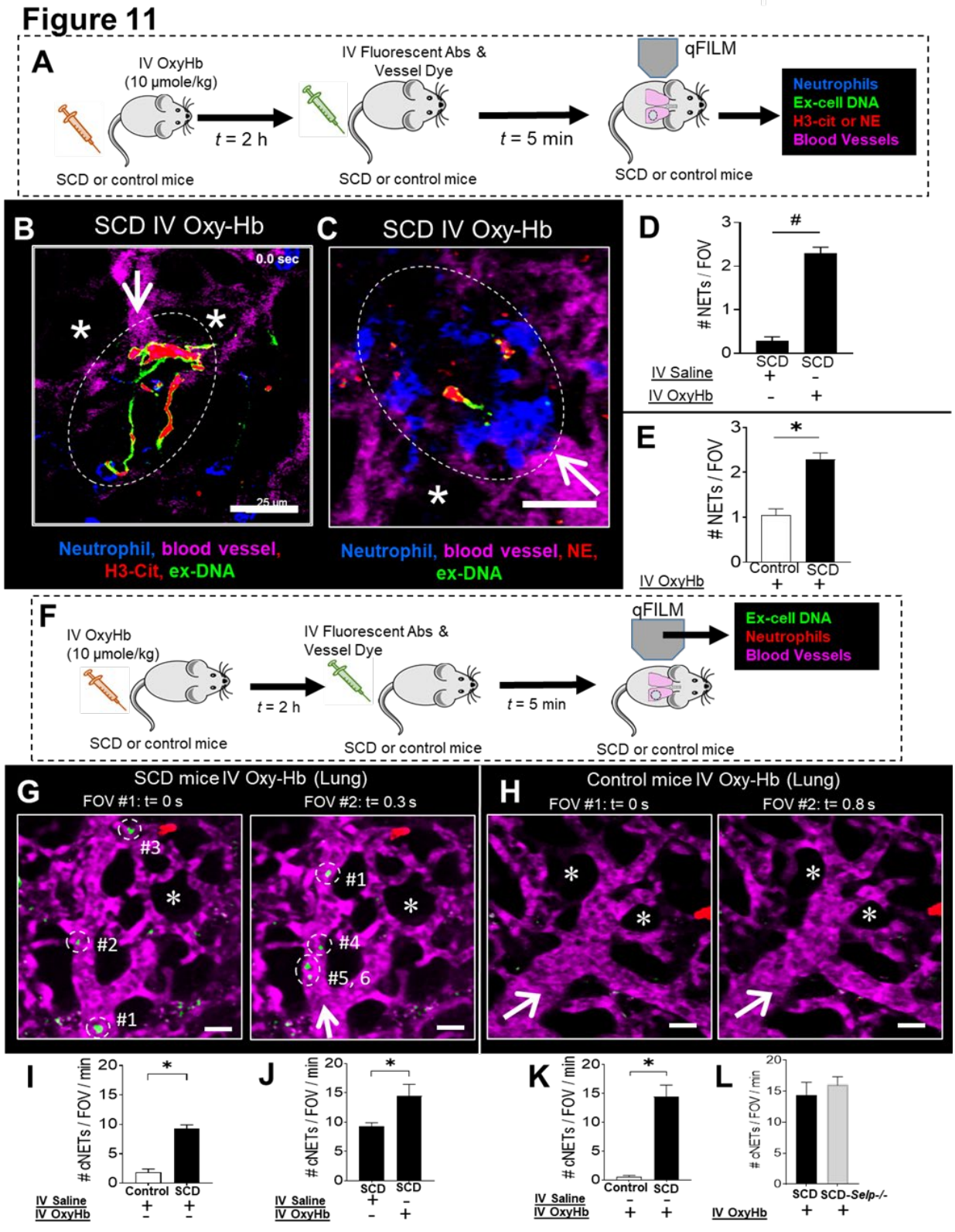


**Figure 11: Circulating NETs arrive in the lung micro-circulation from other organs in SCD mice.**

**Experimental scheme used in A: Control and SCD mice were IV administered 10 µmole/kg oxy-Hb and qFILM was used to assess the absence or presence of NETs within the pulmonary micro-circulation. (B) and (C) shows presence of NETs in the lung micro-circulation of a SCD mice given IV oxy-Hb. Pulmonary microcirculation (pseudo-colored purple), neutrophils (blue), extracellular DNA (green), and citrullinated histones (H3-Cit; red) or neutrophil elastase (NE; red) were labeled in-vivo by IV administration of Evans Blue, Pacific Blue-anti-Ly6G Ab, Sytox Green, and AF546- anti-H3-Cit Ab or AF546-anti-NE Ab, respectively. NETs were identified based on colocalization of Ly6G (blue) with exDNA (green) and (B) H3-cit (red) or (C) NE (red). White arrows denote the direction of blood flow within the pulmonary arterioles. Alveoli are marked with asterisks. Scale bars 20 µm. qFILM FOV size~65,536 µm2. Average number of NETs per FOV (#NETs/FOV) was significantly higher in SCD mice administered IV oxy-Hb (n=4 mice; 44 FOVs) than (D) SCD mice administered IV saline (n=4 mice; 49 FOVs) or (E) control mice administered IV oxy-Hb (n=4 mice; 43 FOVs). # Denotes $p < 0.05$ for SCD IV oxy-Hb compared to SCD IV saline in D. * Denotes $p < 0.05$ for SCD IV oxy-Hb compared to control IV oxy-Hb in E. Means were compared using unpaired Student's t test. Data represent Mean ± SE. (F) Shows the schematic of control and SCD mice administrated with IV Oxy-Hb, and qFILM was performed to look for cNETs in lung micro-circulation. Pulmonary microcirculation (pseudo-colored purple), neutrophils (pseudo-colored red), and extracellular DNA (pseudo-colored green) were labeled in-vivo by IV administration of FITC dextran, Pacific Blue-anti-Ly6G Ab, and Sytox orange, respectively. (G) FOV #1 & #2 of SCD mice with IV oxy-Hb shows cNETs marked in green flowing in the lung micro-circulation. However, no cNETs were seen in control mice given IV oxy-Hb (H). (I) Quantification of cNETs flowing per FOV per min into the lung of SCD mice given IV saline had significantly higher cNETs than control mice given IV saline. (J) and (K) average number of cNETs flowing per FOV per min were statistically higher in SCD mice given IV oxy-Hb in comparison to SCD IV saline, and control IV oxy-Hb. However, no significance reported between SCD IV oxy-Hb and SCD-Selp-/- in average number of cNETs flowing per FOV per min (L). Control IV saline (n = 3 mice; 28 FOVs), SCD IV saline (n = 4 mice; 51 FOVs), SCD IV oxy-Hb (n=4 mice; 44 FOVs), Control IV oxy-Hb (n=4 mice, 43 FOVs), SCD-Selp-/- IV oxy-Hb (n=5 mice; 70 FOVs). qFILM FOV size~65,536 µm2. Data represent mean ± SE and compared using students t-test. * Denotes $p < 0.05$.**

### 4.1.2 Shedding of circulating NETs is P-selectin independent.

As shown in figure 11 L, number of cNETs entering the lung micro-circulation were not different between SCD-*Selp-/-* mice and SCD mice administered IV oxy-Hb. To investigate this study more, we used Imaging flow cytometry to quantify the number of cNETs in the plasma of SCD or SCD-*Selp-/-* mice after IV oxy-Hb challenge. Figure 12 A shows the schematic of imaging flow cytometry of SCD mice plasma and details are mentioned in section 2.1.10. Briefly, SCD or SCD-*Selp-/-* mice were administrated with IV 10 µmole/kg oxy-Hb and blood was collected 3 hours later from the inferior vena cava in tubes containing 3.2% sodium citrate (0.105M) at a ratio of 1:10 (sodium citrate: blood) and processed to generate platelet-poor-plasma (PPP). For each treatment group, 30 µl of PPP was mixed with 70 µl of physiological saline, and incubated with sytox green, AF546-conjugated anti-NE Ab, and AF647-conjugated-anti-H3cit or H2A.X Ab for in situ staining of extracellular DNA, NE, and histones, respectively. Imaging flow cytometry was conducted using AMNIS Image Stream equipment and data was analyzed using IDEAS application software. Figure 12 B shows a representative set of images obtained using imaging flow cytometry. cNETs were identified as fragments (< 3 µm) of ex-DNA (green), that were also positive for both neutrophil elastase (NE; yellow) and citrullinated histones (H3-Cit; red). Further, we quantified cNETs concentration as number of cNETs present in per µl plasma (#cNETs/ µl plasma), and it shows that there was no significance in cNETs concentration between SCD and SCD-Selp-/- mice given IV oxy-Hb (Figure 12 C). Similarly, Imaging flow cytometry was performed on SCD or control human subject blood to quantify number of cNETs concentration. Figure 12 D shows the schematic where blood was collected from SCD or control human subject (details mentioned in section 2.1.3), blood was treated with or without 20 µM hemin and processed to generate PPP. For each treatment group, 30 µl of PPP was mixed with 70 µl of physiological

saline, and incubated with sytox green, AF546-conjugated anti-NE Ab, and AF647-conjugated-anti-H3cit or H2A.X Ab for in-situ staining of extracellular DNA, NE, and histones, respectively. Figure 12 E shows a representative set of images obtained from Imaging flow cytometry. cNETs were identified as fragments (< 3 μm) of ex-DNA (green), that were also positive for both neutrophil elastase (NE; yellow) and citrullinated histones (H3-Cit; red). SCD patients' blood contained significantly higher cNETs per μl of plasma than control human blood (Figure 12 F). After pretreatment of SCD patient's blood with or without 20 μM hemin, significantly higher cNETs per μl of plasma was seen in SCD patient's blood with hemin pretreatment in comparison to without hemin pretreatment (Figure 12 G).

These results suggest that cNETs are significantly elevated in SCD than control mice or patient's plasma, IV administration of oxy-Hb to SCD mice or pretreatment of SCD patient's blood with hemin promotes shedding of cNETs and shedding of cNETs in SCD occurs by a P-selectin independent mechanism.

## Figure 12

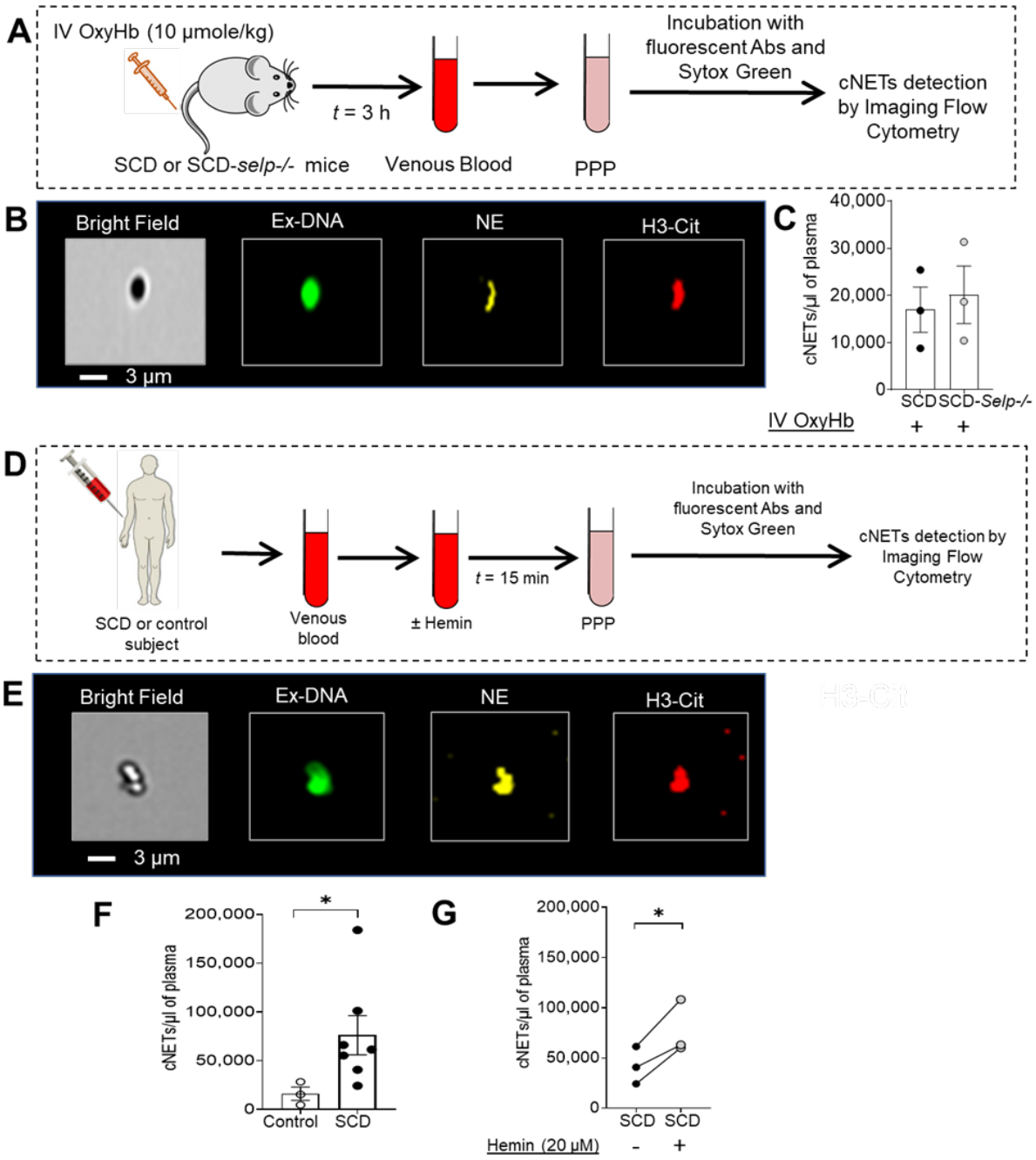


**Figure 12: Shedding of NETs is P-selectin independent.**

**Experimental scheme used in A: SCD or SCD-Selp-/- mice were IV administered 10 µmole/kg oxy-Hb, venous blood was processed to generate Platelet Poor Plasma (PPP), PPP was incubated with sytox green and fluorescent Abs against Neutrophil Elastase (NE) and citrullinated-histones (H3-Cit) and used for detection of cNETs by Imaging Flow Cytometry. (B) A representative imaging flow cytometry image of a cNET in the**

**blood of SCD mice administered IV oxy-Hb. cNETs were identified as particles (< 3 μm) triple-positive for NETs markers-extracellular DNA (green), NE (pseudo-colored yellow) and H3-Cit (pseudo-colored red). Scale bar 3 μm. (C) Imaging flow cytometry data was quantified to estimate concentration of cNETs (#cNETs/μl of plasma). Plasma concentration of cNETs was not different between SCD and SCD-Selp-/- mice (n=3 mice per group) administered IV oxy-Hb. (D) Experimental scheme used for cNETs detection in Control or SCD human blood with or without pretreatment with 20 μM hemin processed to generate PPP and cNETs detected using Imaging Flow Cytometry as in A. (E) A representative imaging flow cytometry image of a cNET in a SCD patient blood pretreated with 20 μM hemin. Scale bar 3 μm. (F) The concentration of cNETs was significantly higher in untreated SCD (n=7) than control (n=3) human subjects blood. (G) Incubation with hemin significantly increased cNETs concentration in SCD patients (n=3) blood. Straight line connects cNETs concentrations in the same SCD patient blood pre- (black circle) and post- (grey circle) hemin treatment. Data in Cand F represent mean ± SE and compared using students t-test. Data in G was compared using a paired t-test. * Denotes $p < 0.05$.**

### 4.1.3 NETs are abundant in the liver of SCD than control mice.

Interestingly, liver is the last organ to drain into inferior vena cava (IVC) before blood reaches lung. The liver vasculature is one of the primary sites for NETs generation during systemic inflammation[57, 65, 66] liver also serves as a sink for heme and hemoglobin released following intravascular hemolysis[65-68], both heme and hemoglobin are potent agonists of NETs generation[2, 65-67, 69, 70], and my recent work showed that liver is significantly inflamed in SCD mice even at baseline[55]. Therefore, we performed qLIM on intact liver of a live SCD or control mice to study the liver histopathology. Experimental detail and design of qLIM[44, 55, 56] is mentioned in section 2.1.6. Briefly as shown in figure 13 A, SCD or control mice were IV administered via tail vein with 10 µmole/kg oxy-Hb. Approximately 2-2.5 hours following IV oxy-Hb, qLIM was conducted using a Nikon multi-photon-excitation fluorescence microscope. Figure 13 B shows qLIM images of FOV# 1 & 2 in revealing numerous NETs and vaso-occlusion in the liver micro-circulation of a SCD mouse given IV oxy-Hb. Besides liver, kidney function is also known to be significantly impaired in both SCD mice and patients[71, 72]. Therefore, we also decided to test the presence or absence of NETs in the kidney microcirculation of SCD mice. Like qLIM, qKIM imaging approach was also developed by me to image intact kidney in a live mouse, details are mentioned in section 2.1.7. Unlike liver micro-circulation, qKIM revealed absence of NETs or vaso-occlusion in the kidney micro-circulation of SCD mice given IV oxy-Hb (Figure 13 C). Quantification of 2D time frames from qLIM and qKIM showed that liver had significantly higher number of NETs than kidney in SCD mice given IV oxy-Hb (Figure 13 D). To further confirm these finding, laser-scanning confocal immunofluorescence microscopy was performed on the fresh cut liver slices of SCD, and control mice given IV oxy-Hb. Detail experiment setup of confocal immunofluorescence microscopy is mentioned in section 2.1.12. Figure 13 E shows

snapshots obtained from confocal immunofluorescence microscopy where large number of NETs were present in liver of SCD mouse given IV oxy-Hb, however relatively very few NETs were seen in liver of SCD mouse given IV oxy-Hb. NETs were identified based on colocalization of neutrophil (white), NE (red), and extracellular DNA (green). Quantification of 1D image data sets obtained from confocal microscopy, showed that liver had almost twice number of NETs present in SCD mice given oxy-Hb in comparison to control mice given oxy-Hb (Figure 13 F).

QLIM, qKIM, and confocal immunofluorescence microscopy experiment all together confirmed that NETs are significantly abundant in the liver than kidney micro-circulation of SCD mice given IV oxy-Hb.

## Figure 13

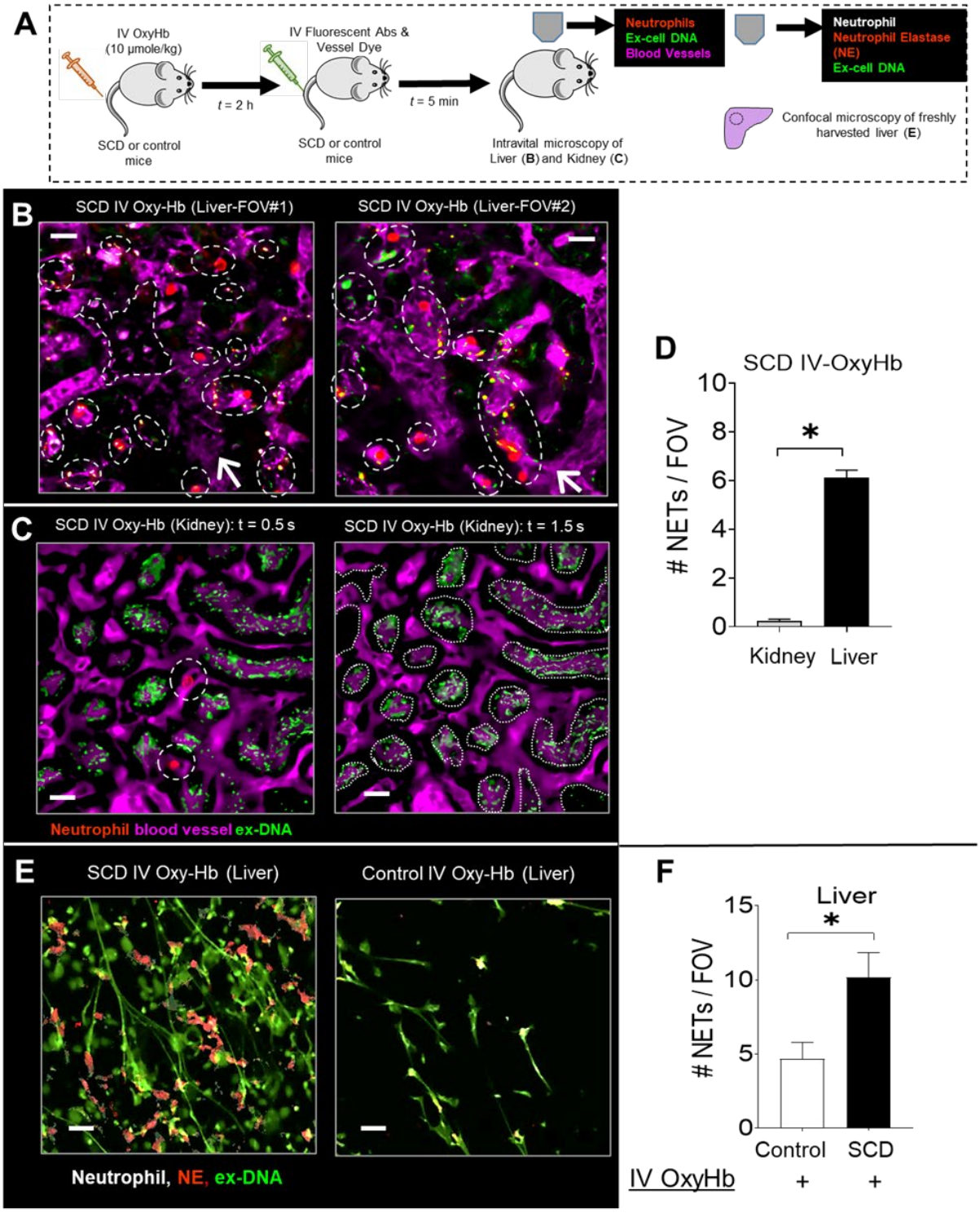


**Figure 13: NETs are abundant in the liver of SCD mice than control mice.**

**(A) Experimental scheme: Control or SCD mice were IV administered 10 µmole/kg oxy-Hb. Intravital fluorescence microscopy was used to assess the absence or presence of NETs and vaso-occlusion within the liver (B), kidney (C). Microcirculation (pseudo-colored purple), neutrophils (pseudo-colored red) and extracellular DNA (pseudo-colored green) were labeled in-vivo by IV administration of FITC or Texas-red dextran, Pacific Blue-anti-Ly6G Ab and Sytox Orange or Green, respectively. Alternatively (E), freshly cut-unfixed slices of excised liver were stained in-vitro for neutrophils (Pacific Blue-anti-Ly6G Ab), extracellular DNA (Sytox Green), and neutrophil elastase (NE; AF546-anti-NE Ab), and confocal microscopy was used to identify NETs based on colocalization of DNA (green) with neutrophils (pseudo colored white) and NE (red). (B) Two representative liver intravital microscopy images (FOVs #1 and #2) reveal numerous NETs (marked with white ellipses) and areas with impaired blood flow evident by slow transit of erythrocytes (dark cells) in the liver microcirculation of SCD mice administered IV oxy-Hb. NETs were identified based on colocalization of neutrophil (red) and extracellular DNA (green). A vaso-occlusion evident by lack of vascular dye (purple) is marked with white dotted polygon in FOV#1. (C) A representative kidney intravital microscopy FOV shown at two different time point reveal two different neutrophils (red; marked with white dotted circles at 0.5 s) rapidly transiting (appearing at 0.5 s and disappearing at 1.5 s) through the kidney microcirculation (purple) in SCD mice administered IV oxy-Hb. The island like structures (outlined by dotted white lines at 1.5 s) interspacing capillaries are glomerular spaces. Unlike liver (panel B), sequestered neutrophils and any associated extracellular-DNA was not present in kidney microcirculation suggestive of the absence of NETs. The green staining in the FOV is primarily DNA dye (sytox green) collecting in the glomerular spaces (islands outlined by dotted lines) due to filtration across the blood-urine barrier. (D) #NETs/FOV was significantly higher in the liver than kidney of SCD mice administered IV oxy-Hb. FOV size~65,536 µm$^2$. SCD IV oxy-Hb kidney (n=3 mice; 35 FOVs), SCD IV oxy-Hb liver (n=4 mice; 42 FOVs). (E) Representative confocal micrographs reveal abundance of NETs (neutrophil-associated DNA strands positive for NE) in the liver of an SCD but rare in the liver of control mouse administered IV oxy-Hb. Neutrophils (pseudo-colored white), NE (red), and extracellular DNA (green). (F) Confocal micrographs were also quantified to reveal significantly more #NETs/FOV in the liver of SCD than control mice administered IV oxy-Hb. n=6 FOVs in each group. FOV size~144,400 µm$^2$. Data represents mean ± SE and compared using students t-test. * Denotes $p < 0.05$. Arrow denotes the direction of blood flow.**

### 4.1.4 Halting blood flow from liver to lung reduces circulating NETs in the lung micro-circulation of SCD mice.

In previous section 4.1.3 we showed that more NETs were present in the liver of a SCD mice given IV oxy-Hb. We hypothesized that NETs are shed in the liver, and then flow with the blood as cNETs to the lung via inferior-vena-cava and right heart as shown in section 2.1.8 for better understanding.

We performed an experiment where blood flow from liver to lung was transiently halted by simultaneously ligating both hepatic artery and portal vein in liver SCD mice. cNETs were counted pre and post ligation in the lung micro-circulation of SCD mice given IV oxy-Hb using qFILM imaging approach. Figure 14 A shows the schematic of the experiment, where SCD or control mice were IV administered via tail vein with 10 µmole/kg oxy-Hb. Approximately 2-2.5 hours following IV administration of fluorescent antibodies and vessel dye, qFILM was conducted without ligation of hepatic artery and portal (pre-liver clamping), 8-10 FOVs were collected pre-liver clamping per mouse, then hepatic artery and portal vein were ligated (post-liver clamping) with the help of silk sutures, further 8-10 FOVs were also collected post-liver clamping. Figure 14 B shows the qFILM snapshot obtained from 2D time-frame data obtained after pre- and post-liver clamping of SCD mouse given IV oxy-Hb. Extra-cellular DNA (green) highlighted by dotted circle is seen entering lung micro-circulation via pulmonary arteriole but not in post-liver clamping in a SCD mouse IV administered oxy-Hb. Quantification of pre- and post-liver clamping data set showed that average number of cNETs entering lung per FOV per min was statistically reduced (~ 60-70 % reduction) post-liver clamping (Figure 14 C).

## Figure 14

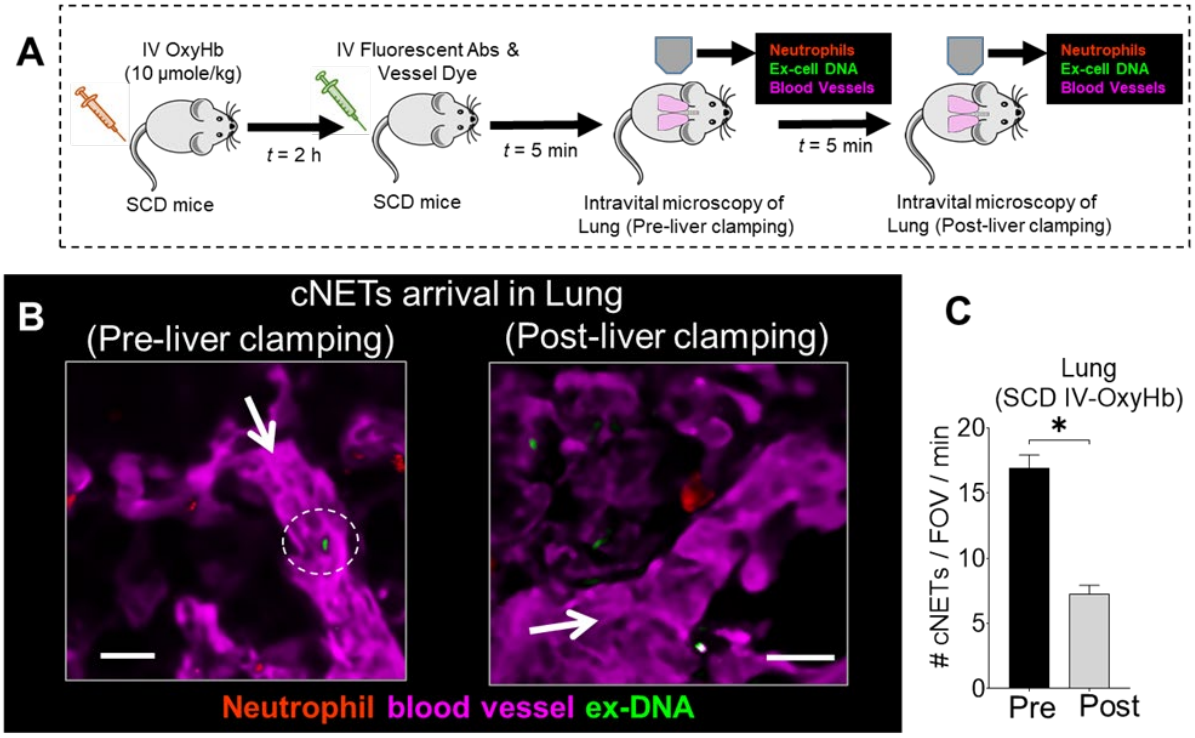


**Figure 14: Halting blood flow from liver to lung reduces cNETs in the lung mirco-circulation of a SCD mice. (A) qFILM schematic of SCD mice given IV oxy-Hb before pre-liver clamping and post-liver clamping to count cNETs entering in the lung micro-circulation. For better visualization neutrophils were pseudo-colored in red, extracellular DNA was pseudo-colored in green, and blood vessels were pseudo-colored in purple. (B) cNETs (green; marked with dotted white circle) are seen entering the pulmonary arteriole pre- but not post-clamping of liver blood flow. (C) Number of cNETs arriving in the lung per FOV over a 1 min duration (#cNETs/FOV/min) were significantly reduced (3-folds) following clamping of liver blood flow in SCD mice administered IV oxy-Hb (n=5 mice; 45 FOVs pre-clamp; 33 FOVs post clamp). FOV size~65,536 µm$^2$. Scale bars 20 µm. Data represents mean ± SE and compared using students t-test. * Denotes $p < 0.05$. Arrow denotes the direction of blood flow.**

## 4.2 Discussion

Based on these results, it can be concluded that cNETs shed in the liver, travel to the lung to promote P-selectin independent lung vaso-occlusion in SCD. However, there were few limitations which are mentioned below, and require further investigation by future studies. First, circulating NETs in the lung micro-circulation of SCD mice should be confirmed by using specific markers like neutrophil-elastase or citrullinated histones followed by 4-color qFILM imaging. For e.g., 1st channel can be used for Pacific Blue Ly6G to fluorescently label neutrophils, 2nd channel can be used for sytox green to fluorescently label extracellular DNA, 3rd channel can be used specific NETs marker like neutrophil elastase or citrullinates histones, and 4th channel can be used for blood label by Evans blue. This combination will enable us to confirm that cNETs flows in the lung micro-circulation of SCD mice. However, this limitation was partly resolved in the current study using imaging flow cytometry of mouse plasma, which confirmed presence of cNET in blood. Second, we have shown that cNETs are P-selectin independent in SCD mice only, but we did not provide any evidence to show cNETs generation in SCD patients is also P-selectin independent. Hence, future studies should investigate the effect of P-selectin inhibition on cNETs generation in SCD human blood. Third, we show that clamping of blood flow from the liver led to 60-70 % partial reduction in delivery of cNETs to the lung of SCD mice, suggesting a contribution of other vascular beds as well besides liver and kidney.

## 4.3 Conclusion

We conclude that cNETs are elevated in SCD than control human blood, and levels are further elevated after hemin treatment. cNETs are very less or absent in control mice but significantly elevated in SCD mice after IV oxy-Hb administered. cNETs are shed by neutrophil-associated intact NETs in the liver and then translocate to the lung with blood flow to promote pulmonary arteriole micro-embolism by neutrophil-platelet aggregates in SCD mice. Finally, cNETs shedding in SCD mice is not attenuated following genetic-deletion of P-selectin.

## 5.0 AIM-3: To determine whether caspase-4/11-dependent activation of neutrophil GSDMD promotes shedding of cNETs and development of ACS in SCD.

*Rationale:* Our preliminary data reveals that GSDMD is active in SCD patient and mice neutrophils, inhibition of GSDMD or its activator caspase-4 (human) or caspase-11 (mouse) or scavenging reactive oxygen species (ROS) prevents cNETs shedding in SCD mice or human blood and inhibiting GSDMD-pathway prevents neutrophil-platelet aggregation-dependent lung vaso-occlusion in SCD mice in-vivo.

*Hypothesis:* Caspase-4/11-dependent activation of neutrophil-GSDMD promotes shedding of cNETs, leading to development of ACS in SCD.

## 5.1 Results

### 5.1.1 Inhibiting GSDMD-signaling prevented cNETs shedding in SCD human blood ex-vivo and SCD mice in-vivo.

To investigate the role of GSDMD-signaling, caspase-4 (in humans), and caspase-11 (in mouse) on shedding of cNETs in SCD human blood and SCD mice, we performed imaging flow cytometry on PPP processed from SCD human or mice blood. As shown in figure 15 A, blood was collected from SCD or control subject (detail mentioned in section 2.1.3), blood was treated with or without 20 µM hemin and processed to generate PPP. Same strategy was used here as described in Aim 2 section 4.1.2 to visualize and quantify cNETs in SCD patient's blood and SCD mice. Treatment of SCD patient's blood with hemin + GSDMD inhibitor (LDC7559) significantly attenuated cNETs per µl of plasma compared to treatment with hemin only as shown in Figure 15 B. Similarly, treatment of SCD patient's blood with hemin + caspase-4 inhibitor (LEVD-CHO) significantly attenuated cNETs per µl of plasma compared to treatment with hemin only as shown in Figure 15 C. To check the role of ROS, we used N-acetyl-cysteine (NAC) antioxidant treatment on SCD patient's blood with hemin. cNETs per µl of plasma were significantly attenuated following hemin + NAC compared to hemin treatment only as shown in Figure 15 D. Similarly, we used Imaging flow cytometry to count the number of cNETs in the plasma of SCD or SCD-*Selp-/-* mice after IV oxy-Hb administration. Figure 15 E shows the schematic of Imaging flow cytometry on SCD, or SCD-*Selp-/-* mice plasma and detail is mentioned in 2.1.11. Average number of cNETs per µl of plasma were reduced in SCD mice given IV oxy-Hb with GSDMD inhibitor (LDC7559) in comparison to SCD mice given IV oxy-Hb only (Figure 15 F). Similarly, average number of cNETs per µl of plasma were reduced in SCD-*Selp-/-* mice given IV oxy-Hb with

GSDMD inhibitor (LDC7559) in comparison to SCD-*Selp-/-* mice given IV oxy-Hb only (Figure 15 G).

These results conclude that inhibiting GSDMD-signaling, and caspase-4 prevented cNETs shedding in SCD human blood, and attenuated cNETs in SCD mice.

Figure 15

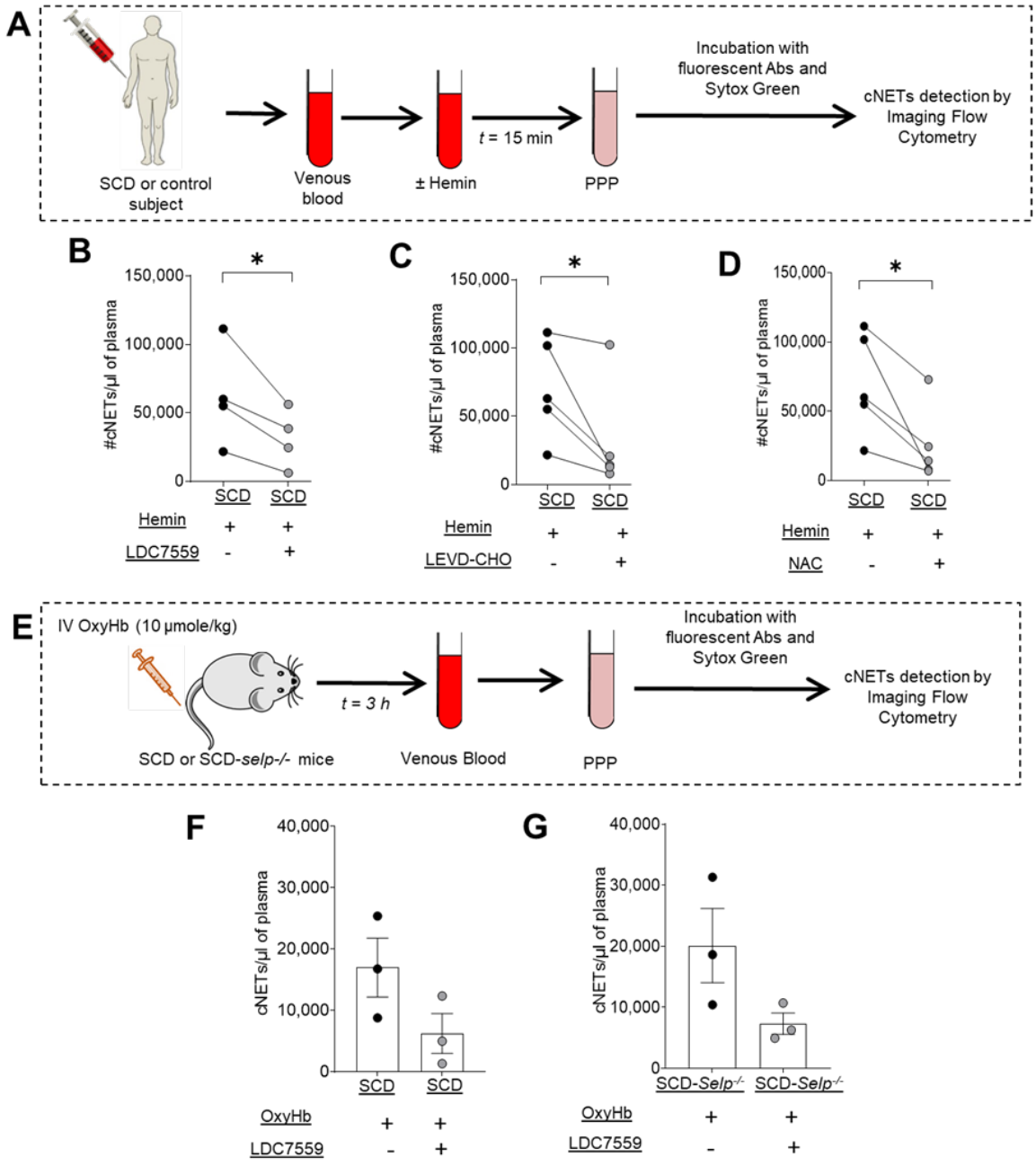


**Figure 15: Inhibiting GSDMD-signaling prevented cNETs shedding in SCD human blood ex-vivo and SCD mice in-vivo.**

**Experimental scheme used in (A) shows SCD patient blood preincubated with 20 µM hemin with or without GSDMD inhibitor (LDC7559) or Caspase-4 inhibitor (LEVD-CHO) or N-acetyl-cysteine (NAC), processed to generate plate-poor-plasma (PPP), PPP incubated with sytox green and fluorescent Abs against Neutrophil**

**Elastase (NE) and citrullinated-histones (H3-Cit), and circulating NETs (cNETs) detected in PPP by Imaging Flow Cytometry. Concentration of cNETs (#cNETs/µl of plasma) was significantly reduced in hemin-treated SCD patient blood following incubation with (B) 10 µM LDC7559 (n=4 patients), (C) 20 µM LEVD-CHO (n=5 patients), and (D) 20 µM NAC (n=5 patients). Straight line connects cNETs concentrations in the same SCD patient blood pre- (black circle) and post- (grey circle) inhibitor treatment. (E) Experimental scheme shows SCD or SCD-*Selp-/-* mice were IV administered 10 µmole/kg oxy-Hb with or without 10 mg/kg GSDMD inhibitor (LDC7559). Venous blood was processed to generate PPP and cNETs detected in PPP using Imaging Flow Cytometry as in A. (F) Plasma concentration of cNETs was significantly less in SCD mice IV administered 10 oxy-Hb + LDC7559 (n=3 mice) than 10 oxy-Hb alone (n=3 mice). (G) Plasma concentration of cNETs was significantly less in SCD-*Selp-/-* mice IV administered 10 oxy-Hb + LDC7559 (n=3 mice) than 10 oxy-Hb alone (n=3 mice). Data in B-D compared using a paired t-test. Data in F-G represents Mean ± SE and compared using Students t-test. * Denotes $p < 0.05$.**

### 5.1.2 NETs generation in liver is controlled by GSDMD-signaling.

To investigate the role of GSDMD-signaling on NETs generation in liver of SCD mice, we have used GSDMD inhibitors and *Gsdmd-/-* mice. qLIM was performed on SCD mice or GSDMD-deficient (*Gsdmd -/-*) mice to count for number of NETs produced in the liver micro-circulation. Figure 16 A shows the schematic, briefly SCD or WT or *Gsdmd -/-* mice were IV administered via tail vein with 10 µmole/kg oxy-Hb. Approximately 2-2.5 hours following IV administration, qLIM was conducted with a Nikon multi-photon-excitation fluorescence microscope. Figure 16 B left image shows the still obtained from qLIM imaging approach which shows large number of NETs (total 6) in the liver micro-circulation of a SCD mouse given IV oxy-Hb, however right image showed only one NETs in the liver micro-circulation of a SCD mouse given IV oxy-Hb with GSDMD-inhibitor LDC7559. After quantification of 2D time-frames image data sets obtained from qLIM, it shows that the average number of NETs per FOV were three times less in the liver micro-circulation of SCD mice given IV oxy-Hb + LDC7559 compared to IV oxy-Hb alone (Figure 16 C). After analyzing the total percent area occluded per FOV in SCD mice given oxy-Hb + LDC7559, shows that there was almost two-folds decrease in the inhibitor group as shown in figure 16 D. Like the above findings, we used WT or *Gsdmd -/-* mice also to conduct qLIM. To generate NETs in the liver and promote lung vaso-occlusion, two times higher dose (20 µmole/kg) of IV oxy-Hb was used on WT and *Gsdmd -/-* mice. Figure 16 E left image shows 6 NETs in the liver of WT mice given IV 20 µmole/kg oxy-Hb. However, relatively fewer NETs were seen in the *Gsdmd -/-* mice liver after administration of IV 20 µmole/kg oxy-Hb. After quantification of data sets obtained from qLIM, the average number of NETs per FOV were significantly decreased in *Gsdmd -/-* mice compared to WT mice given IV 20 µmole/kg oxy-Hb (Figure 16 F). The total percent ischemic area (microcirculation with impaired blood flow) per FOV in the liver was also

significantly decreased in *Gsdmd -/-* mice compared to WT mice given IV 20 µmole/kg oxy-Hb as shown in figure 16 G.

Altogether, these results suggest that NETs generation in the liver of SCD mice is dependent on GSDMD-signaling within neutrophils.

**Figure 16**

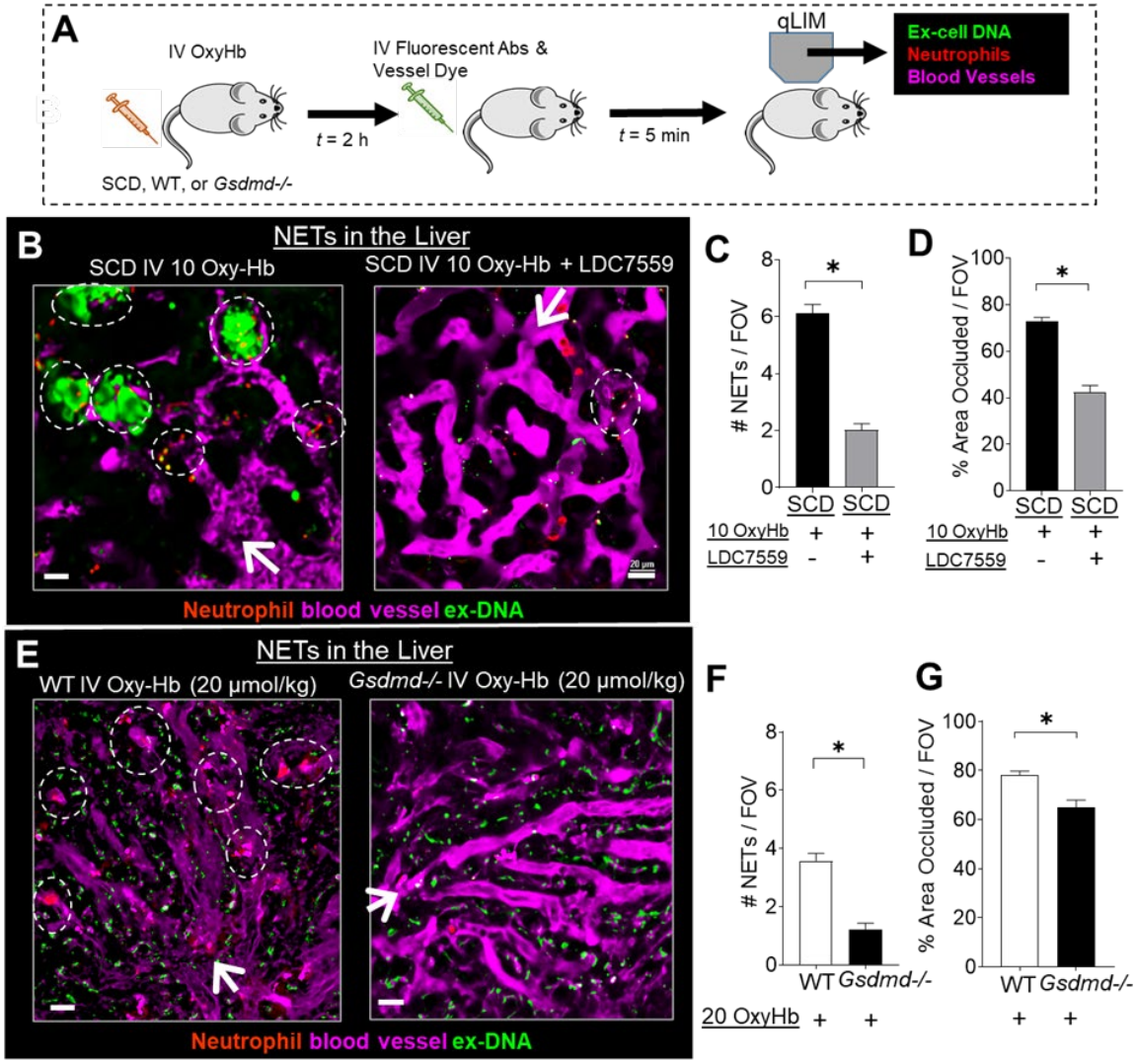


**Figure 16: NETs generation in liver is controlled by GSDMD-signaling.**

**(A) Schematic of qLIM imaging approach, where SCD mice administrated with IV 10 µmole/kg oxy-Hb or WT and *Gsdmd-/-* mice with IV 20 µmole/kg oxy-Hb and qLIM was used to assess the absence or presence of**

**NETs and vaso-occlusion within the liver (B & E). Microcirculation (pseudo-colored purple), neutrophils (pseudo-colored red) and extracellular DNA (pseudo-colored green) were labeled in-vivo by IV administration of FITC or Texas-red dextran, Pacific Blue-anti-Ly6G Ab and Sytox Orange or Green, respectively. (B) qLIM representative image showing NETs in liver of SCD mice given IV oxy-Hb, however only one NETs was seen in SCD mice given IV oxy-Hb with LDC7559. Dotted eclipsed are drawn around NETs to highlight them, arrow denotes the direction of blood flow and scale bar is 20 µm. (C) Average number of NETs per FOV were three times decreased in SCD mice given IV oxy-Hb with LDC7559 (n=4 mice; 42 FOVs) in comparison to SCD IV oxy-Hb (n=4 mice; 44 FOVs) only. (D) percent of area occluded per FOV in SCD mice given IV oxy-Hb with LDC7559 also went down significantly in comparison to SCD IV oxy-Hb. (E) shows qLIM images from WT containing NETs in liver, and *Gsdmd-/-* mice given IV 20 µmole/kg oxy-Hb contains no NETs, and improvement in blood flow. (F) After analysis of qLIM data sets, average number of NETs per FOV were decreased to half in *Gsdmd-/-* mice (n=4 mice; 35 FOVs) in comparison to WT mice (n=4 mice; 38 FOVs). (G) Similarly, percent of area occluded per FOV in *Gsdmd-/-* mice given IV oxy-Hb with LDC7559 also went down significantly in comparison to WT IV oxy-Hb. Data represents mean ± SE and compared using students t-test. * Denotes $p < 0.05$. FOV size~65,536 $\mu m^2$**

### 5.1.3 Arrival of cNETs in the lung of SCD mice were GSDMD dependent.

Next, we investigated the effect of GSDMD pathway inhibition or deletion on delivery of cNETs to the lung. Figure 17 A shows the schematic of qFILM experimental set up. SCD, SCD-*Selp-/-*, WT, or *Gsdmd-/-* mice were IV administered via tail vein with 10 µmole/kg oxy-Hb. Approximately 2-2.5 hours following IV administration, qFILM was conducted with a Nikon multi-photon-excitation fluorescence microscope. Here, the qFILM imaging approach was used to detect and quantify the presence or absence of circulating NETs in the lung micro-circulation of a SCD or control mice after IV administration of oxy-Hb with or without inhibitors. Figure 17 B shows that the average number of cNETs per FOV per min were three-folds decreased in the lung of SCD mice given IV oxy-Hb + pan-caspase inhibitor (Z-VAD-FMK) in comparison to IV oxy-Hb alone. IV administration of oxy-Hb+LDC7559 (GSDMD inhibitor) decreased cNETs per FOV per min in the lung of SCD mice by half in comparison to IV oxy-Hb alone (Figure 17 C). Other GSDMD inhibitor necrosulfonamide (NSA) also led to the decrease in cNETs per FOV per min in the lung of SCD mice shown in figure 17 D. We also quantified the average number of cNETs flowing per FOV per min the lung of SCD-*Selp-/-* mice given IV oxy-Hb or IV oxy-Hb + GSDMD inhibitor LDC7559. Figure 17 E shows more than 3 times decrease in the cNETs per FOV per min in SCD-*Selp-/-* mice given LDC7559 in comparison to IV oxy-Hb alone. Similarly, cNETs per FOV per min were counted in the WT and *Gsdmd-/-* mice given higher dose of oxy-Hb i.e., 20 µmole/kg. *Gsdmd-/-* mice manifested significantly less average number of cNETs per FOV per min in comparison to WT mice as represented in figure 17 F.

## Figure 17

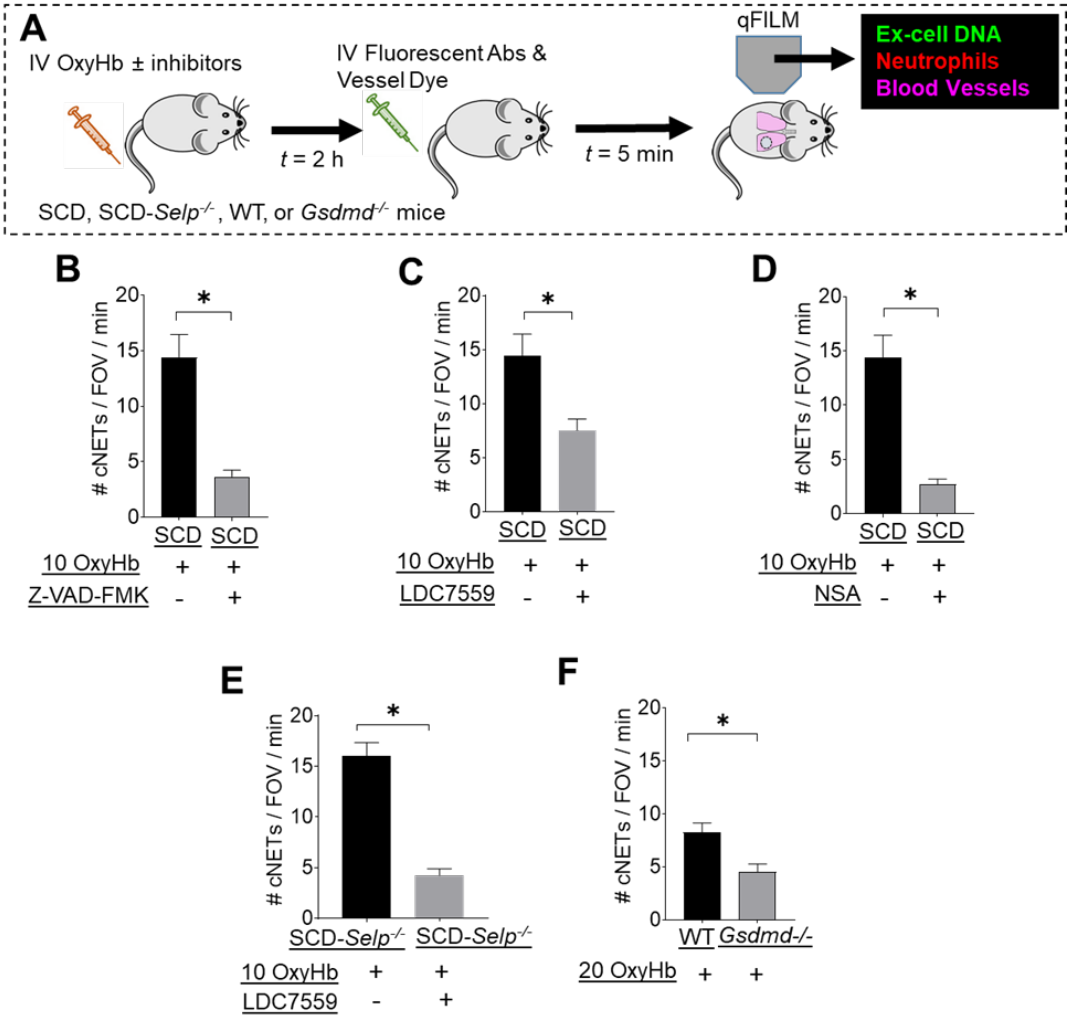


**Figure 17: Arrival of cNETs in the lung of SCD mice were GSDMD independent.**

**(A) Schematic used for qFILM imaging approach to visualize cNETs in the lung micro-circulation of IV SCD 10 µmole/kg oxy-Hb or IV SCD-*Selp-/-* 10 µmole/kg oxy-Hb or IV WT 20 µmole/kg oxy-Hb or IV *Gsdmd-/-* 20 µmole/kg oxy-Hb. (B) #cNETs/FOV/min in the lung were significantly less in SCD mice IV administered 10 oxy-Hb + Z-VAD-FMK (n=4 mice; 51 FOVs), (C) 10 oxy-Hb + LDC7559 (n=4 mice; 41 FOVs), and (D) 10 oxy-Hb + NSA (n=3 mice; 38 FOVs) than 10 oxy-Hb alone (n=4 mice; 44 FOVs). (E) #cNETs/FOV/min in the lung were significantly less (4-folds) in SCD-*Selp-/-* mice IV administered 10 oxy-Hb + LDC7559 (n=3 mice; 35 FOVs) than 10 oxy-Hb alone (n=5 mice; 70 FOVs). (F) #cNETs/FOV/min in the lung were significantly less in *Gsdmd-/-* (n=4 mice; 35 FOVs) than littermate WT mice (n=4 mice; 38 FOVs) IV administered 20 oxy-Hb. Data represents mean ± SE and compared using students t-test. * Denotes $p < 0.05$.**

### 5.1.4 Inhibiting GSDMD-signaling prevented pulmonary vaso-occlusion in SCD mice.

We have shown in above results that inhibiting GSDMD-signaling prevented shedding of NETs in the liver and their translocation to the lung in SCD mice IV administered oxy-Hb. Next, we tested whether this GSDMD-dependent inhibition of the liver to lung translocation of cNETs led to amelioration of pulmonary vaso-occlusion in SCD mice administered IV oxy-Hb. To achieve this, qFILM was used to assess pulmonary vaso-occlusion in the intact lung microcirculation of live control and SCD mice following intravenous (IV) challenge with oxy-Hb with or without inhibitors. The qFILM experimental setup and is mentioned in section 2.1.5 in detail. Briefly as shown in figure 18 A, mice were IV administered via tail vein with 10 μmole/kg oxy-Hb ± inhibitors. Approximately 2-2.5 hours following IV administration, qFILM was conducted with a Nikon multi-photon-excitation fluorescence microscope. QFILM snapshots of SCD mice administered IV oxy-Hb or oxy-Hb + Z-VAD-FMK (pan-caspase inhibitor) or oxy-Hb + LDC7559 or oxy-Hb + NSA (Figure 18 B) revealed that neutrophil-platelet aggregates were blocking pulmonary arteriole-bottlenecks in SCD mice given oxy-Hb but absent in SCD mice given oxy-Hb with inhibitors. Quantitative analysis of several time-series of qFILM images revealed that the total average number of PVOs present in SCD mice given oxy-Hb with Z-VAD-FMK (Figure 18 C) or oxy-Hb with LDC7559 (Figure 18 E) or oxy-Hb with NSA (Figure 18 G) was significantly reduced in comparison to SCD mice given oxy-Hb only. Large PVOs (greater than 1000 μm*2*) also went down significantly in SCD mice administered IV oxy-Hb with Z-VAD-FMK (Figure 18 D) or oxy-Hb with LDC7559 (Figure 18 F) or oxy-Hb with NSA (Figure 18 H) compared to oxy-Hb alone.

## Figure 18

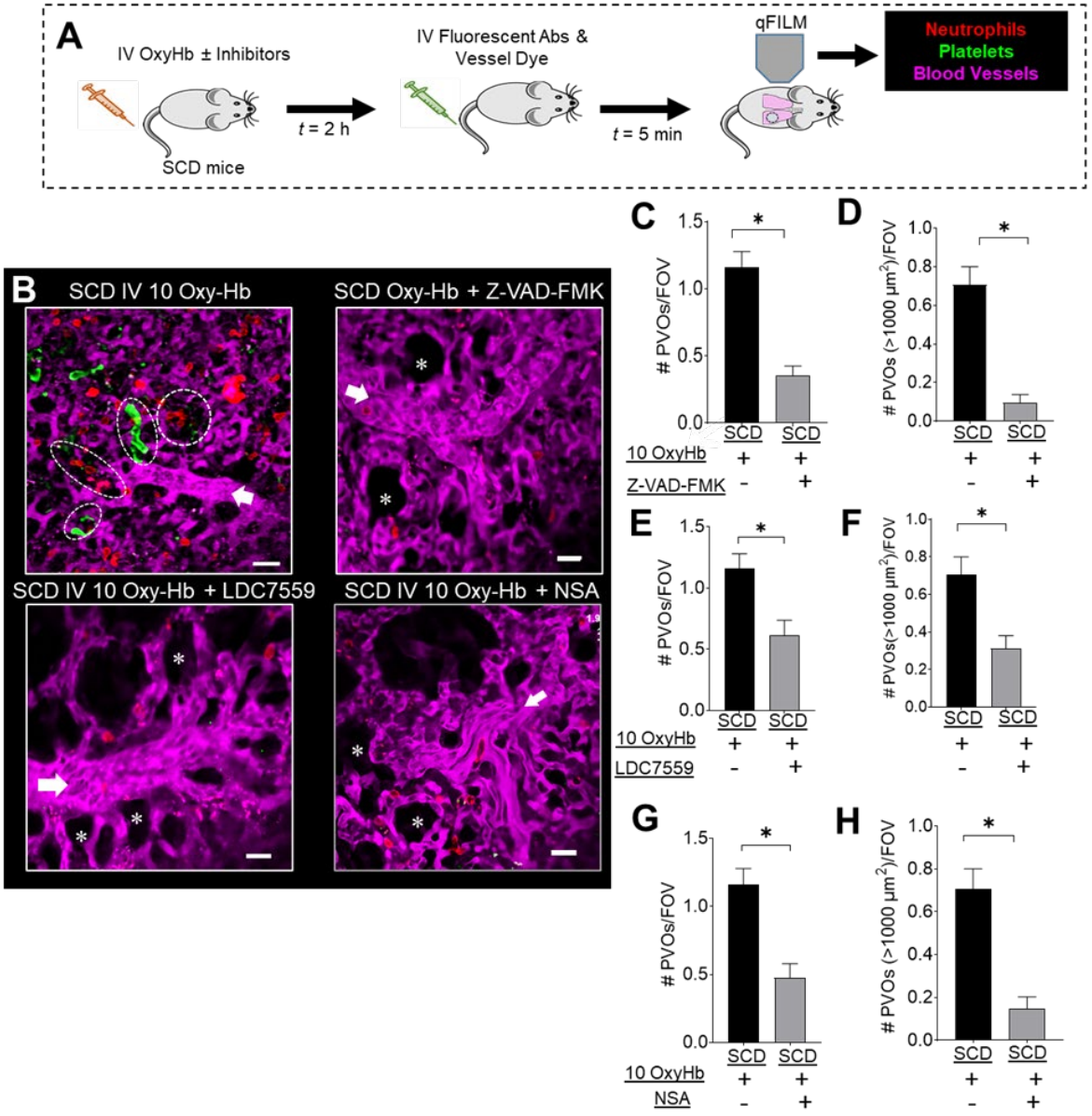


**Figure 18: Inhibiting GSDMD-signaling prevented pulmonary vaso-occlusion in SCD mice.**

**(A) Experimental scheme of SCD mice IV administered with 10 µmole/kg oxy-Hb without or with 0.004 µmol/kg pan-caspase inhibitor (Z-VAD-FMK) or 10 mg/kg GSDMD inhibitor (LDC7559) or 20 mg/kg GSDMD inhibitor necrosulfonamide (NSA). Quantitative fluorescence intravital lung microscopy (qFILM) was used to assess the absence or presence of platelet-neutrophil aggregate mediated pulmonary vaso-occlusion. Pulmonary microcirculation (pseudo-colored purple), neutrophils (red) and platelets (pseudo-colored green) were labeled in vivo by IV administration of FITC dextran, AF546-anti-Ly6G Ab and V450-**

**anti-CD49b Ab, respectively. Representative qFILM images are shown in (B), neutrophil-platelet aggregates were noticed in the bottlenecks of arteriole in SCD mice given IV oxy-Hb, whereas no neutrophil-platelet aggregates were noticed in SCD mice given oxy-Hb with Z-VAD-FMK or SCD oxy-Hb with LDC7559 or SCD oxy-Hb with NSA. Both #PVOs/FOV and #PVOs (with area > 1000 $\mu m^2$) per FOV were significantly less in SCD mice IV administered (C,D) 10 oxy-Hb + Z-VAD-FMK (n=4 mice; 51 FOVs) or (E,F) 10 oxy-Hb + LDC7559 (n=4 mice; 41 FOVs) or (G,H) 10 oxy-Hb + NSA (n=3 mice; 38 FOVs) than SCD mice IV administered 10 oxy-Hb alone (n=5 mice; 75 FOVs). qFILM FOV size~65,536 $\mu m^2$. Data represents mean ± SE and compared using students t-test. * Denotes $p < 0.05$.**

### 5.1.5 Pulmonary vaso-occlusion in the lung of SCD mice were GSDMD and P-selectin dependent.

Here, we evaluated pulmonary arteriole micro-embolism in the lung of SCD, SCD-S*elp-/-*, WT, or *Gsdmd-/-* mice using qFILM. In the current study, qFILM was used to assess pulmonary vaso-occlusion in the intact lung microcirculation of SCD, SCD-*Selp-/-*, WT, or *Gsdmd-/-* mice following intravenous (IV) challenge Oxy-Hb. The qFILM experimental setup is mentioned in section 2.1.5 in detail and schematic is shown in Figure 19. A qFILM snapshot of SCD-*Selp-/-* administered IV 10 µmole/kg oxy-Hb or IV 10 µmole/kg oxy-Hb with LDC7559 or WT mice administered IV 20 µmole/kg oxy-Hb or *Gsdmd-/-* mice administered IV 20 µmole/kg oxy-Hb are shown in Figure 19 B, and it reveals that one neutrophil aggregate is present in the arteriole bottle-neck of a SCD-*Selp-/-* IV 10 µmole/kg oxy-Hb, and one neutrophil aggregate is present in the arteriole bottle-neck of a WT IV 20 oxy-Hb in the lung micro-circulation. However, there is absence of neutrophil-platelet aggregates in the lung micro-circulation of SCD-*Selp-/-* IV 10 µmole/kg oxy-Hb with LDC7559, and *Gsdmd-/-* IV 20 µmole/kg oxy-Hb. Quantitative analysis of several time-series of qFILM images revealed that the total average number of PVOs present in SCD-*Selp-/-* mice given Oxy-Hb is almost twice than SCD-*Selp-/-* mice given oxy-Hb with LDC7559 (Figure 19 C). Average number of PVOs greater than 1000 $\mu m^2$ went down to null per FOV in SCD-*Selp-/-* mice given oxy-Hb with LDC7559 (Figure 19 D). Similarly, quantitative analysis of several time-series of qFILM images reveled that the total average number of PVOs present in WT mice given 20 IV µmole/kg oxy-Hb is almost twice than *Gsdmd-/-* mice given IV 20 µmole/kg oxy-Hb (Figure 19 E), and PVOs greater than 1000 $\mu m^2$ were also significantly reduced in *Gsdmd-/-* mice given IV 20 µmole/kg oxy-Hb (Figure 19 F). These results suggest that

inhibiting GSDMD-signaling prevents P-selectin-independent pulmonary vaso-occlusion in SCD mice.

**Figure 19**

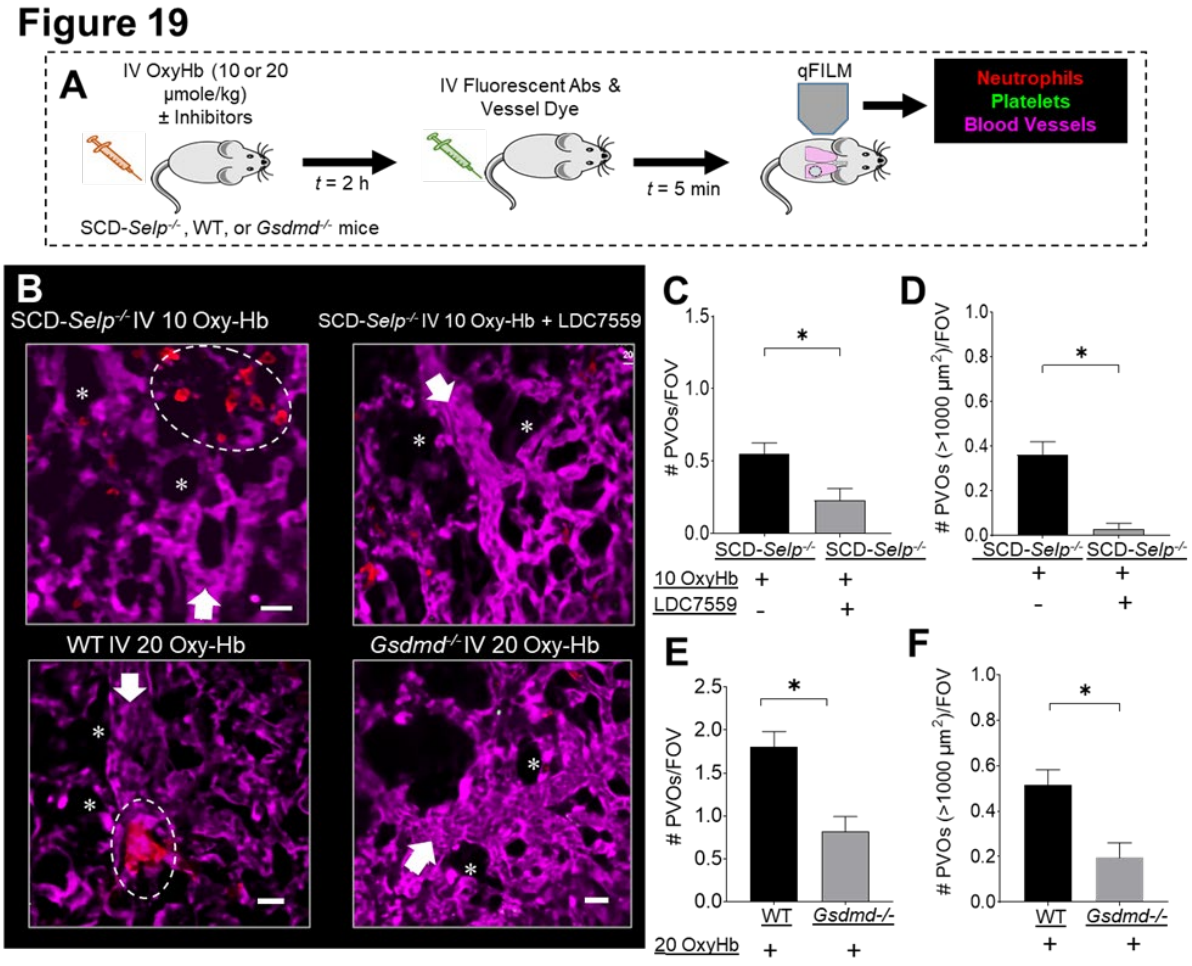


**Figure 19: Pulmonary vaso-occlusion in the lung of SCD mice were GSDMD and P-selectin indendent. (A) Experimental schematic of qFILM imaging approach for SCD-*Selp-/-* mice IV 10 µmole/kg oxy-Hb or SCD-*Selp-/-* mice IV 10 µmole/kg oxy-Hb with LDC7559 or WT 20 µmole/kg oxy-Hb or 20 µmole/kg oxy-Hb *Gsdmd-/-* mice. Quantitative fluorescence intravital lung microscopy (qFILM) was used to assess the absence or presence of platelet-neutrophil aggregate mediated pulmonary vaso-occlusion. Pulmonary microcirculation (pseudo-colored purple), neutrophils (red) and platelets (pseudo-colored green) were labeled in vivo by IV administration of FITC dextran, AF546-anti-Ly6G Ab and V450-anti-CD49b Ab, respectively. Representative qFILM images are shown in (B), pulmonary vaso-occlusion was noticed in the bottlenecks of arteriole in SCD-*Selp-/-* mice given IV oxy-Hb and WT mice IV 20 µmole/kg oxy-Hb, whereas no pulmonary**

**vaso-occlusion was noticed in SCD-*Selp-/-* mice given IV oxy-Hb with LDC7559 or *Gsdmd-/-* mice 20 µmole/kg oxy-Hb. Dotted eclipse represents PVO, arrow shows direction of blood flow, asterisk mark shows air alveoli and scale bar is 20 µm. (C) #PVOs/FOV were significantly reduced and (Q) #PVOs (with area > 1000 µm$^2$) per FOV were absent in SCD-*Selp-/-* mice IV administered 10 µmole/kg oxy-Hb + LDC7559 (n=3 mice; 35 FOVs) compared to SCD-*Selp-/-* mice IV administered 10 µmole/kg oxy-Hb alone (n=5 mice; 69 FOVs). Both (E) #PVOs/FOV and (F) #PVOs (with area > 1000 µm$^2$) per FOV were significantly less in *Gsdmd-/-* (n=3 mice; 28 FOVs) than littermate WT mice (n=3 mice; 31 FOVs) IV administered 20 µmole/kg oxy-Hb. qFILM FOV size~65,536 µm$^2$. Data represents mean ± SE and compared using students t-test. * Denotes $p < 0.05$.**

## 5.2 Discussion

Recently, P-selectin inhibition or deletion was shown to attenuate lung vaso-occlusion in SCD mice by ~50%[3, 12, 48]. In support of these findings, P-selectin Ab therapy was shown to prevent hospitalization by ~50% in SCD patients[35], suggesting a role for P-selectin-independent mechanism in promoting remaining ~50% morbidity. Here, we have used intravital microscopy of lung (qFILM), liver (qLIM), and kidney (qKIM) in SCD mice, imaging flow cytometry of SCD mice or patient plasma and confocal microscopy freshly isolated liver sections to identify this P-selectin independent mechanism of lung vaso-occlusion. We show that IV oxy-Hb triggered occlusion of pulmonary arteriole bottlenecks in the lung of SCD but not control mice, which was secondary to arrival of cNETs from liver to lung microcirculation. These cNETs were found to be shed in the liver of SCD mice in a GSDMD-dependent manner, and then traveled to the lung to promote neutrophil-platelet aggregation in pulmonary arterioles. Surprisingly, the liver to lung translocation of cNETs was not P-selectin-dependent but dependent on ROS, caspase-4 (humans) or caspase-11 (mouse) -dependent activation of neutrophil-GSDMD signaling. Remarkably, inhibition of GSDMD signaling by inhibiting caspase-4/11 or direct GSDMD inhibition/deletion not only prevented cNETs shedding ex-vivo in human blood or in mouse in-vivo but also prevented pulmonary vaso-occlusion by ~50% on SCD and ameliorated pulmonary vaso-occlusion in SCD-*selp-/-* mice, suggesting that GSDMD-pathway promotes P-selectin-dependent pulmonary vaso-occlusion in SCD. Although the current data suggest that GSDMD-signaling contributes to the P-selectin-independent mechanism of ACS, it does not confirm whether this primarily the result of the activation of GSDMD-signaling in neutrophils. However, this can be confirmed in future studies by generating SCD mice lacking GSDMD only in neutrophils ($SCD^{GsdmdLy6g}$). Less than ~50% protection in $SCD^{GsdmdLy6g}$ mice may suggest a role for GSDMD in cells other than

neutrophils as well. Notwithstanding these limitations, my current finding suggests that targeting both P-selectin and GSDMD may provide significant protection from pulmonary vaso-occlusion and development of ACS in SCD.

## 5.3 Conclusion

Inhibiting GSDMD-signaling attenuated cNETs in SCD human blood ex vivo as well in SCD mice in vivo. Inhibiting GSDMD-signaling prevented cNETs shedding, cNETs translocation from liver to lung and attenuated pulmonary vaso-occlusion in SCD mice in vivo. Inhibiting GSDMD-signaling also abolished remaining (~50%) pulmonary vaso-occlusion in SCD-*Selp-/-* mice in vivo.

# 6.0 Additional studies performed during doctoral program.

## 6.1 Role of platelet extracellular vesicles in pulmonary vaso-occlusion

*Note:* Result of this section was previously published as: Ravi Vats*, Tomasz Brzoska*, Margaret F. Bennewitz*, Maritza A. Jimenez*, Tirthadipa Pradhan-Sundd, Egemen Tutuncuoglu, Jude Jonassaint, Edgar Gutierrez, Simon C. Watkins, Sruti Shiva, Melanie J. Scott, Adrian E. Morelli, Matthew D. Neal, Gregory J. Kato, Mark T. Gladwin, and Prithu Sundd. Platelet Extracellular Vesicles Drive Inflammasome–IL-1β–Dependent Lung Injury in Sickle Cell Disease. Am J Respir Crit Care Med Vol 201, Iss 1, pp 33–46, Jan 1, 2020.

*These authors have equally contributed to this manuscript and are co–first authors. Experiments and analysis for figure 5 and figure 6 were conducted by Ravi Vats of this manuscript except isolation of platelet extracellular vesicles.

### 6.1.1 Platelet extracellular vesicles promote lung vaso-occlusion in SCD mice in-vivo.

Figure 20 A shows the schematic of qFILM experiment conducted, where donor SCD or control mice were administrated with IV 1 μg/kg LPS; platelet EVs were isolated from donor SCD or control mice blood and then IV transferred into unchallenged recipient SCD mice[45]. qFILM was done on recipient SCD mice to access lung vaso-occlusion. Figure 20 B-D shows the representative images obtained from qFILM done on recipient SCD mice. qFILM reveals that large neutrophil-platelet aggregates are blocking arteriole bottlenecks in the lung of recipient SCD mice after IV administration of SCD platelet EVs. IV administration of SCD platelet EVs caused a significant increase in the average number of PVO per FOV (Figure 20 E) in comparison to saline IV administration to SCD mice[45]. Average number of PVO per FOV with area greater than 1000 $\mu m^2$ also showed a significant increase in SCD IV platelets EVs mice in comparison to SCD IV saline (Figure 20 F). No difference was noticed when average number of PVO per FOV were compared between IV SCD platelet EVs given to recipient SCD mice group to IV LPS SCD mice (Figure 20 G). Similarly, no difference was noticed in analysis of average number of PVO per FOV with area greater than 1000 $\mu m^2$ compared between both groups (Figure 20 H)[45]. Figure 20 I show the schematic where donor SCD mice was administrated with IV LPS, and then after 3 hours platelet EVs were isolated and stained with chloromethyl-dialkylcarbocyanine (CM-DiI). Further, stained platelet EVs were IV administrated to recipient SCD mice and then qFILM was performed. (J-L) shows representative qFILM images from recipient SCD mice, where SCD platelet EVs (yellow) bound to neutrophil aggregates (red) in the lung arterioles (purple) of recipient SCD mice intravenously administered CM-DiI-stained SCD platelet EVs[45].

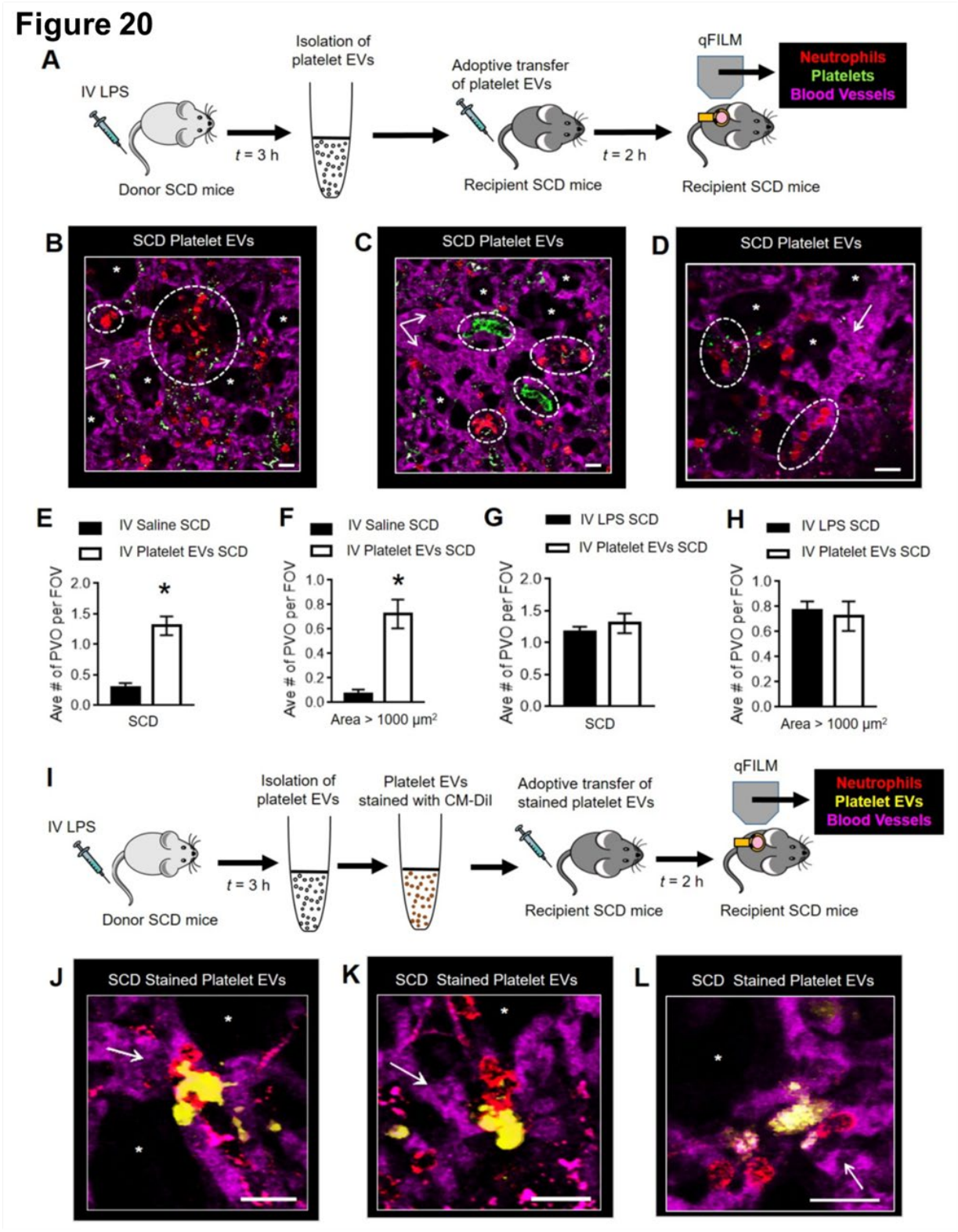


**Figure 20: Platelet extracellular vesciles promote lung vaso-occlusion in SCD mice.**

**This figure is taken with permission from reference[45]. (A) Donor SCD mice were IV administered with LPS (1 μg/kg), platelet EVs were isolated from the blood and adoptively (IV) transferred (~5 x 108 platelet EVs per mouse) into unchallenged recipient SCD mice. Lung vaso-occlusion was assessed in recipient mice using qFILM and compared to lung vaso-occlusion in SCD mice administered IV LPS or saline. (B-D) Three representative qFILM images reveal large neutrophil-platelet aggregates (marked by dotted white circles) blocking arteriolar bottlenecks in the lung of SCD mice IV administered platelet EVs. IV administration of platelet EVs caused a significant increase in the (E) average number of pulmonary vaso-occlusions per FOV and (F) large pulmonary vaso-occlusions with area > 1000 $\mu m^2$ in SCD mice compared to IV saline. (G) The average number of pulmonary vaso-occlusions per FOV and (H) large pulmonary vaso-occlusions (area > 1000 $\mu m^2$) per FOV in SCD mice administered platelet EVs were comparable and not different from those in SCD mice administered 0.1 μg/kg LPS. Saline (n = 2 mice; 44 FOVs), 0.1 μg/kg LPS (n = 5 mice; 116 FOVs) and platelet EVs (n = 3 mice; 49 FOVs). Average number of pulmonary vaso-occlusions per FOV and large pulmonary vaso-occlusions (area > 1000 $\mu m^2$) per FOV were compared between groups using the unpaired Student's t test. Error bars are mean ± SE. * $p < 0.05$. Pulmonary microcirculation (pseudo-colored purple), neutrophils (red) and platelets (pseudo-colored green). (I) Experiments described in scheme (A) were repeated with platelet EVs stained with CM-DiI. (J-L) Three representative qFILM images showing platelet EVs (yellow) bound to neutrophil aggregates (red) in the lung arterioles of SCD mice IV administered CM-DiI-stained platelet EVs. Pulmonary microcirculation (FITC dextran, pseudo-colored purple), neutrophils (Pacific Blue Ly6G, pseudo-colored red) and platelet EVs (CM-DiI, pseudo-colored yellow). Alveoli marked with asterisks. The white arrows denote the direction of blood flow. Scale bars 20 μm[45].**

### 6.1.2 Platelet extracellular vesicle-induced lung vaso-occlusion is IL-1β and caspase-1 dependent.

Figure 21 A shows the schematic representation of experiment performed, where donor SCD mice was administrated with IV LPS 1 μg/kg, platelet EVs were isolated from the blood after 3 hours of IV and then isolated platelet EVs were administrated into IV recipient SCD mice without or with 10 mg/kg IL-1 receptor antagonist (IL-1RA), or 0.004 μmol/kg caspase-1 inhibitor YVAD[45]. Further, lung vaso-occlusion was assessed in recipient SCD mice using qFILM. Representative qFILM images reveal (Figure 21 B) presence of large neutrophil–platelet aggregates (marked by dashed white circles) blocking arteriolar bottlenecks in the lung of a recipient SCD mouse intravenously administered SCD platelet EVs, however (Figure 21 C & D) absence of platelet–neutrophil aggregates in the lung of a recipient SCD mouse intravenously administered SCD platelet EVs with IL-1RA or SCD platelet EVs with YVAD[45]. After analyzing data obtained from qFILM, the average number of PVOs per FOV (Figure 21 E) and large PVOs with area greater than 1000 $\mu m^2$ (Figure 21 F) were significantly reduced in recipient SCD mice administrated with IV SCD platelet EVs and IL-1RA together in comparison to just IV SCD platelet EVs[45]. Similarly, the average number of PVOs per FOV (Figure 21 G) and large PVOs with area greater than 1000 $\mu m^2$ (Figure 21 H) were significantly reduced in recipient SCD mice administrated with IV SCD platelet EVs and YVAD together in comparison to just IV SCD platelet EVs[45].

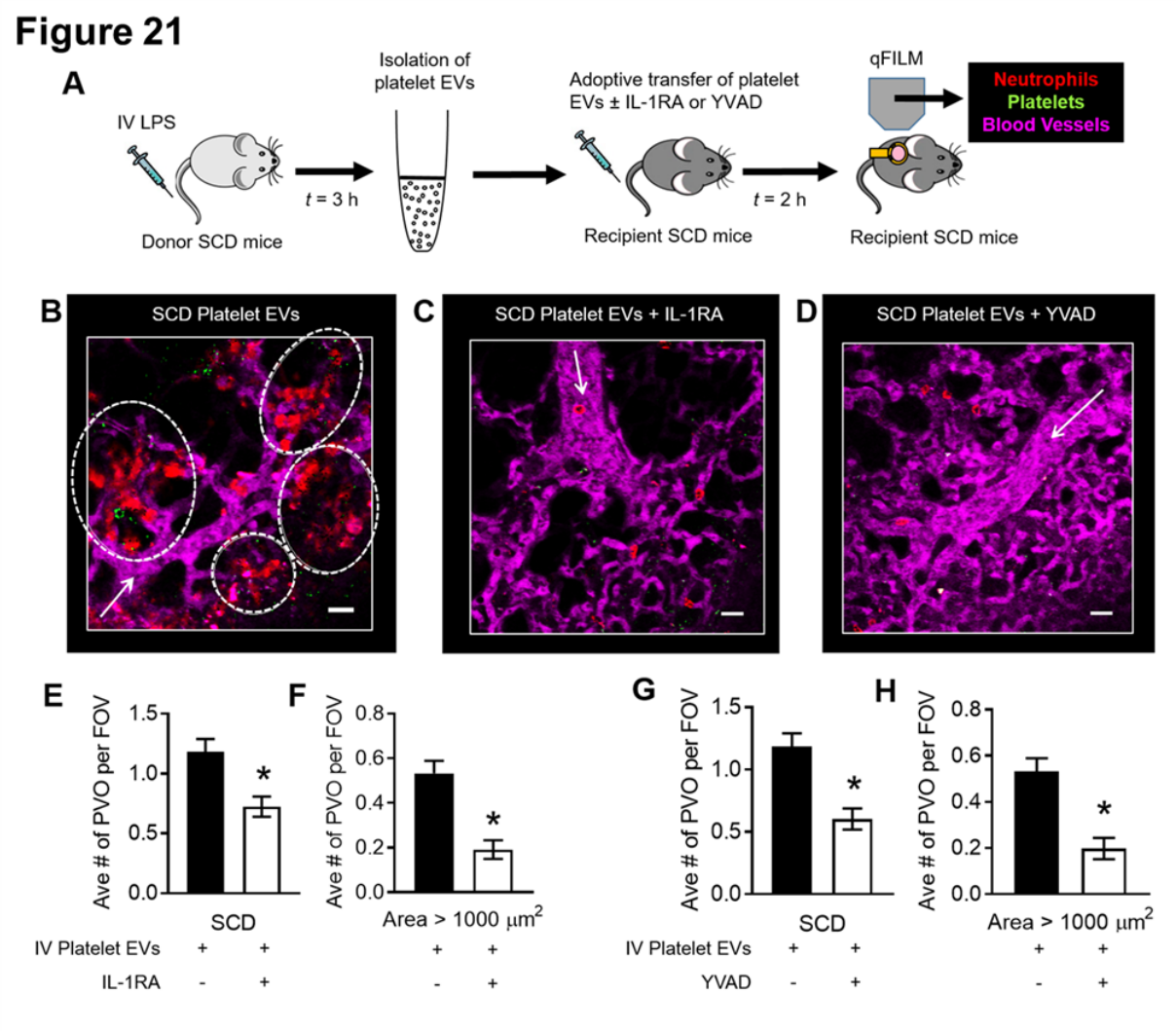


**Figure 21: Platelet extracellular vesicle-induced lung vaso-occlusion is IL-1β and caspase-1 dependent. This figure is taken with permission from reference[45]. (A) Experimental scheme: Donor SCD mice were intravenously administered LPS (1 μg/kg); platelet EVs were isolated from the blood and adoptively (intravenously) transferred into unchallenged recipient SCD mice without (n = 6 mice; 87 FOVs) or with (n = 5 mice; 76 FOVs) 10 mg/kg IL-1 receptor antagonist (IL-1RA), or 0.004 μmol/kg caspase-1 inhibitor YVAD (n = 5 mice; 68 FOVs)[45]. Lung vaso-occlusion was assessed in recipient mice using qFILM. Representative qFILM images reveal (B) presence of large neutrophil–platelet aggregates (marked by dashed white circles) blocking arteriolar bottlenecks in the lung of a recipient SCD mouse intravenously administered SCD platelet EVs and (C and D) absence of platelet–neutrophil aggregates in the lung of a recipient SCD mouse intravenously administered SCD platelet EVs with IL-1RA or SCD platelet EVs with**

**YVAD. (E) The average number of pulmonary vaso-occlusions (PVOs) per FOV and (F) large PVOs (area > 1,000 μm$^2$) per FOV were significantly reduced in recipient SCD mice administered SCD platelet EVs with IL-1RA compared with recipient SCD mice administered SCD platelet EVs only[45]. (G) The average number of PVOs per FOV and (H) large PVOs (area > 1,000 μm$^2$) per FOV were significantly reduced in recipient SCD mice administered SCD platelet EVs with YVAD compared with recipient SCD mice administered SCD platelet EVs only. The average number of PVOs per FOV and large PVOs (area > 1,000 μm$^2$) per FOV were compared between groups using the unpaired student's t test. Error bars are SE. Pulmonary microcirculation (pseudo colored purple), neutrophils (red) and platelets (pseudo colored green) are shown. The white arrows denote the direction of blood flow[45]. Scale bars, 20 μm. *P < 0.054.**

## 6.2 Hepato-pathophysiology of liver in SCD

### 6.2.1 Dysregulated bile transporters and impaired tight junctions during chronic liver injury in mice

*Note:* Result of this section was previously published as: Tirthadipa Pradhan-Sundd, Ravi Vats, Jacquelyn O. Russell, Sucha Singh, Adeola Adebayo Michael, Laura Molina, Shelly Kakar, Pamela Cornuet, Minakshi Poddar, Simon C. Watkins, Kari N. Nejak-Bowen, Satdarshan P. Monga, and Prithu Sundd. Dysregulated Bile Transporters and Impaired Tight Junctions During Chronic Liver Injury in Mice. Gastroenterology 2018; 155:1218–1232.

In this manuscript first time qLIM was introduced and published. All qLIM experiments were designed and conducted by Ravi Vats.

In this manuscript, two experimental models of chronic liver injury were used in mice fed choline deficient, ethionine-supplemented (CDE) or 3,5-diethoxycarbonyl 1,4-dihydrocollidine (DDC) diet, respectively[56]. Using our recently developed quantitative liver intravital microscopy (qLIM) approach, we show that chronic liver injury involves physical breach of blood-bile barrier (BBlB), mixing of blood with bile, and loss of bile transport across hepatocytes[56]. Our data suggest that loss of Tight Junction (TJ) adhesion molecules such as claudins and basolateral or canalicular bile transporters from hepatocytes is the central pathophysiology in chronic liver injury irrespective of the experimental model[56]. Finally, we show that the recovery from liver injury is dictated by the ability of BBlB to regain physical integrity through reappearance of TJ adhesion molecules and bile transporters on hepatocytes[56].

Figure 22 qLIM enables real-time assessment of BBlB in the intact liver of live mice. Time series images of (Figure 22 A) 3 minutes, (Figure 22 B) 10 minutes, and (Figure 22 C) 20 minutes

of liver of mouse fed on normal chow shows localization of carboxyfluorescein (CF) (green) and TXR-dextran (red) in bile canaliculi and sinusoids, respectively[56]. (Figure 22 D) qLIM schematic diagram of liver section of mouse fed with normal chow. Time series images of (Figure 22 E) 3 minutes, (Figure 22 F) 10 minutes, and (Figure 22 G) 20 minutes of (n = 1) liver of mouse fed on CDE diet for 4 days show complete localization of CF (green) and TXR-dextran (red) in liver sinusoids. (Figure 22 H) qLIM schematic diagram of liver section of mouse fed with CDE diet for 4 days[56]. Time series images of (Figure 22 I) 3 minutes, (Figure 22 J) 10 minutes, and (Figure 22 K) 20 minutes of (n = 1) liver of mouse fed on DDC diet for 6 days show localization of CF (green) and TXR-dextran (red) in hepatocytes and sinusoids, respectively[56]. (Figure 22 L) qLIM schematic diagram of liver section of mouse fed with DDC diet for 6 days[56].

Figure 22

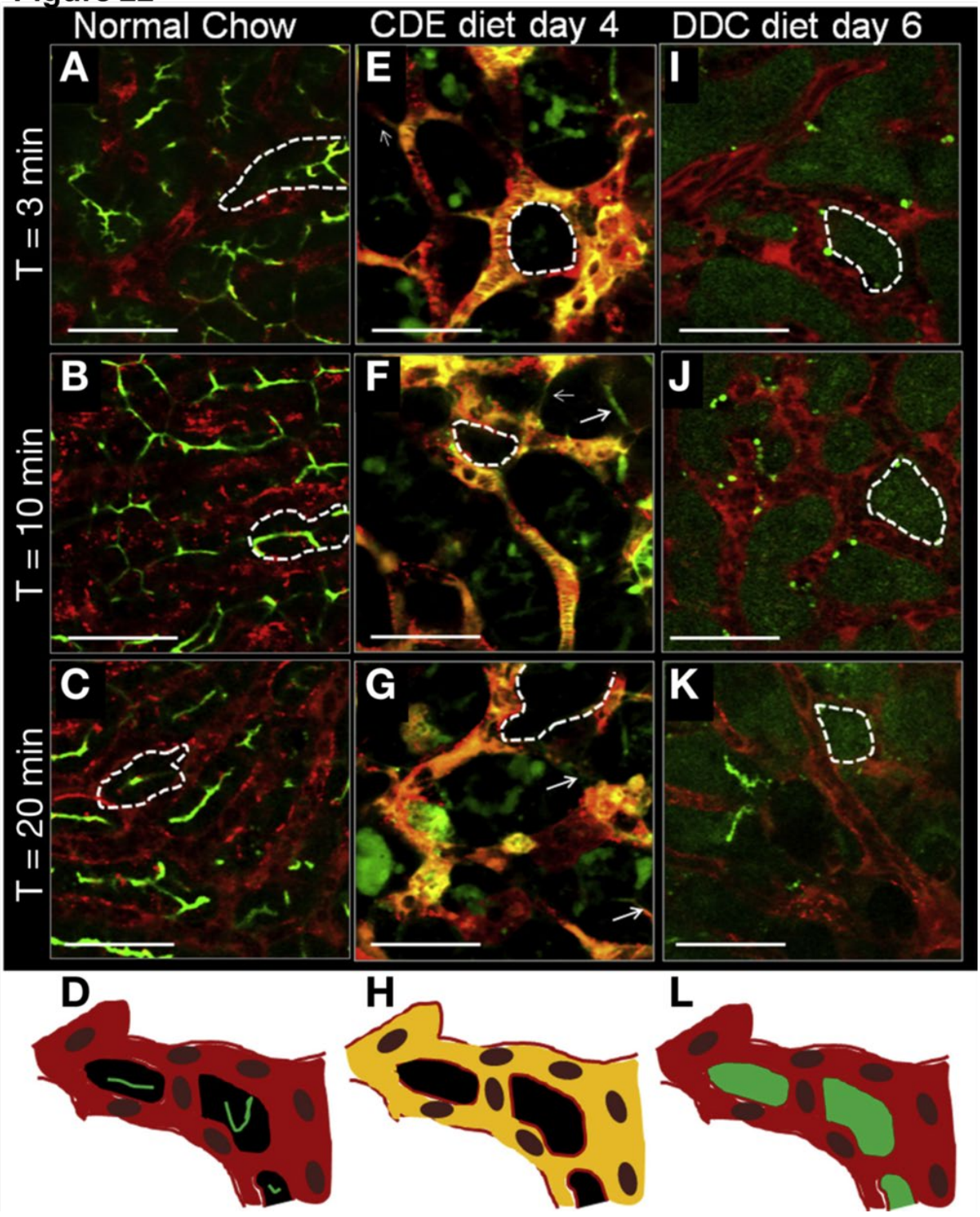


**Figure 22: Dysregulated bile transporters and impaired tight junctions during chronic liver injury in mice.**

**This figure is taken with permission from reference[56]. qLIM shows liver injury progression in CDE and DDC regimen. Time series images of (A) 3 minutes, (B) 10 minutes, and (C) 20 minutes of liver of mouse fed on normal chow shows localization of CF (green) and TXR-dextran (red) in bile canaliculi and sinusoids, respectively[56]. (D) qLIM schematic diagram of mouse liver section fed with normal chow. Time series images of (E) 3 min, (F) 10 min, and (G) 20 min of mice liver fed on CDE diet for 14 days shows localization of CF (green) and TXRdextran (red) in bile canaliculi and sinusoids, respectively. (H) qLIM schematic diagram of mouse liver section fed with CDE diet for 14 days. Time series images of (I) 3 min, (J) 10 min, and (K) 20 min of mouse liver fed on DDC diet for 14 days shows complete localization of CF (green) and TXRdextran (red) in liver sinusoids. (L) qLIM schematic diagram of mouse liver section fed with DDC diet for 14 days. Arrow denotes presence of these conduits through which blood and bile are leaking, and dotted lines represent hepatocytes[56].**

### 6.2.2 Impaired bile secretion promotes hepatobiliary injury in sickle cell disease.

*Note:* Result of this section was previously published as: Ravi Vats, Silvia Liu, Junjie Zhu, Dhanunjay Mukhi, Egemen Tutuncuoglu, Nayra Cardenes, Sucha Singh, Tomasz Brzoska, Karis Kosar, Mikhil Bamne, Jude Jonassaint, Adeola Adebayo Michael, Simon C. Watkins, Cheryl Hillery, Xiaochao Ma, Kari Nejak-Bowen, Mauricio Rojas, Mark T. Gladwin, Gregory J. Kato, Sadeesh Ramakrishnan, Prithu Sundd, Satdarshan Pal Monga, and Tirthadipa Pradhan-Sundd. Impaired Bile Secretion Promotes Hepatobiliary Injury in Sickle Cell Disease. Hepatology, 2020;72:2165-2181.

In this manuscript qLIM was used to show ischemic liver injury in SCD mice. All qLIM experiment were designed and conducted by Ravi Vats.

Figure 23 A shows the schematic of qLIM[44, 56] used in this manuscript and described in detail in section 2.0.6. Figure 23 B, B', B'' shows the representative obtained from qLIM shows that very less blockage of blood flow in the liver of control mice injected with TXR-dextran (red), whereas in Figure 23 C, C', C'' shows the representative images obtained from qLIM shows massive blood stoppage and blockage in the liver of SCD mice injected with TXR-dextran (red)[44]. After analyzing data from qLIM, the total percent area with loss of blood flow in SCD mice is close to 50% whereas in control mice its null as shown in (D). (E) shows the average number of vaso-occlusion per FOV in SCD mice is almost eight time more than in control mice[44].

## Figure 23

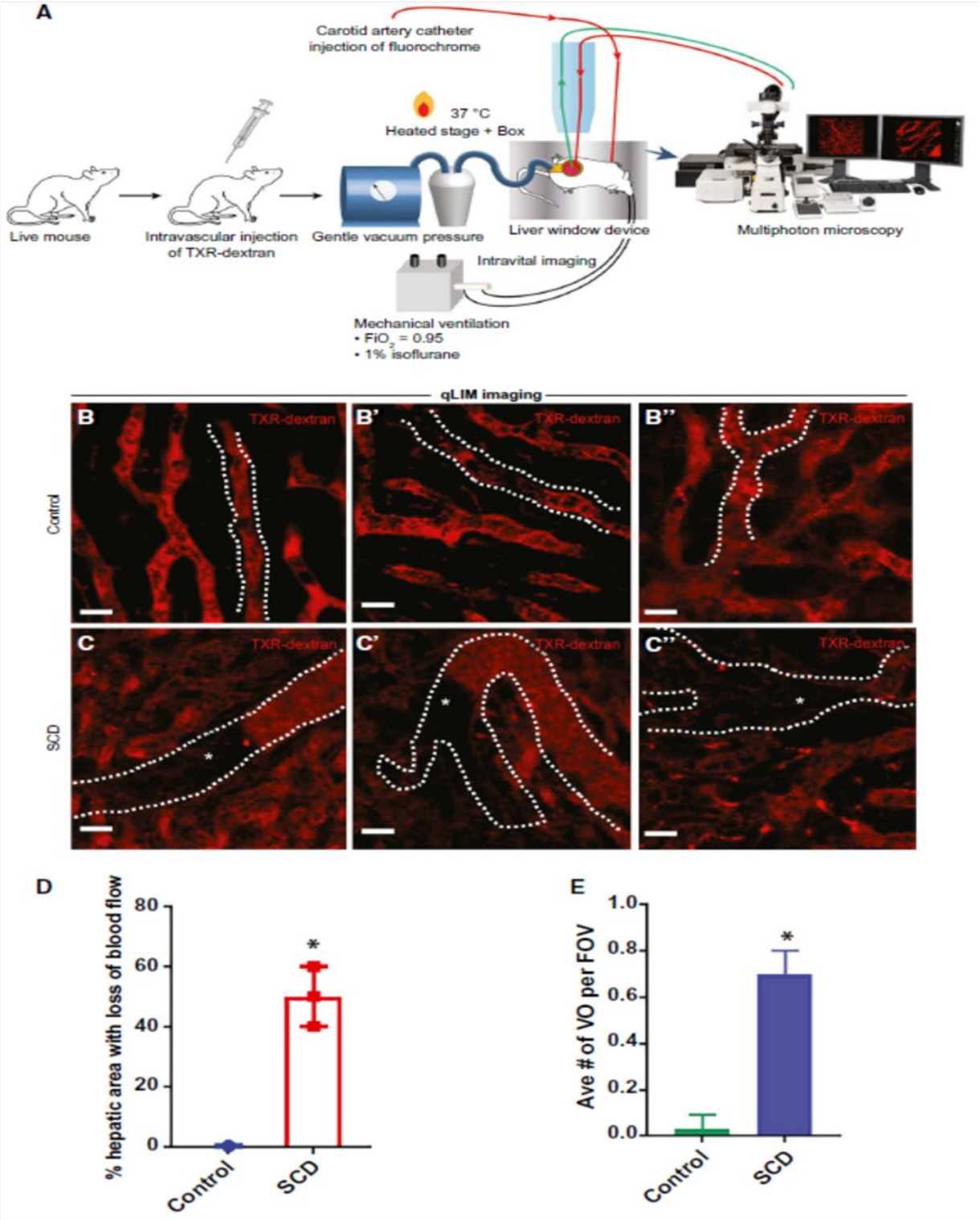


**Figure 23: Imparied bile secretion promote hepatobiliary injury in sickle cell disease.**

**This figure is taken with permission from reference[44]. SCD mice exhibit ischemic liver injury at baseline. (A) Schematic diagram of qLIM of mice using TXR-dextran. qLIM images of three different fields of view of (B-B″) control and (C-C″) SCD liver injected with TXR-dextran[44]. Dotted line marks the sinusoids. Asterisk shows loss of blood flow in SCD liver. (D) Quantification of the total area of liver with loss of blood flow, and (E) average number of vaso-occlusions per field of view in SCD and control mice. *P < 0.05. Scale bar, 30 μm[44].**

Here in Figure 24, qLIM imaging reveals reduced bile flow in SCD liver[44]. (Figure 24 A) Schematic diagram of qLIM imaging of control or SCD mice IV injected with CF and TXR-dextran. (Figure 24 B) Intravital time series images of (b-d′) control and (e-g′) SCD mouse livers at different time points i.e., 1 min, 3 min, and 10 min. In liver of control mice, CF and TXR-dextran are nicely distributed in bile canaliculi and liver sinusoids, respectively[44]. Whereas in liver of SCD mice, CF stays in hepatocytes for long and blockage of blood flow in seen in liver sinusoids as shown by TXR-dextran[44]. (Figure 24 C) Quantification of CF intensity in hepatocytes at 1, 4, and 10 minutes after injection in control and SCD mouse livers. The SCD liver showed a significant increase in CF intensity at 4 and 10 minutes compared to control liver[44].

## Figure 24

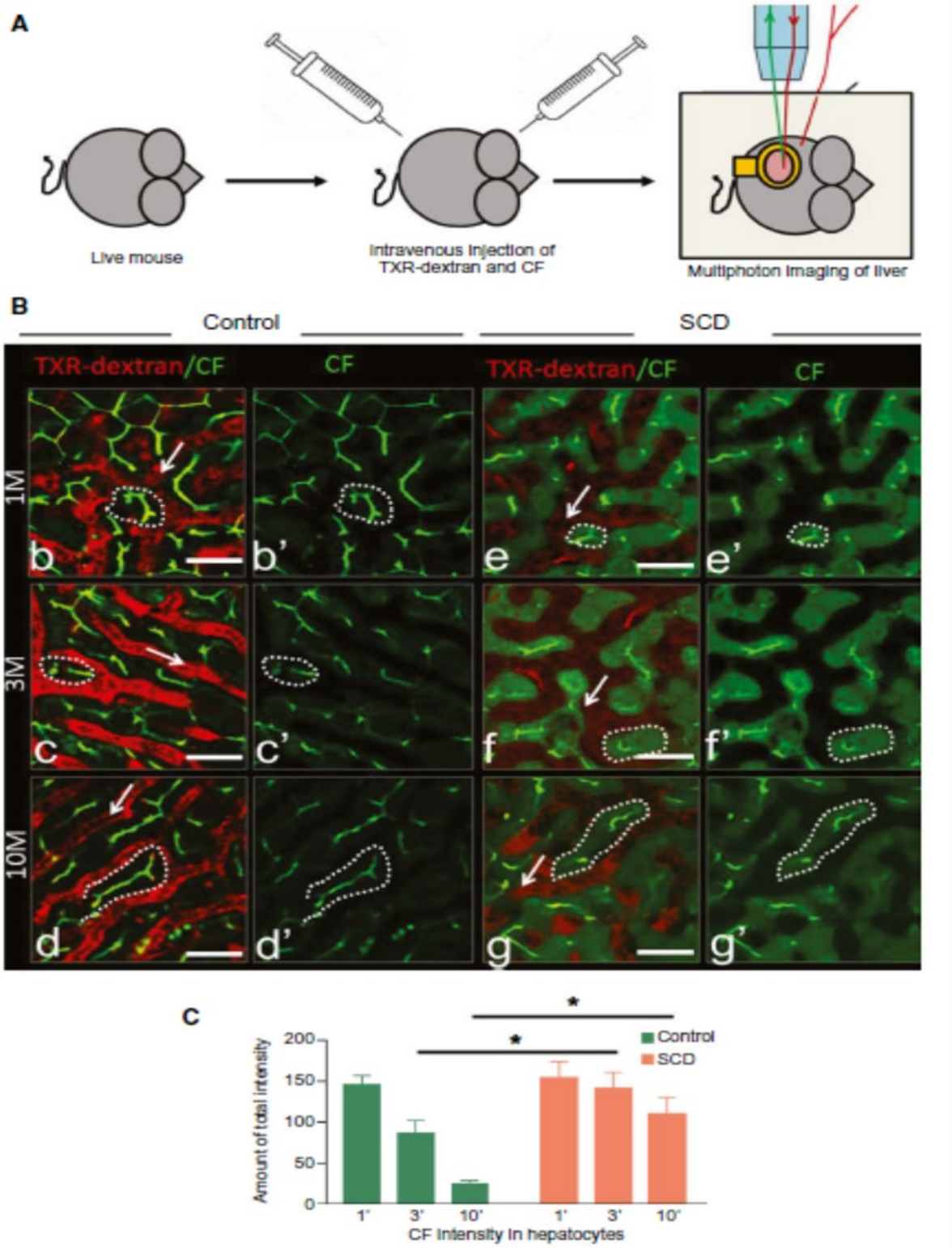


**Figure 24: Impaired bile secretion promotes hepatobiliary injury in SCD mice.**

**This figure is taken with permission from reference[44]. qLIM imaging reveals reduced bile flow in SCD liver. (A) Schematic diagram of qLIM imaging of mice using CF and TXRdextran. (B) Intravital time series images of (b-d and b'-d') control and (e-g and e'-g') SCD mouse livers. Images at 1 min (b,e), 4 min (c,f), and 10 min (d,g) post administration of CF (green) and TXR-dextran (red). (C) Quantification of CF intensity in hepatocytes at 1, 4, and 10 min after injection in control and SCD mouse livers. The SCD liver showed a significant increase in CF intensity at 4 and 10 min compared to control liver. *P < 0.05. Scale bar, 30 µm[44].**

### 6.2.3 P-selectin deficiency promotes liver senescence in sickle cell disease mice.

*Note:* Result of this section was previously published as: Ravi Vats, Tomasz W. Kaminski, Eun-Mi Ju, Tomasz Brozska, Egemen Tutuncuoglu, Jesus Tejero, Enrico M. Novelli, Prithu Sundd, and Tirthadipa Pradhan-Sundd. P-selectin deficiency promotes liver senescence in sickle cell disease mice. Blood 13 May 2021 | volume 137, number 19.

In this manuscript qLIM was used to show that p-selectin deficiency promotes blockage of blood flow and liver injury in sickle cell disease mice. All qLIM experiment were designed and conducted by Ravi Vats.

Figure 25 A shows the schematic representation of qLIM performed in this manuscript[55]. Here SCD or SCD-*Selp-/-* mice were used. CF and TXR-dextran were IV administrated to visualize bile canaliculi and blood flow, respectively. Further qLIM was performed[55]. Figure 25 B top row shows the representative images obtained from qLIM where massive blockage of blood flow is noticed in SCD mice shown by dotted circle. However, very few blockages and increase in blood flow was noticed in SCD-*Selp-/-* mice bottom row (Figure 25 B). After quantification of qLIM data, percent area with vaso-occlusion in SCD-*Selp-/-* mice were significantly decreased in comparison to SCD mice (Figure 25C). (Figure 25 D) shows the percentage of total number of vaso-occlusion per FOV, and it shows that in SCD-*Selp-/-* mice this was significantly reduced in comparison to SCD mice[55].

# Figure 25

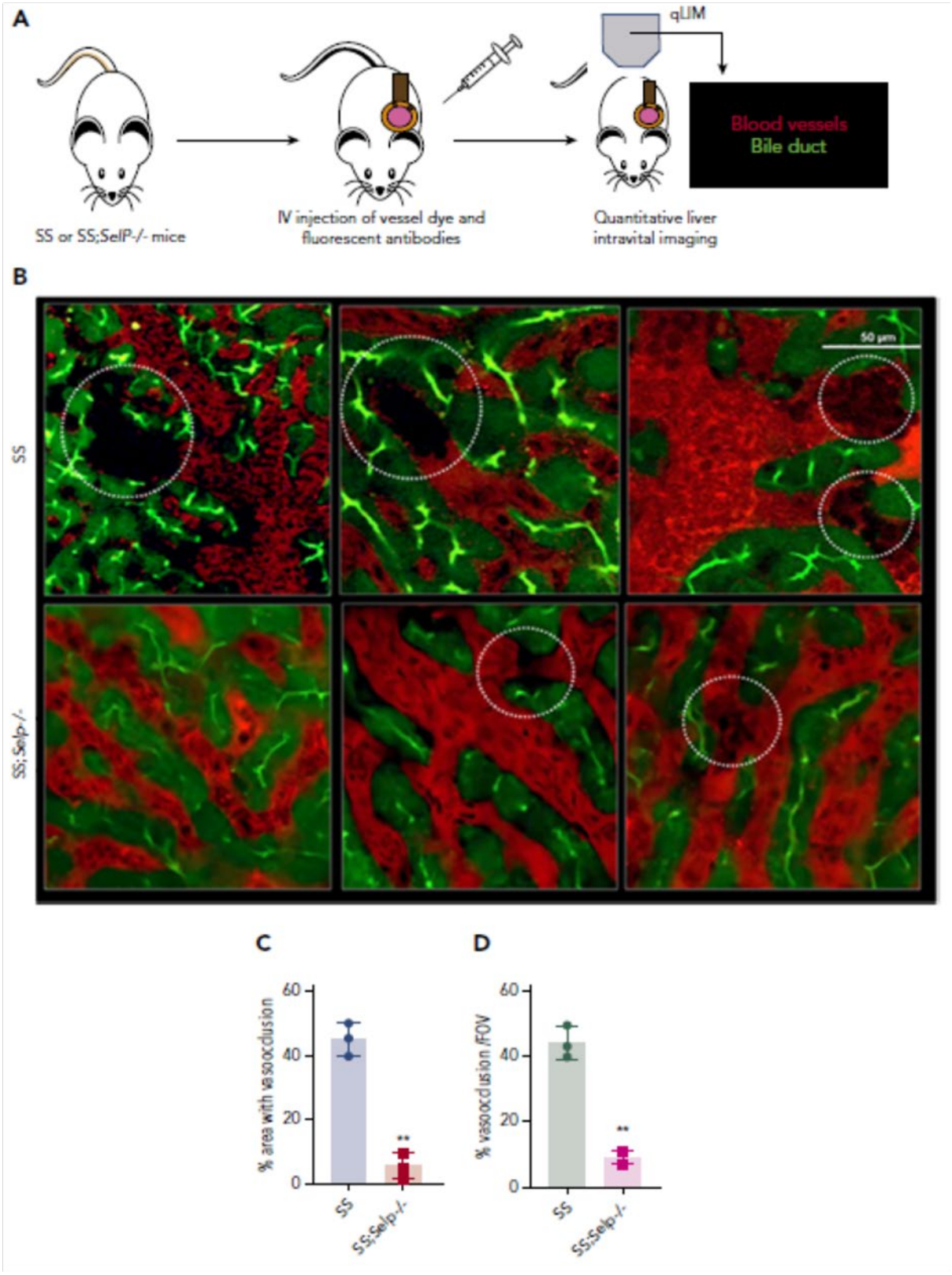
A
qLIM
Blood vessels
Bile duct
SS or SS;Selp-/- mice
IV injection of vessel dye and fluorescent antibodies
Quantitative liver intravital imaging
B
SS
SS;Selp-/-
50 µm
C
% area with vasoocclusion
60
40
20
0
**
SS
SS;Selp-/-
D
% vasoocclusion /FOV
60
40
20
0
**
SS
SS;Selp-/-

**Figure 25: P-selectin deficiency promotes liver senescence in SCD mice.**

**This figure is taken with permission from reference[55]. P-selectin–deficient SCD mice exhibit amelioration of ischemic liver injury at baseline. (A) Schematic diagram of qLIM imaging of mice using TXR-dextran and CF to visualize blood flow and bile canaliculi, respectively. (B) qLIM images of 3 different FOVs of SS and P-selectin–deficient SCD liver (SS-*Selp-/-*) injected with TXR-dextran and CF. Dotted circle shows loss of blood flow in SCD liver, which was significantly improved in SS-*Selp-/-* liver. Scale bar is 50 µm. (C) Quantification of the total area (%) of liver with loss of blood flow in SS and SS-*Selp-/-* liver. (D) Percentage of total number of vaso-occlusion/FOV. **P < .01[55].**

## 6.3 Role of DNase-1, PAD4 inhibitor, neutrophil elastase inhibitor in controlling pulmonary vaso-occlusion and NETs generation in SCD mice.

This section contains work which I conducted during my doctoral program to set up my hypothesis. This section results may not be part of paper, but following experiments were performed to look for role of alternative pathways in promoting pulmonary vaso-occlusion and NETs generation in SCD mice.

It has been shown that DNase-1 digests NETs into smaller fragments[10], however there has been no data showing the effect of DNase-1 on pulmonary vaso-occlusions in SCD mice. Hence, we have also used DNase-1 to evaluate its role on PVOs, NETs generation, and cNETs. Similarly, PAD4 inhibitor has been shown to inhibit NETs generation by preventing citrullination-dependent decondensation of nuclear DNA[19, 21, 62]. Recently, a new mechanism has been identified in infectious models cytosolic release of neutrophil elastase from neutrophil granules was shown to promote GSDMD-dependent generation of NET[24]. Hence, we also studied the effect of DNase-1, PAD4 inhibition or NE inhibition on shedding of cNETs, liver to lung translocation of cNETs and development of pulmonary vaso-occlusion in SCD mice administrated IV oxy-Hb.

Figure 26 A shows the schematic of qFILM experimental setup. qFILM was used to assess pulmonary vaso-occlusion in the intact lung microcirculation of live SCD mice following intravenous (IV) challenge with oxy-Hb with or without inhibitors. The qFILM experimental setup is mentioned in section 2.1.5 in detail. Figure 26 B shows the representative images obtained from qFILM where SCD mice administered with IV 10 µmole/kg oxy-Hb and 10 mg/kg DNase-1 or IV 10 µmole/kg oxy-Hb and 10 mg/kg PAD4 inhibitor (GSK 484) or SCD mice administrated with IV 10 µmole/kg oxy-Hb and 10 mg/kg neutrophil elastase inhibitor (BAY-85-8501). Absence of

PVOs can be seen in the all the qFILM images in Figure 26 B. Blood vessels are pseudo colored in purple, neutrophils are pseudo colored in red, and platelets are pseudo colored in green. Quantification of data obtained from qFILM shows that the average number of PVOs per FOV was significantly reduced in SCD mice given IV oxy-Hb and DNase-1 (Figure 26 C) or SCD mice given IV oxy-Hb and PAD-4 inhibitor (Figure 26 D) or SCD mice given IV oxy-Hb and NE inhibitor in comparison to SCD IV oxy-Hb only (Figure 26 E). Similarly, Large PVOs (> 1000 $\mu m^2$) were also significantly decreased in SCD mice administered IV oxy-Hb with DNAse-1 (Figure 26 F) or PAD4 inhibitor (Figure 26 G) or NE inhibitor (Figure 26 H) compared to SCD mice administered IV oxy-Hb alone.

## Figure 26

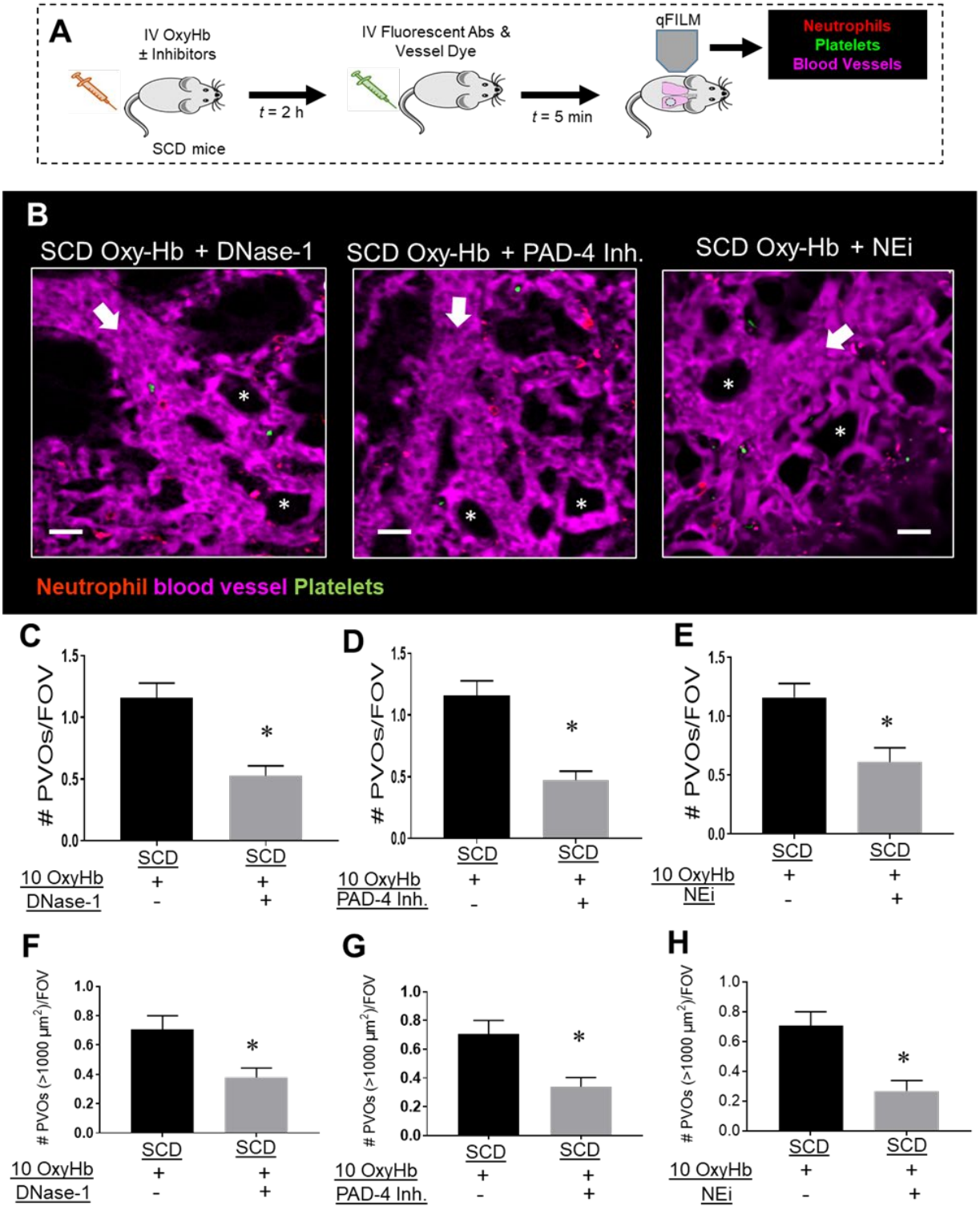


**Figure 26: PVOs decreased by using DNase-1, PAD-4 inhibitor, and neutrophil elastase inhibitor.**

**(A) Schematic of qFILM to acquire absence or presence of PVOs in the lung micro-circulation of a SCD mice. (B) representative images obtained from qFILM 2D data sets shows absence of PVO in SCD mice administrated with IV oxy-Hb and DNase-1 or IV oxy-Hb and PAD-4 inhibitor or IV oxy-Hb with neutrophil elastase inhibitor. Arrow indicates the direction of blood flow, asterisk sign represent air alveoli and scale bar is 20 μm. Average number of PVOs per FOV were significantly decreased in SCD mice administrated with IV oxy-Hb and DNase-1 (C), IV oxy-Hb and PAD-4 inhibitor (D), and IV oxy-Hb with neutrophil elastase inhibitor (E). Larger PVOs greater than 1000 $\mu m^2$ were also significantly reduced in SCD mice administrated with IV oxy-Hb and DNase-1 (F), IV oxy-Hb and PAD-4 inhibitor (G), and IV oxy-Hb with neutrophil elastase inhibitor (H). SCD mice IV oxy-Hb and DNase-1 (n = 4 mice and FOVs 54), SCD IV oxy-Hb and PAD-4 inhibitor (n = 4 mice and FOVs 54), IV oxy-Hb with neutrophil elastase inhibitor BAY-85-8501 (n = 3 mice and FOVs 35). Data represents mean ± SE and compared using students t-test. * Denotes $p < 0.05$.**

In figure 27, A shows the schematic of qFILM experimental setup. qFILM was used to assess NETs and cNETs in the intact lung microcirculation of live SCD mice following intravenous (IV) challenge oxy-Hb with or without inhibitors. The qFILM experimental setup and is mentioned in section 2.1.5 in detail. The average number of NETs per FOV in SCD mice given IV oxy-Hb and DNase-1 shows significant reduction in NETs in comparison to SCD mice given IV oxy-Hb (Figure 27 B). Similar results were obtained in SCD mice given IV oxy-Hb with PAD-4 inhibitor (Figure 27C), and SCD mice IV oxy-Hb with neutrophil elastase inhibitor (Figure 27 D). After analyzing the average number of cNETs flowing per FOV per min, significant reduction was seen in all three inhibitors groups in comparison to just IV oxy-Hb (Figure 27 E), (Figure 27 F), and (Figure 27 G).

Figure 27

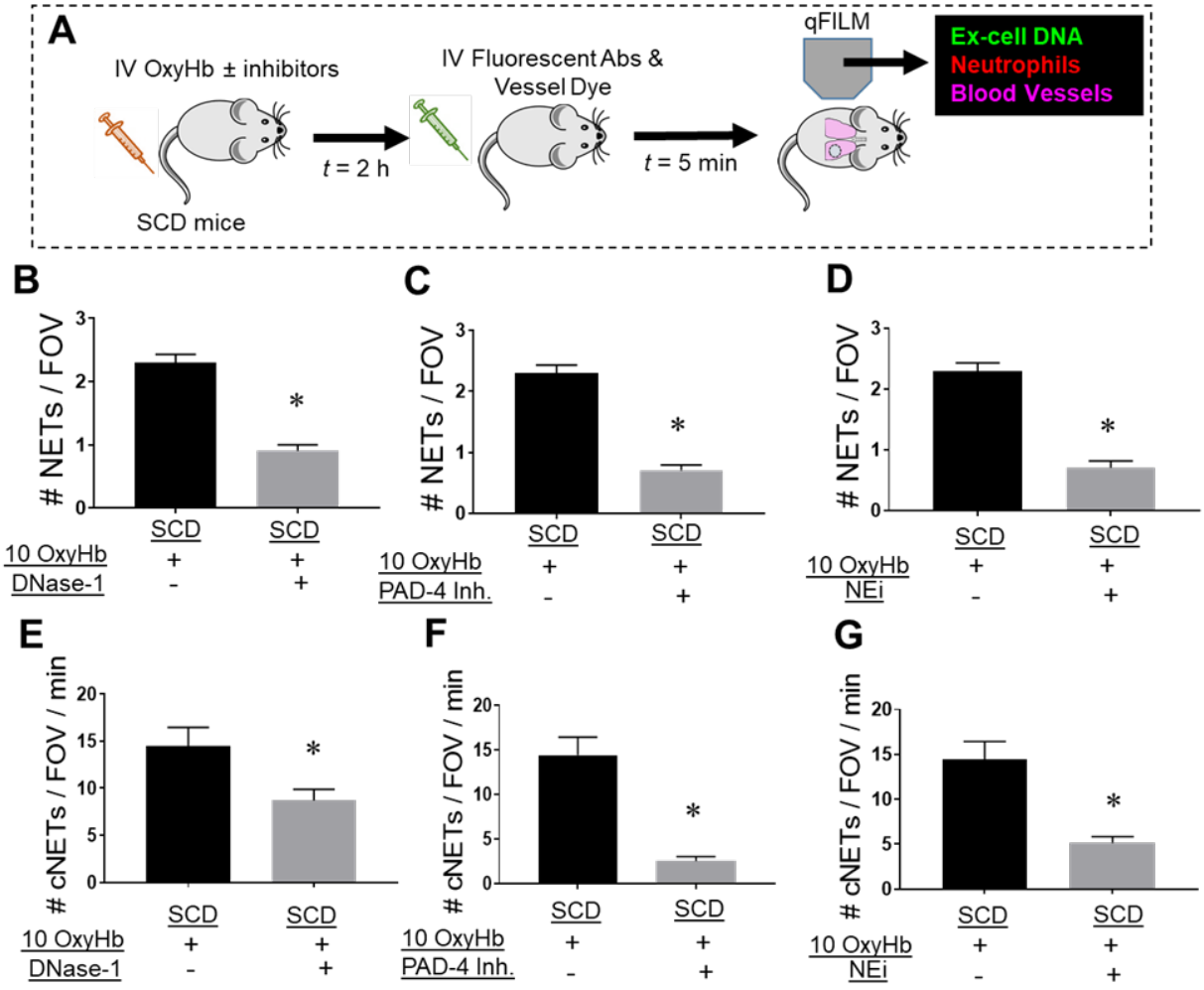


**Figure 27: NETs and cNETs attenuated after using DNase-1, PAD-4 inhibitor, and neutrophil-elastase inhibitor.**

**(A) Schematic of qFILM to acquire NETs and cNETs in the lung micro-circulation of a SCD mice with or without inhibitors. Average number of NETs per FOV were significantly decreased in SCD mice administered with IV oxy-Hb and DNase-1 (B), IV oxy-Hb and PAD-4 inhibitor (C), and IV oxy-Hb with neutrophil elastase inhibitor (D). Average number of cNETs flowing per FOV per min were also significantly reduced in SCD mice administrated with IV oxy-Hb and DNase-1 (E), IV oxy-Hb and PAD-4 inhibitor (F), and IV oxy-Hb with neutrophil elastase inhibitor (G). SCD mice IV oxy-Hb and DNase-1 (n = 4 mice and FOVs 54), SCD IV Oxy-Hb and PAD-4 inhibitor (n = 4 mice and FOVs 54), IV oxy-Hb with neutrophil**

**elastase inhibitor BAY-85-8501 (n = 3 mice and FOVs 35). Data represents Mean ± SE and compared using Students t-test. * Denotes $p < 0.05$.**

## 7.0 Future work

The primary focus during this study was to identify the molecular mechanism leading to shedding of circulating NETs and neutrophil-platelet aggregate-dependent pulmonary vaso-occlusion in SCD. In future, it would to be beneficial to study the role of other blood cells that may contribute to lung vaso-occlusion, such as RBC, monocytes, natural killer cells. Since natural killer cells have been shown to play a role in vaso-occlusion of SCD[73-75]. Additionally, this study tested how eDAMPs like oxy-hemoglobin and hemin affected neutrophil-platelets aggregates formation, NETs formation, and cNETs shedding in the lung micro-circulation of a SCD mice. However, there are other many proinflammatory stimuli released into the blood after hemolysis like ADP, tissue factor, etc[2]., hence their affects can also be tested on vaso-occlusion and lung injury in SCD. These proinflammatory factors can be helpful in evaluating the role on neutrophil-platelet aggregates formation, NETs generation and cNETs shedding.

We have shown that NETs are generated in liver of SCD mice in large amount. These NETs in liver shed and travel via inferior vena cava through heart to lung. Once these cNETs enter lung micro-circulation they form neutrophil-platelet aggregates and block arteriole bottlenecks, which leads to ACS in SCD. However, after post-clamping of hepatic artery and portal vein of SCD mice still few cNETs were noticed in the lung micro-circulation, which opens the possibility of cNETs coming from other organs besides liver. To address this, evaluation of cNETs shedding by in vivo imaging of mesentery, cremaster, and skin microcirculation that are known to be site of vaso-occlusion in SCD[2] should be done in future. Alternatively, this finding may also suggest that DNA-fragments from sources other than NETs may contribute to ACS.

Although the current data suggest that GSDMD-signaling contributes to the P-selectin-independent mechanism of ACS, it does not confirm whether this primarily the result of the activation of GSDMD-signaling in neutrophils. However, this can be confirmed in future studies by generating SCD mice lacking GSDMD only in neutrophils ($SCD^{GsdmdLy6g}$). Less than ~50% protection in $SCD^{GsdmdLy6g}$ mice may suggest a role for GSDMD in cells other than neutrophils as well. To address this, the effect of GSDMD inhibitor on ACS in SCD mice can be assessed following depletion of monocytes/macrophages with clodronate liposomes[76, 77]. To assess the role of endothelial GSDMD, $Gsdmd^{fl/fl}$ mice can be crossed with VECadherin Cre+ mice[78] to generate endothelium-specific Gsdmd-deficient (Gsdmd-VECadh-Cre) mice. Bone marrow can be transferred from SCD to lethally irradiated Gsdmd-VECadh-Cre mice to generate chimeric SCD mice lacking Gsdmd in endothelial cells, and pulmonary arteriole micro-embolism assessed. Less than ~50% protection from ACS in SCD-*casp-11-/-* mice would suggest a contribution of caspase-11-independent activation of GSDMD as well. In such case, one may assess the effect of neutrophil elastase inhibition or deletion on GSDMD activation[24] and ACS in SCD mice.

Franks et. al. 2020 created a humanized porcine model of Sickle Cell Disease, which express human α-, β- and γ-globin genes[79]. SCD mouse models have been valuable in understanding the pathophysiology of SCD, however, use of mouse models have limited application in translational (bench to bedside) studies due to anatomical and physiological variations between mice and humans[79]. This porcine model of SCD is a unique large-animal platform, which will offer more physiological and anatomical similarity to SCD human patients in future studies[79].

Due to the limitations on SCD patient availability, we were unable to include any SCD patients that were suffering with active VOE or ACS prior to treatment. VOE has a major effect

on patients and is the leading cause of emergency medical care[2]. Using Imaging flow cytometry to study platelet-neutrophil interactions, and cNETs generation in crisis patients may provide unique insight into the mechanistic changes that exists in SCD patients at baseline versus crisis. Furthermore, many patients are prescribed HU to reduce hemolysis via induction of fetal hemoglobin and the occurrence of VOE[32]. A study looking at the possible differences between HU and non-HU patients would show the effects the drug may have on cell behavior and cell counts. Using Imaging flow cytometry, one could visualize the cells in each patient to determine if there are any changes between the patients.

In this study most of the result shown are in-vivo in SCD mice or ex-vivo in SCD patient blood, we have not shown shedding of cNETs from neutrophil or NETs in real-time in SCD patient blood. However, this experiment is feasible in our lab using quantitative Microfluidic Fluorescence Microscopy (qMFM)[80] in future studies.

# 8.0 Conclusion

Based on in-vivo studies done in SCD mice and autopsy of SCD patients, pulmonary vaso-occlusion is believed to promote the development of ACS in SCD[2, 17]. The etiological mechanism that triggers ACS remains poorly understood and the current therapy is primarily supportive[81]. 10-20% of SCD patients hospitalized with acute systemic painful vaso-occlusive episodes develop ACS within next few days, suggesting that molecular events surrounding vaso-occlusion contribute to lung injury[1]. This epidemiology also offers a therapeutic window to halt the development of ACS, provided that targeted therapies are identified[2]. Understanding the molecular events that promulgate pulmonary vaso-occlusion will allow us to identify new therapies for ACS. So far four drugs are approved by FDA for SCD, but none of them are lifesaving. Recently, we have published a study where anti-p-selectin drug prevents 50 % of PVOs in the SCD mice challenged with IV LPS[3]. However, the remaining percent of PVOs seems to be driven by other pathways. Like our findings, crizanlizumab (a humanized anti-p-selectin antibody, FDA approved for SCD) has also shown similar results[35]. Hence, the primary focus of this study is to evaluate the remaining 45-50 % of VOEs which has been noticed in patients given crizanlizumab. It would be beneficial to visualize the effect of other pathways on VOE. This study focuses on our new finding that circulating fragments of neutrophil extracellular traps (cNETs) promote gasdermin D (GSDMD)-dependent lung vaso-occlusion in SCD.

Chapter 3 established a role of neutrophil-platelet aggregates in the onset of PVOs after administration with eDAMPs viz. oxy-hemoglobin and hemin. Oxy-Hb and hemin promoted neutrophil-platelet aggregates formation in the arteriole bottleneck of the lung micro-circulation of SCD mice. However, minimal, and significantly less PVOs were noticed in control mice after

Oxy-Hb and hemin administration. We have also shown that Tandem P-selectin−glycoprotein ligand−immunoglobulin (TSGL-Ig) fusion molecule containing four P-selectin binding sites, significantly attenuated intravenous (IV) oxy-hemoglobin triggered lung vaso-occlusion in SCD mice by inhibiting P-selectin-mediated adhesive events[12]. These findings highlight the therapeutic potential of TSGL-Ig in preventing VOE and ACS in SCD[12].

In chapter 4 using qFILM we showed that oxy-Hb induces shedding of cNETs in liver micro-circulation of SCD mice in-vivo and SCD patient blood ex-vivo, and these cNETs are shed by a P-selectin-independent mechanism. Liver being a hypoxic organ and most of the free heme is metabolized in liver, we noticed abundance of NETs in liver of a SCD mice using qLIM. Finally, it was proved that halting blood flow from liver to lung reduces circulating NETs in the lung micro-circulation of a SCD mice. These results support that cNETs shed in the liver, travel to lung to promote p-selectin independent pulmonary arteriole micro-embolism in SCD.

In chapter 5 we have shown the role of GSDMD-signaling and caspse-4 (in humans) / caspase-11 (in mice) signaling on cNETs. Inhibiting GSDMD-signaling, and caspase-4/11 prevents cNETs shedding in SCD human blood, attenuated cNETs in SCD mice. Moreover, inhibiting GSDMD-signaling prevented cNETs shedding in the liver, and their translocation to the lung in SCD mice. Finally, inhibiting GSDMD-signaling prevented pulmonary vaso-occlusion in SCD mice in vivo. Combining these results, we believe that pulmonary vaso-occlusion in SCD mice is GSDMD and P-selectin dependent, and this was shown by inhibiting GSDMD-signaling on a SCD-*Selp-/-* mice where PVOs were further reduced to minimal, thus highlighting the therapeutic potential of targeting both P-selectin and GSDMD-pathway. Figure 28 shows the schematic of my aims and results.

## Figure 28

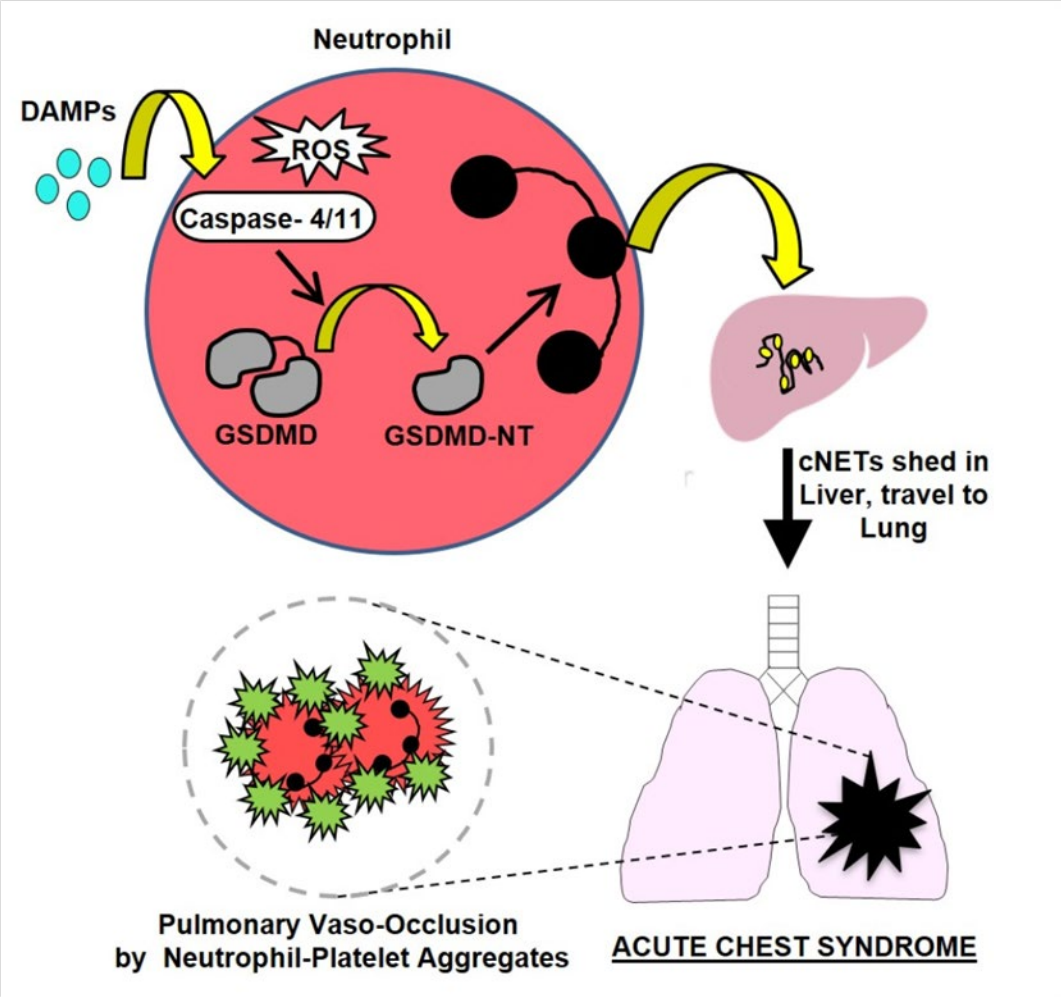


**Figure 28: Schematic of my aims.**

**The sterile inflammatory milieu (DAMPs, IFN-I signaling and ROS) in SCD promotes caspase-4 (humans) or caspase-11 (mouse)-dependent cleavage of neutrophil GSDMD into the active form GSDMD-NT, leading to shedding of NETs in the liver microcirculation. Once shed, these NETs are carried by the blood as circulating NETs (cNETs) to the lung, where they promote neutrophil-platelet aggregation in the pulmonary arterioles, leading to pulmonary vaso-occlusion and lung injury (Acute Chest Syndrome). SCD, Sickle Cell Disease; DAMPs, Damage Associated Molecular Pattern molecules; IFN-I, Type-I interferon (α and β); ROS, Reactive oxygen species; GSDMD, Gasdermin-D; GSDMD-NT, N-terminus (active) domain of Gasdermin-D; NETs, Neutrophil extracellular traps.**

# Appendix

SUNDD LAB PROTOCOLS

The following methods are used in Sundd lab to conduct experiment and analysis.

## Appendix A.1.1 Quantitative Fluorescence Intravital Lung Microscopy

Quantitative fluorescence intravital lung microscopy (qFILM) has been used widely for in-vivo assessment of pulmonary vaso-occlusion in SCD mice[3, 12, 45, 48, 52, 59]. In the current study, qFILM was used to assess pulmonary vaso-occlusion and detect neutrophil extracellular traps (NETs) in the intact lung microcirculation of live SCD, Control, SCD-*Selp-/-*, *Gsdmd-/-* and WT mice following intravenous (IV) challenge with saline, oxy-hemoglobin (oxy-Hb) or hemin with or without pretreatment with GSDMD inhibitors LDC7559[25] or NSA[53] or the pan-caspase inhibitor Z-VAD-FMK[54]. The qFILM experimental setup and approach has been described elsewhere in detail[3, 52]. Briefly, mice were IV administered via tail vein with 80 µl of either: 1) saline or vehicle, 2) 10 µmole/kg oxy-Hb, 3) 20 µmole/kg hemin, 4) 0.004 µmol/kg Z-VAD-FMK or 10 mg/kg LDC7559 or 20 mg/kg NSA, 30 min prior to 10 µmole/kg oxy-Hb. Approximately 2-2.5 hours following IV administration, qFILM was conducted with a Nikon multi-photon-excitation fluorescence microscope using an excitation wavelength of 850 nm and an APO LWD 25x water immersion objective with 1.1 NA. Time-series of 2D qFILM images were collected at ~15 frames per second (fps) using a resonant scanner. Each field of view (FOV) was 256 µm x 256 µm (~65,536 $\mu m^2$) with a resolution of ~0.5 µm per pixel in the x-y plane. Fluorescent light received from the sample was collected in several band pass filters including

450/20 nm (detector 1 for collection of V450 or Pacific Blue), 525/50 nm (detector 2 for collection of FITC), 576/26 nm (detector 3 for collection of AF546), and 685/70 nm (detector 4 for collection of Evans Blue). Mice were anesthetized with an intraperitoneal (IP) injection of 100 mg/kg ketamine HCl and 20 mg/kg xylazine. A cannula was inserted into the right carotid artery and a tracheotomy was performed to facilitate mechanical ventilation with 95% O2 and supply maintenance anesthesia (1-2% isoflurane). The left lung was surgically exposed, and a small portion of the lung was immobilized against a coverslip using a vacuum enabled micro-machined device as described elsewhere[3, 82]. Just prior to qFILM, ~125 µg/mouse FITC-dextran or 50 µl Evans Blue, 5 µg/mouse Sytox Orange or Green, 10 µg/mouse AF546-conjugated anti-NE Ab, 10 µg/mouse AF546-conjugated anti-citrullinated-histone-3 (H3cit) Ab, 12 µg/mouse AF546 or Pacific Blue-conjugated anti-Ly6G mAb and 7 µg/mouse V450-conjugated anti-mouse CD49b mAb were injected into the carotid artery catheter for visualization of the pulmonary microcirculation, extracellular DNA and in vivo staining of NE, citrullinated-histones, neutrophils and platelets, respectively. qFILM was performed on a mouse for a total period of 30 minutes and the presence or absence of vaso-occlusion, presence, or absence of NETs, and counts of circulating NETs (cNETs) were assessed for 30 seconds in each FOV. The resulting series of qFILM images were processed using image subtraction, a median filter, a noise-reduction algorithm, and adjustment of intensity histograms as described previously[3, 12, 45]. As described in the figure legends, some of the channels were pseudo-colored to enhance contrast. Pulmonary vaso-occlusions were assessed in ~10-15 FOVs in each mouse and across multiple mice per test group (n = 3 to 6) as previously described[3, 12, 45]. Figure 29 shows the schematic of qFILM used in this study with slight modifications[52].

Figure 29

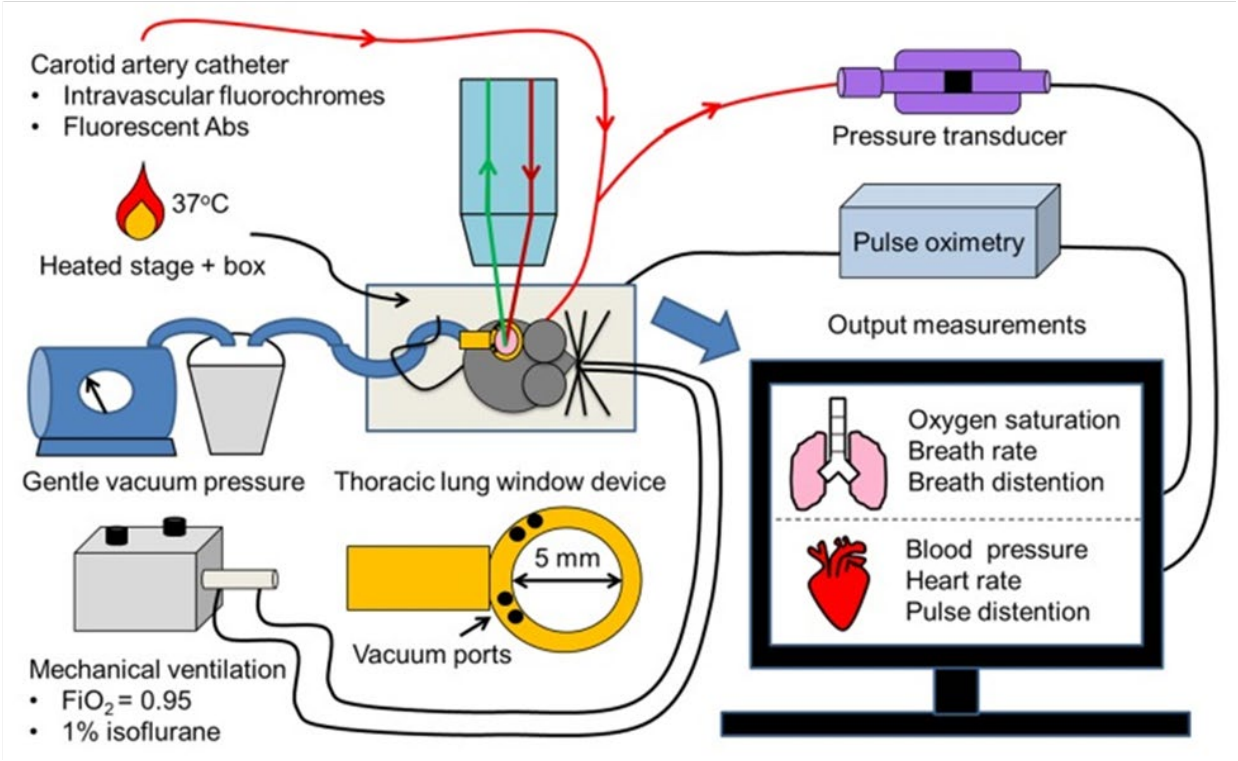


**Figure 29: Schematic diagram of quantitative Fluorescence Lung Intravital Microscopy.**

**Figure taken with permission from reference[52].**

## Appendix A.1.2 Quantitative Liver Intravital Microscopy

Recently, we developed quantitative liver intravital microscopy (qLIM) to study liver pathophysiology in SCD mice[44, 56]. In the current study, qLIM was used to assess vaso-occlusion and detect NETs generation in the intact liver microcirculation of live mice. qLIM was conducted on same strains of mice as described under qFILM studies. The qLIM experimental setup has been described previously in detail[44, 55, 56]. Briefly, mice were IV administered via tail vein with 80 µl of either: 1) saline, 2) 10 µmole/kg oxy-Hb, 3) 0.004 µmol/kg Z-VAD-FMK

or 10 mg/kg LDC7559 or 20 mg/kg NSA, 30 min prior to 10 µmole/kg oxy-Hb. Mice were anesthetized with an IP injection of 100 mg/kg of body weight ketamine HCl and 20 mg/kg of body weight xylazine. Following anesthetization, mice were IP administered 1 ml physiological saline (maintained at room-temperature) and placed on a heated stage in the supine position. A tracheotomy was performed, and a short length of PE90 tubing was inserted into the incision site and tied to the trachea using a silk suture. Next, the right carotid artery was cannulated with heparinized PE10 tubing. Mice were repositioned in the supine position, the right lobe of the liver was exposed and gently immobilized against a coverslip using a vacuum-enabled micro-machined liver-imaging window described elsewhere[44, 55, 56]. Next, ~125 µg/mouse FITC-dextran, 5 µg/mouse Sytox Orange/Green, and 12 µg/mouse AF546 or Pacific Blue-conjugated Ly6G mAb were injected into the carotid artery catheter for visualization of the liver microcirculation, extracellular DNA, and in vivo staining of neutrophils, respectively, and intravital observations were conducted in the intact mice liver with a Nikon Multi-Photon-Excitation fluorescence microscope using an excitation wavelength of 850 nm and an APO LWD 25x water immersion objective (1.1 NA) as described elsewhere in detail[44, 55, 56]. Figure 28 shows the schematic of qLIM with slight modifications[56].

## Figure 30

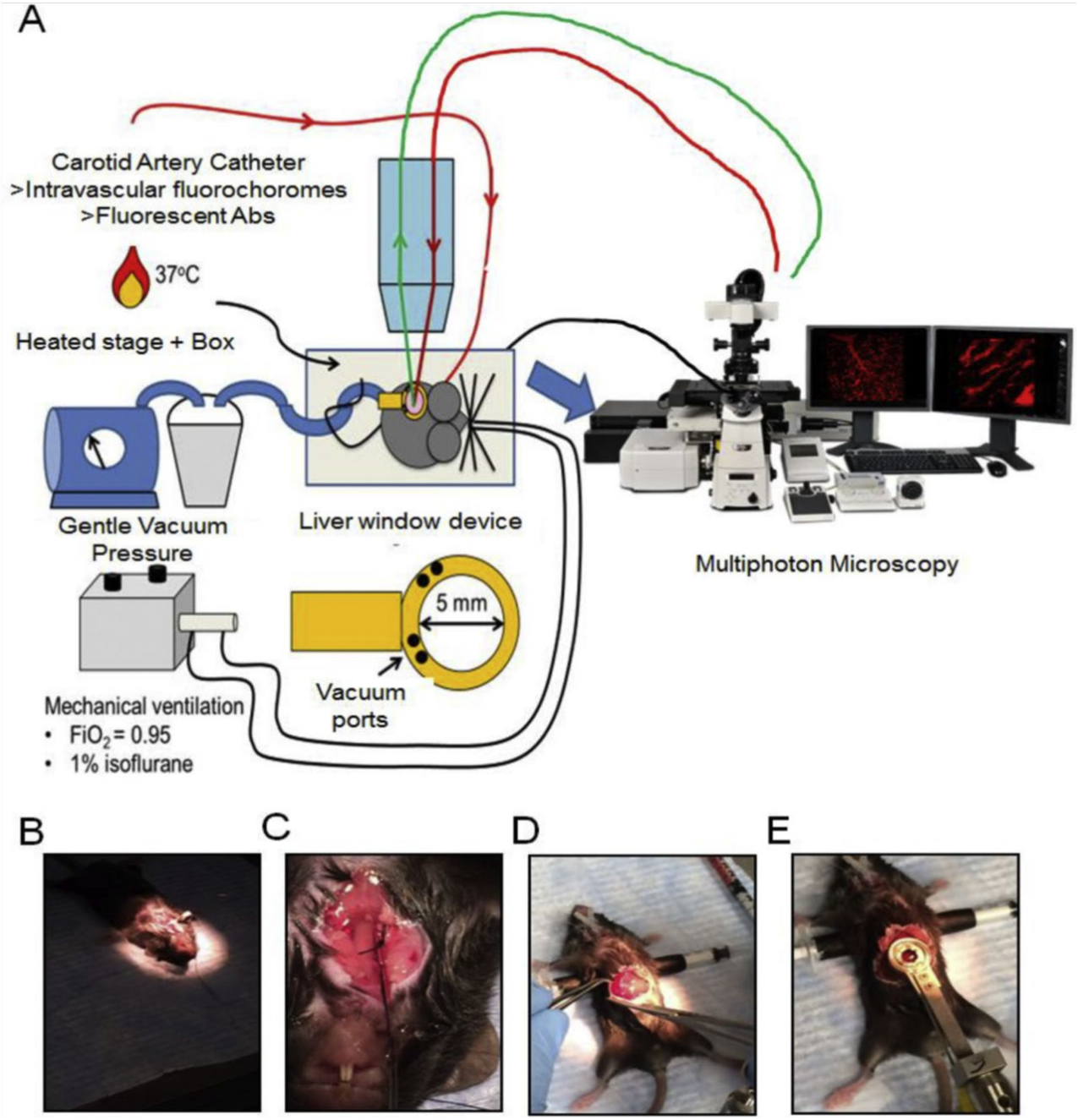


**Figure 30: Schematic of quantitative Liver Intravital Microscopy.**

**(A) Shows the schematic of quantitative Lung Intravital Microscopy (qLIM). (B) Shows the position of a mouse under a binocular. (C) Shows the image taken after carotid artery cannulation. (D) Shows the position of a mouse before starting liver surgery. (E) Shows the position of clamp placed over liver for stabilization. Figure is taken with permission from reference[56].**

**Appendix A.1.3 Quantitative Kidney Intravital Microscopy**

We have also developed quantitative Kidney Intravital Microscopy (qKIM) approach, which enables in vivo visualization of blood flow, blood cell trafficking and detection of NETs in the intact kidney of SCD mice. qKIM uses an experimental set-up and approach identical to the one used for qLIM imaging with few modifications. Briefly, control and SCD mice were intravenously (IV) injected via tail vein with 10 μmole/kg oxy-Hb, anesthetized with an IP injection of 100 mg/kg of body weight ketamine HCl and 20 mg/kg of body weight xylazine. Following anesthetization, mice were IP administered 1 ml physiological saline (maintained at room-temperature) and placed on a heated stage in the supine position. A tracheotomy was performed, and a short length of PE90 tubing was inserted into the incision site and tied to the trachea using a silk suture. Next, the right carotid artery was cannulated with heparinized PE10 tubing. Mice were repositioned in the supine position, the right kidney was exposed and gently immobilized against a coverslip using a vacuum-enabled micro-machined kidney-imaging window. Next, ~125 μg/mouse FITC-dextran, 5 μg/mouse Sytox Orange/Green, and 12 μg/mouse AF546 or Pacific Blue-conjugated Ly6G mAb were injected into the carotid artery catheter for visualization of the kidney microcirculation, extracellular DNA, and in vivo staining of neutrophils, respectively, and intravital observations were conducted in the intact mice kidney with a Nikon Multi-Photon-Excitation fluorescence microscope using an excitation wavelength of 850 nm and an APO LWD 25x water immersion objective (1.1 NA).

## Appendix A.1.4 Imaging Flow Cytometry

Image Flow Cytometry was conducted using Image Stream equipment Amnis Imagestream and data was analyzed using IDEAS application software version 6.2.187.0. cNETs were identified as particles (< 3 μm) triple-positive for NETs markers-extracellular DNA, NE, and histones. As shown by the representative images in Figure 12 B & E, Channel 1 showed the bright field image, channel 2 showed extracellular DNA (green), channel 3 showed neutrophil elastase (yellow) and channel 4 showed histones (red). Concentration of cNETs was reported as number of cNETs per μL of plasma and compared between treatment groups. Figure 29 shows the picture of Imaging flow cytometry used in this study, and it is in Department of Immunology BST E1005 at the University of Pittsburgh. ImageStream-10 is equipped with 6 lasers: 375 nm, 405 nm, 488 nm, 561 nm, and 642 nm. It offers 3 multi-magnifications i.e., 20 X, 40X, and 60X. Figure 29 shows the picture of AMNIS ImageStream-10 (Imaging Flow Cytometer) available at the Flow Cytometry Core within the Department of Immunology at the University of Pittsburgh.

Figure 31


**Figure 31: AMNIS Image stream-10.**

**AMNIS ImageStream-10 (Imaging Flow Cytometer) available at the Flow Cytometry Core within the Department of Immunology at the University of Pittsburgh.**

## Bibliography


1. Rees, D.C., T.N. Williams, and M.T. Gladwin, *Sickle-cell disease.* Lancet, 2010. **376**(9757): p. 2018-31.

2. Sundd, P., *Pathophysiology of Sickle Cell Disease.* 2019.

3. Bennewitz, M.F., et al., *Lung vaso-occlusion in sickle cell disease mediated by arteriolar neutrophil-platelet microemboli.* JCI Insight, 2017. **2**(1): p. e89761.

4. Kato, G.J., et al., *Sickle cell disease.* Nat Rev Dis Primers, 2018. **4**: p. 18010.

5. *Global, regional, and national age-sex specific all-cause and cause-specific mortality for 240 causes of death, 1990-2013: a systematic analysis for the Global Burden of Disease Study 2013.* Lancet, 2015. **385**(9963): p. 117-71.

6. Herrick, J.B., *Peculiar elongated and sickle-shaped red blood corpuscles in a case of severe anemia. 1910.* Yale J Biol Med, 2001. **74**(3): p. 179-84.

7. SYDENSTRICKER, V.P., *FURTHER OBSERVATIONS ON SICKLE CELL ANEMIA.* Journal of the American Medical Association, 1924. **83**(1): p. 12-17.

8. Pauling, L., et al., *Sickle Cell Anemia, a Molecular Disease.* Science, 1949. **110**(2865): p. 543-548.

9. Mark T. Gladwin, G.J.K., Enrico M. Novelli, *Sickle Cell Disease*. 2021: McGraw Hill.

10. Belcher, J.D., et al., *Heme triggers TLR4 signaling leading to endothelial cell activation and vaso-occlusion in murine sickle cell disease.* Blood, 2014. **123**(3): p. 377-90.

11. Barabino, G.A., M.O. Platt, and D.K. Kaul, *Sickle cell biomechanics.* Annu Rev Biomed Eng, 2010. **12**: p. 345-67.

12. Vats, R., et al., *Tandem P-selectin glycoprotein ligand immunoglobulin prevents lung vaso-occlusion in sickle cell disease mice.* Exp Hematol, 2020. **84**: p. 1-6 e1.

13. Novelli, E.M. and M.T. Gladwin, *Crises in Sickle Cell Disease.* Chest, 2016. **149**(4): p. 1082-93.

14. Rifkind, J.M., J.G. Mohanty, and E. Nagababu, *The pathophysiology of extracellular hemoglobin associated with enhanced oxidative reactions.* Front Physiol, 2014. **5**: p. 500.

15. Gregory J. Kato, M.T.G., *Hemolysis and Endothelial Dysfunction*, in *Sickle Cell Disease*, G.J.K. Mark T. Gladwin, Enrico M. Novelli, Editor. 2021, Mc Gras Hill. p. 73-108.

16. Yang, H., et al., *New Insights into Neutrophil Extracellular Traps: Mechanisms of Formation and Role in Inflammation.* Front Immunol, 2016. **7**: p. 302.

17. Desai, P.C. and K.I. Ataga, *The acute chest syndrome of sickle cell disease.* Expert Opin Pharmacother, 2013. **14**(8): p. 991-9.

18. Chaturvedi, S., et al., *Rapidly progressive acute chest syndrome in individuals with sickle cell anemia: a distinct acute chest syndrome phenotype.* Am J Hematol, 2016. **91**(12): p. 1185-1190.

19. Jorch, S.K. and P. Kubes, *An emerging role for neutrophil extracellular traps in noninfectious disease.* Nat Med, 2017. **23**(3): p. 279-287.

20. Papayannopoulos, V., *Neutrophil extracellular traps in immunity and disease.* Nat Rev Immunol, 2018. **18**(2): p. 134-147.

21. Sollberger, G., D.O. Tilley, and A. Zychlinsky, *Neutrophil Extracellular Traps: The Biology of Chromatin Externalization.* Dev Cell, 2018. **44**(5): p. 542-553.

22. Rosazza, T., J. Warner, and G. Sollberger, *NET formation - mechanisms and how they relate to other cell death pathways.* Febs j, 2020.

23. Schimmel, M., et al., *Nucleosomes and neutrophil activation in sickle cell disease painful crisis.* Haematologica, 2013. **98**(11): p. 1797-803.

24. Kambara, H., et al., *Gasdermin D Exerts Anti-inflammatory Effects by Promoting Neutrophil Death.* Cell Rep, 2018. **22**(11): p. 2924-2936.

25. Sollberger, G., et al., *Gasdermin D plays a vital role in the generation of neutrophil extracellular traps.* Sci Immunol, 2018. **3**(26).

26. Broz, P., P. Pelegrín, and F. Shao, *The gasdermins, a protein family executing cell death and inflammation.* Nat Rev Immunol, 2020. **20**(3): p. 143-157.

27. Liang, F., et al., *The advances in pyroptosis initiated by inflammasome in inflammatory and immune diseases.* Inflamm Res, 2020. **69**(2): p. 159-166.

28. Shi, J., W. Gao, and F. Shao, *Pyroptosis: Gasdermin-Mediated Programmed Necrotic Cell Death.* Trends Biochem Sci, 2017. **42**(4): p. 245-254.

29. Broz, P. and V.M. Dixit, *Inflammasomes: mechanism of assembly, regulation and signalling.* Nat Rev Immunol, 2016. **16**(7): p. 407-20.

30. Chen, K.W., et al., *Noncanonical inflammasome signaling elicits gasdermin D-dependent neutrophil extracellular traps.* Sci Immunol, 2018. **3**(26).

31. *3rd World Sickle Cell Day*. Available from: http://www.unesco.org/new/en/unesco/events/all-

events/?tx_browser_pi1%5BshowUid%5D=4087#:~:text=Through%20advocacy%20of%20the%20Sickle,sickle%20cell%20disease%20as%20a.

32. Agrawal, R.K., et al., *Hydroxyurea in sickle cell disease: drug review.* Indian J Hematol Blood Transfus, 2014. **30**(2): p. 91-6.

33. Li, H. and P.S. Frenette, *Vaso-Occlusion in Sickle Cell Disease*, in *Sickle Cell Disease*. 2021, Mx Graw Hill. p. 55-72.

34. Sadaf, A. and C.T. Quinn, *L-glutamine for sickle cell disease: Knight or pawn?* Exp Biol Med (Maywood), 2020. **245**(2): p. 146-154.

35. Ataga, K.I., et al., *Crizanlizumab for the Prevention of Pain Crises in Sickle Cell Disease.* N Engl J Med, 2017. **376**(5): p. 429-439.

36. Vichinsky, E., et al., *A Phase 3 Randomized Trial of Voxelotor in Sickle Cell Disease.* N Engl J Med, 2019. **381**(6): p. 509-519.

37. Telen, M.J., et al., *Randomized phase 2 study of GMI-1070 in SCD: reduction in time to resolution of vaso-occlusive events and decreased opioid use.* Blood, 2015. **125**(17): p. 2656-64.

38. Manwani, D., et al., *Single-dose intravenous gammaglobulin can stabilize neutrophil Mac-1 activation in sickle cell pain crisis.* Am J Hematol, 2015. **90**(5): p. 381-5.

39. Jakubowski, J.A., et al., *The effect of prasugrel on ADP-stimulated markers of platelet activation in patients with sickle cell disease.* Platelets, 2015. **26**(5): p. 474-9.

40. Heeney, M.M., et al., *A Multinational Trial of Prasugrel for Sickle Cell Vaso-Occlusive Events.* N Engl J Med, 2016. **374**(7): p. 625-35.

41. Rees DC, K.Y., Unal S, et al. , *Double-blind, randomized study of canakinumab treatment in pediatric and young adult patients with sickle cell anemia.* . 61st ASH Annual Meeting and Exposition, 2019. **Abstract 615**.

42. Alexis Leonard, J.F.T., *A pause in gene therapy: Reflecting on the unique challenges of sickle cell disease.* Molecular Therapy, 2021. **29**(4): p. 1355-1356.

43. Wu, L.C., et al., *Correction of sickle cell disease by homologous recombination in embryonic stem cells.* Blood, 2006. **108**(4): p. 1183-8.

44. Vats, R., et al., *Impaired Bile Secretion Promotes Hepatobiliary Injury in Sickle Cell Disease.* Hepatology, 2020. **72**(6): p. 2165-2181.

45. Vats, R., et al., *Platelet Extracellular Vesicles Drive Inflammasome-IL-1β-Dependent Lung Injury in Sickle Cell Disease.* Am J Respir Crit Care Med, 2020. **201**(1): p. 33-46.

46. Ghosh, S., et al., *Extracellular hemin crisis triggers acute chest syndrome in sickle mice.* J Clin Invest, 2013. **123**(11): p. 4809-20.

47. Sparkenbaugh, E.M., et al., *Thrombin activation of PAR-1 contributes to microvascular stasis in mouse models of sickle cell disease.* Blood, 2020. **135**(20): p. 1783-1787.

48. Bennewitz, M.F., et al., *P-selectin-deficient mice to study pathophysiology of sickle cell disease.* Blood Adv, 2020. **4**(2): p. 266-273.

49. Shi, J., et al., *Cleavage of GSDMD by inflammatory caspases determines pyroptotic cell death.* Nature, 2015. **526**(7575): p. 660-5.

50. Denk, W., J.H. Strickler, and W.W. Webb, *Two-photon laser scanning fluorescence microscopy.* Science, 1990. **248**(4951): p. 73-6.

51. Xu, C., et al., *Multiphoton fluorescence excitation: new spectral windows for biological nonlinear microscopy.* Proc Natl Acad Sci U S A, 1996. **93**(20): p. 10763-8.

52. Bennewitz, M.F., S.C. Watkins, and P. Sundd, *Quantitative intravital two-photon excitation microscopy reveals absence of pulmonary vaso-occlusion in unchallenged Sickle Cell Disease mice.* Intravital, 2014. **3**(2): p. e29748.

53. Rathkey, J.K., et al., *Chemical disruption of the pyroptotic pore-forming protein gasdermin D inhibits inflammatory cell death and sepsis.* Sci Immunol, 2018. **3**(26).

54. Pagano, N., et al., *Effect of caspase inhibitor Z-VAD-FMK on bovine sperm cryotolerance.* Reprod Domest Anim, 2020. **55**(4): p. 530-536.

55. Vats, R., et al., *P-selectin deficiency promotes liver senescence in sickle cell disease mice.* Blood, 2021. **137**(19): p. 2676-2680.

56. Pradhan-Sundd, T., et al., *Dysregulated Bile Transporters and Impaired Tight Junctions During Chronic Liver Injury in Mice.* Gastroenterology, 2018. **155**(4): p. 1218-1232.e24.

57. Kolaczkowska, E., et al., *Molecular mechanisms of NET formation and degradation revealed by intravital imaging in the liver vasculature.* Nat Commun, 2015. **6**: p. 6673.

58. Yipp, B.G., et al., *Infection-induced NETosis is a dynamic process involving neutrophil multitasking in vivo.* Nat Med, 2012. **18**(9): p. 1386-93.

59. Brzoska, T., et al., *Live Imaging of the Lung.* Curr Protoc Cytom, 2020. **95**(1): p. e80.

60. Tejero, J., et al., *Low NO concentration dependence of reductive nitrosylation reaction of hemoglobin.* J Biol Chem, 2012. **287**(22): p. 18262-74.

61. Barbaux, S., et al., *The adhesion mediated by the P-selectin P-selectin glycoprotein ligand-1 (PSGL-1) couple is stronger for shorter PSGL-1 variants.* J Leukoc Biol, 2010. **87**(4): p. 727-34.

62. Lewis, H.D., et al., *Inhibition of PAD4 activity is sufficient to disrupt mouse and human NET formation.* Nat Chem Biol, 2015. **11**(3): p. 189-91.

63. Raat, N.J., et al., *Direct sGC activation bypasses NO scavenging reactions of intravascular free oxy-hemoglobin and limits vasoconstriction.* Antioxid Redox Signal, 2013. **19**(18): p. 2232-43.

64. Anea, C.B., et al., *Pulmonary platelet thrombi and vascular pathology in acute chest syndrome in patients with sickle cell disease.* Am J Hematol, 2016. **91**(2): p. 173-8.

65. Smith, A. and W.T. Morgan, *Hemopexin-mediated heme transport to the liver. Evidence for a heme-binding protein in liver plasma membranes.* J Biol Chem, 1985. **260**(14): p. 8325-9.

66. Slaba, I., et al., *Imaging the dynamic platelet-neutrophil response in sterile liver injury and repair in mice.* Hepatology, 2015. **62**(5): p. 1593-605.

67. Tolosano, E., et al., *Heme scavenging and the other facets of hemopexin.* Antioxid Redox Signal, 2010. **12**(2): p. 305-20.

68. Nielsen, M.J., H.J. Møller, and S.K. Moestrup, *Hemoglobin and heme scavenger receptors.* Antioxid Redox Signal, 2010. **12**(2): p. 261-73.

69. Chen, G., et al., *Heme-induced neutrophil extracellular traps contribute to the pathogenesis of sickle cell disease.* Blood, 2014. **123**(24): p. 3818-27.

70. Gladwin, M.T. and S.F. Ofori-Acquah, *Erythroid DAMPs drive inflammation in SCD.* Blood, 2014. **123**(24): p. 3689-90.

71. Nath, K.A. and R.P. Hebbel, *Sickle cell disease: renal manifestations and mechanisms.* Nat Rev Nephrol, 2015. **11**(3): p. 161-71.

72. Vichinsky, E., *Chronic organ failure in adult sickle cell disease.* Hematology Am Soc Hematol Educ Program, 2017. **2017**(1): p. 435-439.

73. Wallace, K.L. and J. Linden, *Adenosine A2A receptors induced on iNKT and NK cells reduce pulmonary inflammation and injury in mice with sickle cell disease.* Blood, 2010. **116**(23): p. 5010-20.

74. Chantrathammachart, P., et al., *Tissue factor promotes activation of coagulation and inflammation in a mouse model of sickle cell disease.* Blood, 2012. **120**(3): p. 636-46.

75. Zennadi, R., *MEK inhibitors, novel anti-adhesive molecules, reduce sickle red blood cell adhesion in vitro and in vivo, and vasoocclusion in vivo.* PLoS One, 2014. **9**(10): p. e110306.

76. Dutra, F.F., et al., *Hemolysis-induced lethality involves inflammasome activation by heme.* Proc Natl Acad Sci U S A, 2014. **111**(39): p. E4110-8.

77. Ferenbach, D.A., et al., *Macrophage/monocyte depletion by clodronate, but not diphtheria toxin, improves renal ischemia/reperfusion injury in mice.* Kidney Int, 2012. **82**(8): p. 928-33.

78. Alva, J.A., et al., *VE-Cadherin-Cre-recombinase transgenic mouse: a tool for lineage analysis and gene deletion in endothelial cells.* Dev Dyn, 2006. **235**(3): p. 759-67.

79. Franks, T.M., et al., *Engineering, Generation and Preliminary Characterization of a Humanized Porcine Sickle Cell Disease Animal Model.* bioRxiv, 2020: p. 2020.09.15.291864.

80. Jimenez, M.A., et al., *Quantitative microfluidic fluorescence microscopy to study vaso-occlusion in sickle cell disease.* Haematologica, 2015. **100**(10): p. e390-3.

81. Miller, A.C. and M.T. Gladwin, *Pulmonary complications of sickle cell disease.* Am J Respir Crit Care Med, 2012. **185**(11): p. 1154-65.

82. Looney, M.R., et al., *Stabilized imaging of immune surveillance in the mouse lung.* Nat Methods, 2011. **8**(1): p. 91-6.